University of Stavanger

Faculty of Science and Technology

MASTER'S THESIS

Study program/ Specialization: Petroleum Engineering/ Production Engineering	Spring semester, 2014 Open
Writer: Maevskiy Evgeny	…… (Writer's signature)
Faculty supervisor: Aly Anis Hamouda	
Thesis title: Mechanism of Primary and Secondary Oil Flooding for Recovery from Chalk by Low Salinity Water.	
Credits (ECTS): 30	
Key words: - Enhanced oil recovery - Low salinity waterflooding - Dissolution of calcite - Chalk - Calcium - pH - Pressure drop	Pages: 96 + enclosure: 4 Stavanger, 16th June, 2014. Date/year

Acknowledgments

I want to use the opportunity to express my gratitude to my supervisor, Dr. Aly Anis Hamouda, for his guidance, motivation and encouragement during the work on my MSc thesis. I found the topic very interesting and have got a lot of positive experience.

I would also like to thank my co-workers at the laboratory, Rinad Munaev and Aleksandr Mamonov, for their support and pleasant working environment.

Finally, thanks to my family and friends for believing in me.

Abstract

This research work is performed with the intention to bring the contribution in the ongoing discussion of implementing the low salinity brines as the injection fluid in carbonate reservoirs. The work contains theoretical review of the materials connected to the topic, experimental part, interpretation of acquired data, discussion of results, simulation and proposed mechanism.

In this thesis the effect of changing the injection water salinity on oil recovery was studied. The porous media is represented by the Stevns Klint chalk cores. Synthetic oil that was used is the mixture of n-decane and stearic acid. Synthetic sea water was acquired by diluting salts in distilled water (total salinity is 33388 ppm). Low salinity brines represent the dilution of synthetic sea water 5 times, 10 times, 15 times, 20 times and 25 times.

Synthetic sea water and low salinity brines were studied during primary recovery water flooding on 4 PV/day flowrate and 16 PV/day flowrate. The recovery using different salinity gave different results both on low flowrate and on high flowrate. The data acquired during the flooding process, including pressure drop, pH of the effluent and the injection fluid, ions chromatography analysis, were interpreted and support the discussion about the observed recovery results. Based on these data the mechanism of the recovery increase with low salinity is proposed. It includes the brine/rock interaction which induces the dissolution of calcite. The dissolution leads to peeling off calcite particles and fine migration in core. Fines then block the pore throats and this increases the sweep efficiency. The proposed reason for the difference in dissolution rates between different salinity brines lies in physical properties of these brines, such as pH of injection fluid and IFT. The pH of brine decreases with lowering of salinity, which enhance the dissolution process. However, IFT between the injection fluid and synthetic oil increases with lowering of salinity, which increases the amount of capillary trapped oil. These two parameters working together can give the distribution of results as it was observed. The simulation of relative permeability curves in Sendra supports the proposed mechanism.

The implementing of 10 times diluted synthetic sea water as a secondary recovery fluid brought incremental oil. This shows the potential of implementing low salinity brine as an EOR fluid. However, the incremental oil is only equal to 0.3% OOIC. This was connected to the damaging of the core by synthetic sea water on high flowrate during primary flooding.

Contents

List of Figures

List of Tables

Nomenclature

A	Total cross-sectional area of the rock
A_r	Cross-sectional area
BHP	Bottom-hole flowing pressure
BOPD	Barrel of oil per day
c	Molar concentration
dp/dx	Pressure gradient
E	Overall displacement efficiency
E_A	Areal sweep efficiency
E_D	Microscopic displacement efficiency
E_l	Vertical sweep efficiency
EOR	Enhanced oil recovery
E_V	Macroscopic displacement efficiency
I	Ionic strength
IFT	Interfacial tension
IHP	Inner Helmholtz plane
IOR	Improved oil recovery
IWS	Initial water saturation
K	Thermodynamic equilibrium constant
k	Effective permeability
k_g	Effective permeability for gas
k_o	Effective permeability for oil
k_{rg}	Relative permeability for gas
k_{ro}	Relative permeability for oil
k_{rw}	Relative permeability for water
k_{rw}^o	The end point of the water relative permeability
k_w	Effective permeability for water
LSW	Low salinity water
M	Mobility ratio
m_d	Weight of dried core
m_{sat}	Weight of the core with SSW inside
N_C	Capillary number
OHP	Outer Helmholtz plane
OOIC	Original oil in core
OOIP	Original oil in place
P_C	Capillary pressure
p_c	External pressure at the drainage radius

P_{COW}	Capillary pressure for an oil-water system
P_o	Pressure in the oil phase
PV	Pore volume
ppm	Particles per millions
P_w	Pressure in the water phase
p_{wf}	Bottom-hole flowing pressure
q	Volumetric flowrate
q_g	Flow rate for gas
q_o	Flow rates for oil
q_w	Flow rates for water
r	Pore radius
SA	Stearic acid
SGC	Stern-Gouy-Chapman model
SI	Spontaneous imbibition
S_{or}	Residual oil saturation
SSW	Synthetic sea water
SW	Sea water
S_{wi}	Irreducible water saturation
S_{wn}	Normalized water saturation
TDS	Total dissolved solids
WAG	Water-alternating-gas
z	Charge number
ζ	Zeta potential
θ	Contact angle
θ_A	Advancing contact angle
θ_R	Receding contact angle
μ	Viscosity
μ_g	Viscosity of gas
μ_o	Viscosity of oil
μ_w	Viscosity of water
ρ_{ssw}	Synthetic sea water density
σ	Interfacial tension
σ_{os}	Interfacial energy between oil and solid
σ_{ow}	Interfacial energy between oil and water
σ_{ws}	Interfacial energy between water and solid
υ	Darcy velocity
ψ_δ	Potential at Stern layer

1 Introduction

Among all reservoirs existing in the world, carbonate reservoirs contain more than 50% of the world's total known oil reserves. Also, more than 40% of the daily world oil production is coming from naturally fractured carbonate reservoirs (Ahmadi and Shadizadeh, 2013).

The behavior of carbonate reservoirs is different in many ways from sandstone reservoirs, mainly because of the very complex pore structure. The percentage of original oil in place recovered from carbonate reservoir rocks is often very low (less than 20%). Their origin, composition, and the diagenetic and catagenetic processes determine in large measure the petrophysical properties and behavior of carbonate reservoirs (Chilingar et al., 2012). Also for fluid flow the wetting properties of carbonate reservoirs are fundamental. Wettability is important to the understanding of fluid flow in all aspects of oil production, particularly during water flooding. The aging of carbonate rock, which contain water and oil, turns the initially water-wet rocks into mixed-wet or even oil-wet. This means that oil can adhere to the surface of pores inside carbonate rock and it is therefore harder to produce. Most carbonate reservoirs are believed to be mixed-wet or oil-wet. (Gomari, 2009)

Highly naturally fractured conventional oil reservoirs (e.g., carbonate reservoirs), where the oil-recovery mechanisms are imbibition and gravity drainage, are considered non-classical conformance problems. In these reservoirs there are often unusually large and conductive natural fractures that contribute to conformance problems and poor oil recovery (Sydansk and Romero-Zerón, 2011). However, there are examples of exceptionally successful waterflooding in carbonate reservoirs. Waterflooding the Ekofisk fractured chalk is one of them (Hermansen et al., 2000). The exceptional good response of seawater injection into the Ekofisk formation is an indication of a special rock-water interaction, which improves the spontaneous displacement of oil (Austad et al., 2005). Such success induced many research programs, aimed for studying brine/rock/oil interactions. One of the main parameters studied in those works is the salinity of the injection brine.

The impact of brine salinity and ion composition on oil recovery has been an area of research in recent years. Evidence from laboratory studies, supported by some field tests targeting mainly sandstones, has distinctly shown that injecting low-salinity water has a significant impact on oil recovery. Although the potential for carbonates has not been thoroughly investigated, some reported studies have excluded carbonates from this effect (Yousef et al., 2011).

The main goal of this work is to study the effect of changing the injection brine salinity on the recovery from chalk cores. The low salinity brines are studied both as a primary injection fluid (low salinity is flooded from the beginning), and as a secondary injection fluid (low salinity is implemented after flooding with sea water). The discussion of recovery results is supported by pressure drop measurements, pH measurements, ion chromatography analysis and simulation.

2 Theory

2.1 Carbonates

Carbonates are anionic complexes of $(CO_3)^{2-}$ and divalent metallic cations such as Ca, Mg, Fe, Mn, Zn, Ba, Sr, Cu, and also a few less common others. Naturally carbonates occur as sediments and reefs in modern tropical and temperate oceans, as ancient rocks, and also as economically important mineral deposits (Ahr, 2008). Carbonate rocks include rocks consisting mainly of carbonate minerals formed by the organic or inorganic precipitation from aqueous solution of carbonates of calcium ($CaCO_3$) – limestone, or calcium plus magnesium ($CaMg(CO_3)_2$) – dolostone (Chilingar et al., 2012). The distinction between these two rocks is in percentage of different carbonates composing the rock. Limestones are composed of more than 50% $CaCO_3$. Dolomites are composed of more than 50% $CaMg(CO_3)_2$. Most dolomites have formed by replacement of limestone, and the result is that in many cases the original structures are poorly preserved (Tucker, 2003).

The common carbonates are grouped into families based of their crystal lattice structure (the internal arrangement of atoms). The following crystal systems exist: the hexagonal, orthorhombic, and monoclinic crystallographic systems. The most common carbonate minerals, namely, calcite ($CaCO_3$) and dolomite ($CaMg(CO_3)_2$), are in the hexagonal system. Aragonite has the same composition as calcite, $CaCO_3$, but it crystallizes in the orthorhombic system. Calcite and aragonite are polymorphs of calcium carbonate because they have the same composition but different crystal structures. Aragonite is common in the modern oceans but it is rare in the ancient rocks; hence it is possible to state that carbonate reservoirs and aquifers are composed of minerals calcite and dolomite — limestones and dolostones. Together, those two rocks amount for about 90% of all naturally occurring carbonates (Ahr, 2008).

As hydrocarbon reservoirs carbonates are important due to the high porosity which they sometimes contain (Selley, 2000). Chilingar and Yen (1982) pointed out that carbonate rocks constitute only 15 to 30% of the total volume of all sedimentary rocks, whereas about 65% of the world total oil and gas reserves reside in carbonate reservoirs (Chilingar et al., 2012). However, porosity distribution is complex and has deserved considerable amount of research (Selley, 2000). Porosity in modern carbonate sediments lies within about 40% to 70%, but it is reduced to about 5% – 15% in ancient rocks (Ahr, 2008).

2.1.1 Chalk

Chalk is formed by the stacking of small single-cell algae called coccoliths. The porosity of the modern chalk is high, but the permeability is low or very low (about 1 millidarcy) due to the very small size of pores (0,2 to 2 μm in diameter) (Cossé, 1993). Chalk is a soft white biomicrite formation, consisting of individual coccolithic plates and rings (Bell et al., 1999). These building blocks give the

chalk material a rather open structure, where the dimensions of the pore space may be considerably greater than the dimensions of the individual grains. On the other hand, due to the smallness of the grains, the pore throats will be narrow, and the permeability will be rather small (Risnes et al., 2003). Generally, chalk represents a remarkably pure limestone. For example, the English Chalk has a carbonate content mostly exceeding 98% and rarely falling below 96% (Bell et al., 1999). An image of a typical high porosity chalk is presented in Figure 2.1 (Risnes et al., 2003).

Figure 2.1 – Image of high porosity chalk (5000x magnification) (Risnes et al., 2003).

High porosity chalk represents an important hydrocarbon reservoir rock both in the Norwegian and in the Danish part of the central North Sea. Although burial depth often exceeds 3 km these carbonate reservoirs have preserved high porosities. Studies of samples of Upper Cretaceous chalk from various reservoir and outcrop localities within the North Sea revealed, that most chalk is pure (>95% carbonate), highly porous (>40%) and low permeable (<10 mD). Specific surface area of chalk is bout 1–2 m^2/g (Hjuler and Fabricius, 2009). The reason for such high porosity values in case of North Sea is that the diagenetic processes which usually compact and strengthen the rock matrix have been largely suppressed by the early invasion of hydrocarbons (Risnes et al., 2003).

Porosity together with permeability determines the quality of the reservoir (Ahr, 2008). Improved oil recovery from low-permeable chalk reservoirs is regarded as a great challenge, because of their complexity and heterogeneity (Zahid, 2012).

2.2 Oil recovery

The recovery ranges for each type of reservoir result from the properties the fluids, the thermodynamic conditions, the petrophysical properties, and from the variations due to the architecture and the heterogeneities of the reservoir, and to the production rate (Cossé, 1993). For example, reservoirs composed of fluvial rocks with water drive or gas-cap expansion drive may have

recovery efficiencies in the range of 35-50%, whereas barrier strand-plain reservoirs with gas-cap expansion may have much higher recovery efficiencies of 50-70% (Gudmestad et al., 2010).

Traditionally oil recovery operations have been subdivided into three stages: primary, secondary, and tertiary. Historically, these stages described the reservoir production in a chronological sense (Green and Willhite, 1998). Primary oil recovery involves oil produced solely by means of the natural energy and forces existing within the reservoir. Reservoir-wide primary production occurs when there are only production wells in the field, and there are no any oil-recovery flooding operations involved. Primary oil recovery includes production from naturally flowing wells and also the aid of artificial-lift (Sydansk and Romero-Zerón, 2011). Secondary recovery usually was implemented after primary production declined. The secondary recovery is now almost synonymous with waterflooding, although the term itself includes besides waterflooding such processes as pressure maintenance and gas injection. Tertiary recovery is the third stage of production. It was obtained after waterflooding (or any other secondary process that was used). Tertiary processes used miscible gases, various chemicals, and thermal energy to produce additional oil after the secondary recovery process became uneconomical (Green and Willhite, 1998).

Several decades ago, the term "improved oil recovery" (IOR) was introduced. It includes all methods and techniques that lead to the increase in oil recovery. IOR means planning and execution of various measures intended to increase or accelerate oil recovery from a hydrocarbon field in a profitable manner compared to current plans and forecasts. IOR may be achieved by using conventional methods including improved reservoir management and cost-reducing measures, or by using advanced methods, in which case it is called "enhanced oil recovery" (EOR) (Gudmestad et al., 2010). Various methods of EOR are specifically designed to recover oil commonly described as residual oil, left in the reservoir after both primary and secondary recovery methods have been exploited to their respective economic limits (Ahmed and Meehan, 2011).

The drawback to the division of recovery in the three stages based on chronological sequence is that many reservoir production operations are not conducted in the specified order. A method considered to be a tertiary process in a chronological depletion sequence, can be used as the first, and perhaps final, method of recovery in some specific cases. As an example for this a production of heavy oils can be used. They are very viscous and therefore cannot be produced just by waterflooding. For them as the first method of recovery thermal energy is used. Because of such situations, the term "tertiary recovery" is used less in petroleum engineering literature and was substituted with the term EOR (Green and Willhite, 1998).

2.2.1 Primary recovery

Primary recovery operations use natural energy present in a reservoir as the main source of energy for displacement of oil to producing wells (Green and Willhite, 1998). Cossé, 1993 indicated that pressure for these operations may result from several forces, called driving mechanisms:

- One-phase expansion in gas or undersaturated oil reservoir. It is considerate for gases, but allows the recovery of only a few per cent for oil.
- Expansion of gases coming out of solution, called dissolved gas drive or solution gas drive.
- Expansion of the water of an aquifer associated with the reservoir, which limits the pressure drop of an oil reservoir and drains it, called water drive. For a gas reservoir it could be harmful because of trapping high-pressure gases behind the gas/water interface.
- Expansion of a gas cap overlying the oil (saturated oil reservoir), called gas-cap drive.
- Imbibition. It is important for very heterogeneous reservoirs. Very slow mechanism.
- Gravitational forces causing the segregation of fluids, particularly between gas and oil.
- Rock compressibility. It is relatively important for one-phase oil.

The particular mechanism of lifting oil to the surface, when it reached a wellbore, is not a part of the classification (Green and Willhite, 1998).

At some point of time, the reservoir pressure will fall. Petroleum production can decrease because of different reasons. For example, for gas-cap drive the gas can occupy the emptied pore spaces, which reduces the permeability of the rock, making it more difficult for oil to flow through. In case of solution gas drive the fall in pressure and the loss of dissolved gas increases the surface tension and viscosity of the oil (Speight, 2009). Primary recovery techniques usually produce 5–10% of the total reserves (Sen, 2008).

2.2.2 Secondary recovery

Secondary oil recovery means using of "conventional" methods to add energy to the reservoir to produce oil beyond primary oil recovery. Secondary recovery largely involves physical displacement processes to produce additional oil. The most widely applied secondary oil-recovery methods are natural gas injection (for pressure maintenance) and waterflooding (Sydansk and Romero-Zerón, 2011). The gas is injected into the reservoir above the oil and forces the oil downwards. Water is injected below the oil and forces it upwards. Sometimes the gas which has just been released during primary recovery is used in secondary recovery for pressure maintenance. The disadvantage of using this gas is that it is a marketable product on its own. However, this gas can be used in secondary recovery operations if its transporting is costly (Speight, 2009). An immiscible gas displacement is not as efficient as waterflooding and it is used rarely as a secondary recovery method today, in earlier times it was used much more prevalently. Nowadays, waterflooding is almost synonymous with the term secondary recovery (Green and Willhite, 1998). The main advantages which make waterflooding an essential process for most of the mature fields are: (1) water is easily available and inexpensive agent; (2) it is relatively easy to inject into formation and efficient for displacing oil; (3) water is associated with relatively low capital investment and operating costs (Romero-Zerón, 2012).

Surguchev et al., 2005 indicated that the secondary recovery methods most widely employed on Norwegian fields so far have been:

- Horizontal and multilateral wells
- Water-alternating-gas (WAG) injection
- Gas injection
- Waterflooding in chalk reservoirs
- Increasing the well density
- Well shut-off methods

Recovery efficiencies in the secondary stage vary from 10% to 40% of the original oil in place (Sen, 2008). Recently there have been some encouraging trends relating to conventional-technique oil-recovery factors and operations. For example the Statfjord oilfield in the Norwegian North Sea is reported to have attained an extraordinary 66% recovery efficiency during conventional production. Such encouraging conventional oil-recovery factors are likely attributed to some combination of sound reservoir management and newer oil-recovery technologies, such as conformance improvement by accurately targeting horizontal wells within the oil reservoirs in order to maximize mobile oil recovery (Sydansk and Romero-Zerón, 2011).

2.2.3 Tertiary recovery

Approximately 60–70% of oil reserves cannot be recovered by conventional methods (Fink, 2012). Most of the present world oil production comes from mature fields. Therefore increasing oil recovery from the aging resources becomes a major concern for oil companies and authorities. Furthermore, the rate of replacement of the produced reserves by new discoveries has been declining steadily in the last decade. In these conditions the increase of the recovery factors from mature fields is a critical issue to meet the growing energy demand in the coming years (Surguchev et al., 2005). The primary production and the secondary techniques bring normally recovery factors of no greater than 0.45 because of the problems with mobility and capillary barriers in oil reservoirs. For improvement of production performance, the implementation of tertiary oil production techniques is required (Ahmadi and Shadizadeh, 2013).

The term EOR means the process of enhancing oil recovery by reducing oil saturation below the residual oil saturation. The target of EOR methods varies considerably for different hydrocarbons. Figure 2.2 shows the fluid saturations and the target of EOR for typical light and heavy oil reservoirs (Ahmed and Meehan, 2011).

EOR involves principally the injection of gases or liquid chemicals and the use of thermal energy (Green and Willhite, 1998). It also involves bacteria or bacterial nutrient solutions. It is the most expensive approach (Speight, 2009).

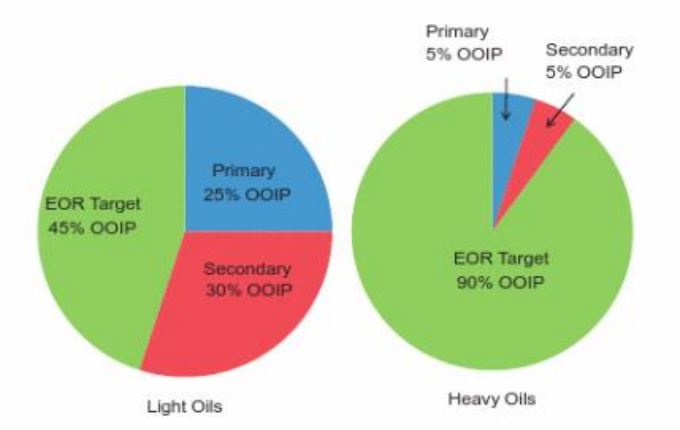

Figure 2.2 – Target for different crude oil systems (Ahmed and Meehan, 2011).

Thermal energy can be obtained from the use of steam, combustion, or electric heating (Fink, 2012). When high-pressure steam is injected, it heats the oil, making its density and viscosity decrease and its flow rate increase. Sometimes, some of the oil in the reservoir is deliberately set on fire. This process increases the flow rate of the oil ahead of the combustion front (Speight, 2009).

Gas floods are usually determined by the type of injected fluid (carbon dioxide, flue gas, nitrogen, or hydrocarbon) (Fink, 2012). Generally, the use of a gas presents in itself an EOR method if the recovery efficiency significantly depends on a mechanism, and not just on immiscible frontal displacement characterized by high-interfacial-tension (IFT) permeabilities. A number of liquid chemicals are known to be available for using, including polymers, surfactants, and hydrocarbon solvents (Green and Willhite, 1998).

Chemicals are often combined, for example, polymer slugs usually follow surfactant or alkaline slugs for improving the sweep efficiency. It may be required to inject materials that plug permeable channels for injection profile control and for preventing or reducing premature water or gas breakthrough (Fink, 2012). Detergents which can be injected reduce the viscosity of the oil and act as surfactants, reducing the ability of the oil to stick to the rock surface and thus making it easier to flush up oil to the surface (Speight, 2009).

Another tertiary recovery technique is based on injecting of bacteria into the oil field. Some bacteria produce polysaccharides which reduce the permeability of the water-filled pores of the reservoir rock, and this can force the injected water to move into the oil-filled pores, pushing the oil out. Other bacteria produce carbon dioxide which helps to increase pressure within the rock pores, which also forces the oil out. Other bacteria can produce surfactants and/or chemicals that reduce the viscosity of the oil (Speight, 2009).

It is well known that projects involving EOR methods have been strongly influenced by economics and crude oil prices. The initiation of such projects depends on the preparedness and willingness of investors to deal with the EOR risks and also on the availability of more attractive investment options. For example, in the USA chemical and thermal EOR projects have been in

constant decline since middle 1980's, with gas injection methods as the preferred recovery methods in the last decade (Surguchev et al., 2005). Despite all technological challenges, harsh reservoir conditions (carbonate complexity, high-pressure, high-temperature, high-salinity), strict regulations, and costly implementation that ordinary keep oil companies from using EOR techniques, it is expected that EOR will grow in the following years and perform extremely well in the world market. However, some challenges still remain in understanding the best EOR technique to be used for specific reservoir and what controlling parameters one should focus on for designing the best production/recovery scenario (Jabbar et al., 2013).

2.3 Multiphase flow concepts

Oil recovery in any displacement process depends on the volume of reservoir contacted by the injected fluid (Green and Willhite, 1998). This will depend on the reservoir quality and continuity, and the rate at which the displacement takes place. At higher rates, displacement will take place even more preferentially in the high permeability layers, and the macroscopic displacement efficiency will be reduced (Jahn et al., 2008). The term volumetric (macroscopic) sweep efficiency represents the fraction (or percent) of pore volume in porous media that is swept by the injected fluid. Volumetric sweep efficiency is expressed by (Sydansk and Romero-Zerón, 2011):

$$E_V = E_A E_l \qquad (2.1)$$

where

E_A areal sweep efficiency (the fraction of the pattern area swept by the displacing fluid)

E_l vertical sweep efficiency (the fraction of the pattern thickness swept by the displacing fluid)

Four factors generally control how much of a reservoir will be contacted by a displacement process: (1) the properties of the injected fluids, (2) the properties of the displaced fluids, (3) the properties and geological characteristics of the reservoir rock, and (4) the geometry of the injection and production well pattern (Green and Willhite, 1998).

Overall displacement efficiency in a process can be viewed conceptually as a product of the volumetric sweep, E_V, and the microscopic efficiency, E_D (Green and Willhite, 1998):

$$E = E_V E_D \qquad (2.2)$$

where

E overall hydrocarbon displacement efficiency

E_V macroscopic displacement efficiency

E_D microscopic hydrocarbon displacement efficiency

On a microscopic scale, even in parts of the reservoir which have been swept by water, some oil remains as residual oil. The surface tension at the oil-water interface is so high that as the water attempts to displace the oil out of the pore space through the small capillaries, the continuous phase of

oil breaks up, leaving small droplets of oil (snapped off, or capillary trapped oil) in the pore space (Jahn et al., 2008). Microscopic displacement efficiency, E_D, largely determines the success or failure of a EOR process. For crude oil, E_D is reflected in the magnitude of the residual oil saturation in places contacted by the displacing fluids. Capillary and viscous forces govern phase trapping and mobilization of fluids in porous media and thus microscopic displacement efficiency. An understanding and appreciation of the magnitude of these forces is required to understand the recovery mechanisms involved in EOR processes (Green and Willhite, 1998).

Another important force which determines flow behavior is the gravity force. The effect of the gravity force is to separate fluids according to their density. During displacement in the reservoir, both gravity forces and viscous forces play a major role in determining the shape of the displacement front (Jahn et al., 2008).

Figure 2.3 shows a number of situations in which oil is left in the reservoir, using a water drive reservoir as an example (Jahn et al., 2008).

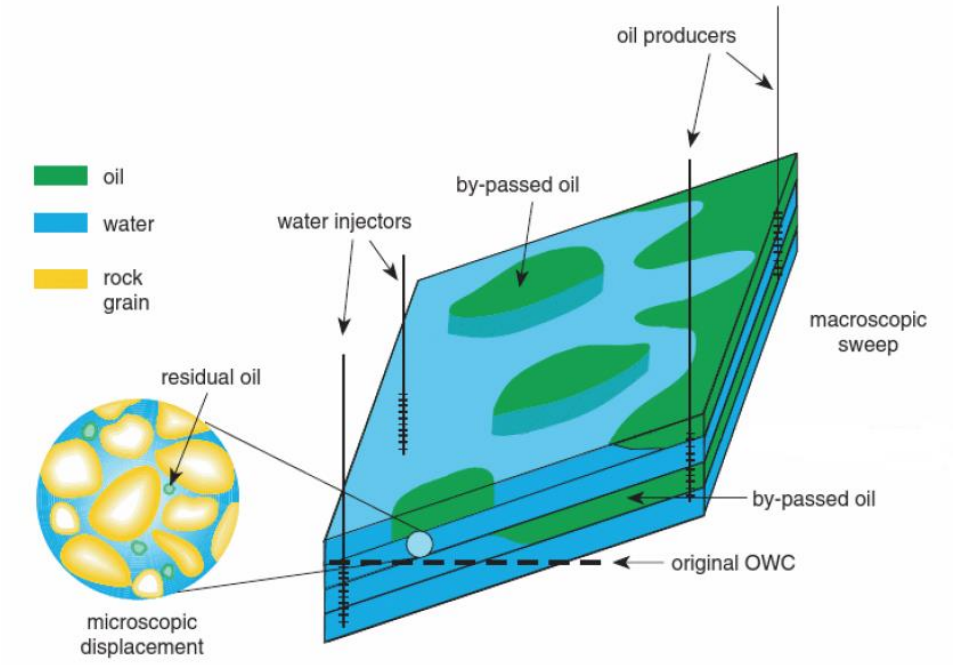

Figure 2.3 – Macroscopic and microscopic displacement (Jahn et al., 2008).

Several basic concepts are necessary to understand multiphase flow, namely they are interfacial tension, wettability, and contact angle. These concepts lead naturally to a discussion of capillary pressure, mobility, and fractional flow (Fanchi, 2005).

2.3.1 Interfacial tension

At the interface of two immiscible fluids, the forces acting on the molecules of each of these fluids are not the same as within each phase, and the system behaves as though the two phases were separated by a membrane (Cossé, 1993). Interfacial tension (IFT) means the tension between two

liquids at a liquid-liquid interface. Surface tension refers to the tension between two fluids at a gas-liquid interface (Fanchi, 2005). IFT can be interpreted as a measure of miscibility; the lower the IFT, the closer two phases approach miscibility. For example, at the critical point the properties of the liquid phase become indistinguishable from those of the vapor phase. Consequently, approaching the critical point makes the IFT to become zero (Willhite, 1986).

IFT is the energy per unit of surface area of the interface, or force per unit length. The units of IFT are typically expressed in milli-Newtons per meter or in the equivalent dynes per centimeter. The value of interfacial tension depends on the composition of the two fluids at the interface between two phases (Fanchi, 2005). There are different methods for measuring IFT, which include sessile drop, pendant drop, and spinning drop techniques (Willhite, 1986).

2.3.2 Capillary number and mobility ratio

The magnitude of the reduction residual oil saturation and mobilization of oil by an EOR process is controlled by two major factors: capillary number and mobility ratio (Ahmed and Meehan, 2011).

The residual oil saturation depends on the capillary and viscous forces present at the time of trapping. It is verified by the extensive experiments for water-wet porous media. It was proposed by different scientists that the residual oil saturation should be a function of a dimensionless group representing the ratio of viscous forces to capillary forces (Willhite, 1986). The capillary number is defined as the ratio between viscous force (depends on the viscosity of the displacing fluid and Darcy velocity) and interfacial tension force (Ahmed and Meehan, 2011):

$$N_c = \frac{Viscous\ force}{Interfacial\ tension\ force} = \frac{\upsilon\mu}{\sigma} \qquad (2.3)$$

where

υ Darcy velocity

μ viscosity of the displacing fluid

σ interfacial tension

The reduction of the interfacial tension between the displacing and displaced fluids is perhaps the only practical option in mobilizing residual oil by increasing capillary number (Ahmed and Meehan, 2011).

For any given oil reservoir, the sweep efficiency depends on the viscosity of the drive fluid. Within a reservoir with a given degree of permeability heterogeneity, as the viscosity of the displacing fluid decreases, the degree of the poor sweep efficiency increases. The mathematical term that relates the viscosity of the oil recovery drive fluid to conformance and sweep efficiency is the mobility ratio (Sydansk and Romero-Zerón, 2011). The mobility ratio by definition is the ratio between the displacing fluid mobility and the displaced fluid mobility (Ahmed and Meehan, 2011):

$$M = \frac{\lambda_{displacing}}{\lambda_{displaced}} = \frac{(k/\mu)_{dispacing}}{(k_0/\mu_0)_{dispaced}} \qquad (2.4)$$

where

k effective permeability

μ viscosity

The mobility ratio influences both the microscopic (pore-level) and macroscopic (areal and vertical sweep) displacement efficiencies. If the value of mobility ratio exceeds one, it is considered unfavorable because it indicates that the displacing fluid flows more readily than the displaced fluid (oil) (Ahmed and Meehan, 2011). Thus, a large viscosity contrast between the displacing fluid and the displaced fluid causes a large mobility ratio, which promotes the fingering of water through the more viscous oil (Figure 2.4) and reduces the oil recovery efficiency. As such mobility ratio can be improved by increasing the drive water viscosity using polymers (Romero-Zerón, 2012).

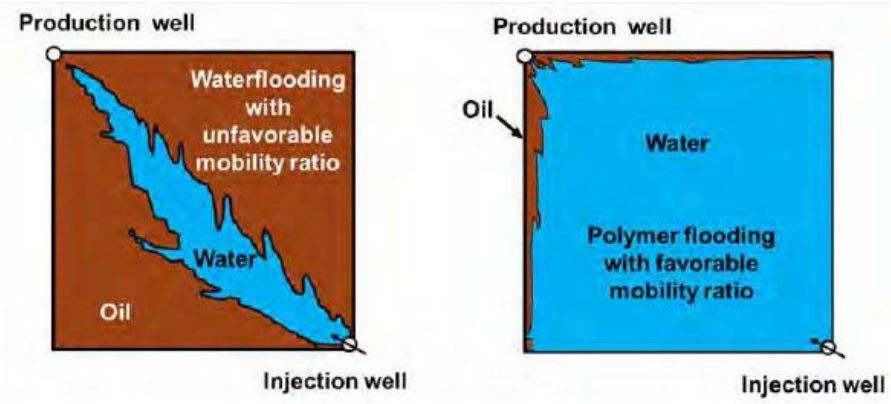

Figure 2.4 - Waterflooding with different mobility ratios (Romero-Zerón, 2012).

2.3.3 Wettability

Interaction between the fluid phases confined in the pore space and the surface of the reservoir rock pores influences fluid distribution inside rock as well as flow properties. When two immiscible phases are placed in contact with a solid surface, usually one of the phases is attracted to the surface more strongly than the other. This phase is called the wetting phase while the other phase is the non-wetting phase (Willhite, 1986).

Wettability is the ability of one fluid phase to wet a solid surface preferentially in the presence of another immiscible phase (Fanchi, 2005). Wettability is related to rock mineralogy as well as the properties of the fluid pairs (Willhite, 1986).

The parameter which influences the wetting, or wettability, condition in a rock/fluid system is the interfacial tension. Changing the type of rock or fluid can change IFT and, consequently, the wettability of the system. Adding some chemicals such as surfactant, polymer, corrosion inhibitor, or scale inhibitor can alter wettability (Fanchi, 2005). Defining the relative wetting behavior of fluids in a rock is complex matter because the spreading behavior itself varies at points, or areas, within the rock

and the measured wettability represents an average of the physical and chemical interactions of the fluids (Tiab and Donaldson, 2011).

The wettability influences the relative permeability, electric properties, nuclear magnetic resonance relaxation times, and saturation profiles in the reservoir. The wetting state can impact waterflooding and aquifer encroachment into a reservoir. Reservoir wettability preference can be determined by measuring the contact angle of crude oil and formation water on silica or calcite crystals or by measuring the characteristics of core plugs either in an Amott imbibitions test or in a United States Bureau of Mines (USBM) test (Gudmestad et al., 2010). These measuring techniques are subjects to some difficulties when applying them in carbonate reservoirs. From a practical point of view, the heterogeneous nature of carbonate reservoirs which originated from wide spectrum of environments in which carbonate are deposited, causes significant impact on wettability measurements, and hence on residual oil saturation, capillary pressure, electrical properties and last but of course not the least the oil recovery (Gomari, 2009).

As wettability of a reservoir is an important parameter affecting both the fluid distribution and the flow of different fluids in the rock, in order to improve oil recovery from the carbonate reservoir in most cases it is needed to alter the wetness of the reservoir towards more water-wet (Jabbar et al., 2013).

Austad et al., 2005 indicated that normally the wetting conditions of carbonates depend on the following parameters, which, of course, also depend on each other:

- pH of the equilibrium brine
- Temperature of the reservoir
- Crude oil properties, e.g. acid-/base number
- Composition of the equilibrium brine, e.g. potential determining ions (Ca^{2+}, CO_3^{2-})

Wettability is usually measured in the laboratory, and there are several factors that can affect such laboratory measurements. Wettability can be changed during making of the core by contact with drilling fluids or fluids on the rig floor, and by contact of the core during core handling with oxygen or water from the atmosphere. Laboratory fluids should also be at reservoir conditions for obtaining the most reliable measurements of wettability (Fanchi, 2005).

2.3.4 Contact angle

When the liquid-liquid interface is in intimate contact with solid surface, the interface intersects the solid surface at an angle θ, which is a function of the relative adhesive tension of the liquids to the solid (Tiab and Donaldson, 2011). Wettability thus can be explained quantitatively by examining the force balance between two immiscible fluids at the contact line between these two fluids (water and oil) and the solid surface, as shown in Figure 2.5 (Willhite, 1986).

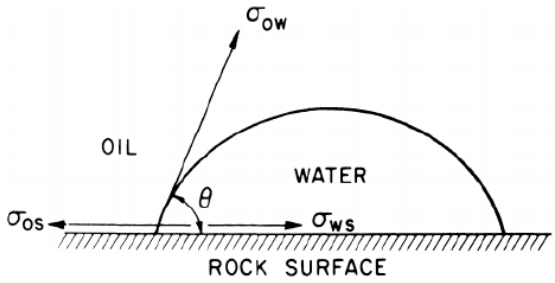

Figure 2.5 – Wettability of oil/water/solid system (Willhite, 1986).

The water phase spreads out over the surface in preference to the oil. There are forces at the contact line, namely σ_{os}, the IFT between the solid and the oil phase; σ_{ws} the IFT between the solid and the water phase; and σ_{ow}, the IFT between the oil and water phases. The contact angle, θ, is measured through the water phase to σ_{ow}, the tangent to the interface at the contact line. At equilibrium, the sum of the forces acting along the contact line must be equal zero (Willhite, 1986). It is not possible to measure the solid-fluid surface tensions directly (Tiab and Donaldson, 2011). Instead wettability is measured by contact angle. Contact angle is always measured through the denser phase and is related to interfacial energies by the following equation (Fanchi, 2005):

$$\sigma_{os} + \sigma_{ws} = \sigma_{ow} cos\theta$$

where

σ_{os} interfacial energy between oil and solid (dyne/cm)

σ_{ws} interfacial energy between water and solid (dyne/cm)

σ_{ow} interfacial energy, or IFT, between oil and water (dyne/cm)

θ contact angle at oil-water-solid interface measured through the water phase (degrees)

For a liquid spreading on a uniform nondeformable solid (idealized case), there is only one contact angle (the equilibrium value), but in case of the real surface (practical systems) a number of stable angles can be measured. From them two angles can be measured, which are relatively reproducible: largest, advancing angle θ_A and smallest, receding angle θ_R. Advancing angle is measured by advancing the periphery of the drop over the surface (e.g., by adding more liquid to the drop). Receding angle is measured by pulling the liquid back across the surface (e.g., by removing some liquid from the drop) (Tharwat, 2012). A modification of the sessile drop method can be used to measure advancing and receding contact angles. Two polished mineral plates are mounted horizontally with a small gap between them: one plate is fixed and the other can be moved smoothly. A drop of oil is placed between the plates and allowed to age until the contact angle no longer changes; then the mobile plate is moved, creating the advancing contact angle, as shown on Figure 2.6 (Tiab and Donaldson, 2011).

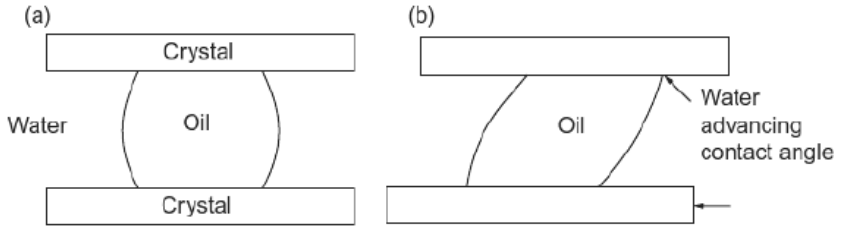

Figure 2.6 – Method for measuring advancing and receding contact angles (Tiab and Donaldson, 2011).

The difference between the advancing and receding contact angles is called "contact angle hysteresis". The reasons for this hysteresis lie in penetration of wetting liquid into pores and in the surface roughness (Tharwat, 2012).

Prior to the 1950s, oil reservoirs were thought to be all water-wet. Later it was discovered that oil reservoirs can have wide range of wettabilities, i.e., water-, intermediate-, and oil-wet. However, most oil reservoirs have a non-uniform wettability named mixed-wet (Meybodi et al., 2011).

Examples of water-wet and oil-wet systems are shown in Figure 2.7 (Willhite, 1986).

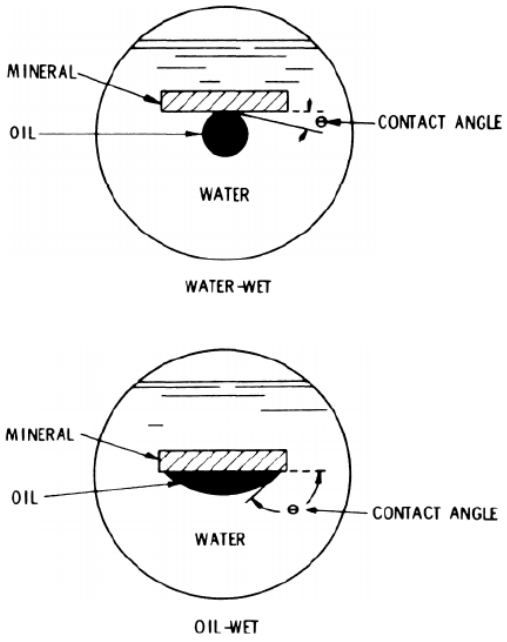

Figure 2.7 – Contact angles measured through the aqueous phase (Willhite, 1986).

Table 2.1 presents examples of contact angle for different wetting conditions (Fanchi, 2005). In the past the considerable amount of work has been directed towards explaining the mechanisms responsible for oil reservoirs being oil-wet, water-wet or mixed-wet. Factors that may influence the reservoir wettability to be altered from one state to another include oil composition, brine chemistry, rock surface characteristics, capillary pressure, and temperature. Among these factors, oil composition is known to be key factor, because it includes wettability-altering components such as polar components. The influence of the other factors is either to increase the effect of oil composition in

altering the wetting surface or to decrease this effect (Gomari, 2009). Based on laboratory tests, most known reservoirs have intermediate wettability and are preferentially water-wet (Fanchi, 2005).

Table 2.1 – Examples of contact angle (Fanchi, 2005).

Wetting condition	Contact angel (degrees)
Strongly water-wet	0-30
Moderately water-wet	30-75
Neutrally wet	75-105
Moderately oil-wet	105-150
Strongly oil-wet	150-180

2.3.5 Capillary pressure

The concept of capillary pressure as a characteristic of a porous rock media evolved from the observation of capillary phenomena in capillary tubes. An oil/water interface or an air/water interface in a tube with a large diameter is flat because the wetting forces at the walls of such tube are distributed over a large perimeter and do not penetrate into the interior to any extent. Hence, the pressures of the fluids at the interface between them are equal (Willhite, 1986). Let us consider a cylindrical capillary tube, immersed in a receptacle containing water. The water rises in the tube to some height above the interface in the container. It is also found that the water/air interface is spherical, with the center of curvature in the air. This simple fact implies that, in the neighborhood of the interface, the pressure of the air is higher than that of the water (which is the wetting fluid since it tends to spread) (Cossé, 1993). Pores in reservoir rocks are analogous to capillary tubes in that the diameters are too small. When diameters are small enough, surface forces (induced by preferential wetting of the solid by one of the fluids) extend over the entire interface, creating significant pressure differences between the two fluid phases across the interface (Willhite, 1986).

The pressure difference across the curved interface formed by two immiscible fluids in a small capillary tube is called capillary pressure, and it is equal to the difference between pressure in nonwetting phase and pressure in wetting phase (Fanchi, 2005). As an example, let’s consider the oil/water interface in the horizontal glass capillary tube with a small diameter, it is in static equilibrium and shown in Figure 2.8. Water strongly wets the glass surface with a contact angle approaching zero. If sensitive pressure gauges were attached to each end of the capillary tube to measure the water-phase pressure and the oil-phase pressure, they would show that the oil-phase pressure is always larger than the water-phase pressure, regardless of the length of the tube. Oil will be displaced spontaneously from the tube if the pressure of the oil phase is reduced, even though the

pressure in the water phase is less than the pressure in the oil phase. Water can be displaced from the capillary tube by injecting oil into the tube (Willhite, 1986).

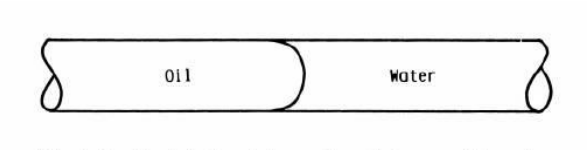

Figure 2.8 – The interface between the oil phase and the water phase in a horizontal water-wet capillary tube (Willhite, 1986).

Expressing capillary pressure for porous media in terms of force up per unit area gives the following expression (Fanchi, 2005):

$$P_c = \frac{2\sigma cos\theta}{r} \qquad (2.5)$$

where

r pore radius (cm)

σ interfacial (or surface) tension (mN/m or dynes/cm)

θ contact angle (degrees)

Equation above shows that increasing of the pore radius will cause a reduction in capillary pressure while decreasing of IFT will also cause a decrease in capillary pressure (Fanchi, 2005).

Oil is the nonwetting phase in a water-wet oil-water reservoir. Capillary pressure for an oil-water system is (Fanchi, 2005):

$$P_{cow} = P_o + P_w \qquad (2.6)$$

where

P_o pressure in the oil phase (psia)

P_w pressure in the water phase (psia)

Capillary pressure increases when the wetting fluid is drained out and decreases when the wetting fluid is imbibed. When the pressure difference is equal zero, no fluid movement is occurring (Figure 2.9). Injection of a wetting fluid will enhance its pressure and therefore enhance recovery due to further imbibitions. Following lines you can see on Figure 2.9: (1) Primary drainage where the wetting fluid (water) is forced out of the rock by the non-wetting fluid (oil); (2) spontaneous imbibition curve of the wetting fluid (water) as the wetting fluid naturally enters the rock; (3) forced imbibition of the wetting fluid (water) as the wetting fluid is injected under pressure into the rock; (4) spontaneous secondary drainage of the non-wetting fluid (oil) as the non-wetting fluid enters the rock; (5) forced secondary drainage as the non-wetting phase (oil) is injected under pressure into the rock (Gudmestad et al., 2010).

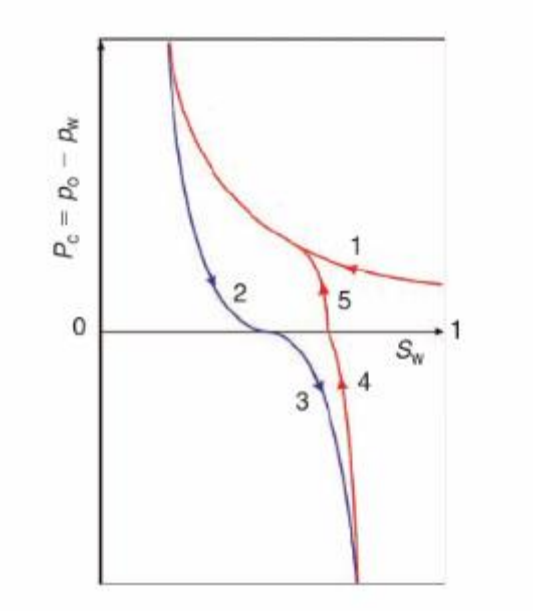

Figure 2.9 - Capillary pressure as a function of water saturation (Gudmestad et al., 2010).

2.3.6 Darcy's law

On a microscopic scale, the most important equation governing fluid flow in the reservoir is Darcy's law. For a single fluid flowing through a section of reservoir rock, Darcy showed that the superficial velocity of the fluid is proportional to the pressure drop, and inversely proportional to the viscosity of the fluid (Jahn et al., 2008).

For a horizontal linear system, this relationship is (Ahmed and Meehan, 2011):

$$\upsilon = \frac{q}{A} = -\frac{k}{\mu}\frac{dp}{dx} \qquad (2.7)$$

where

υ apparent velocity (cm/s)

q volumetric flowrate (cm^3/s)

A total cross-sectional area of the rock (cm^2)

In other words, A includes the area of the rock material as well as the area of the pore channels. The fluid viscosity is expressed in centipoise units, and the pressure gradient dp/dx is in atmospheres per centimeter, taken in the same direction as υ and q (Ahmed and Meehan, 2011). k is called the permeability coefficient, and is independent of the fluid considered as a first approximation. It is the absolute or specific permeability of the sample in the direction considered. Permeability is expressed like an area, in Darcy units (Cossé, 1993). It is dependent on the pore size distribution (Jahn et al., 2008). The negative sign is added because the pressure gradient dp/dx is negative in the direction of flow as shown on Figure 2.10 (Ahmed and Meehan, 2011).

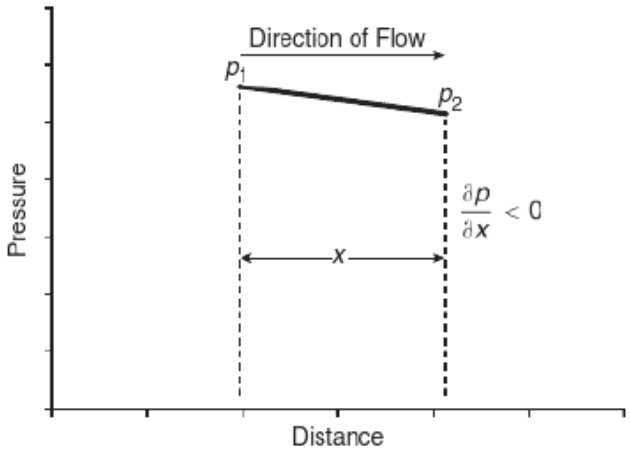

Figure 2.10 – Pressure vs. distance in a linear flow (Ahmed and Meehan, 2011).

In a radial flow system, all fluids move toward the producing well from all directions. However, before flow can take place, a pressure differential must exist. Thus, if a well is to produce oil, which implies a flow of fluids through the formation to the wellbore, the pressure in the formation at the wellbore must he less than the pressure in the formation at some distance from the well. The pressure in the formation at the wellbore of a producing well is known as the bottom-hole flowing pressure (flowing BHP, p_{wf}) (Ahmed and Meehan, 2011).

Figure 2.11 schematically illustrates the radial flow of an incompressible fluid toward a vertical well.

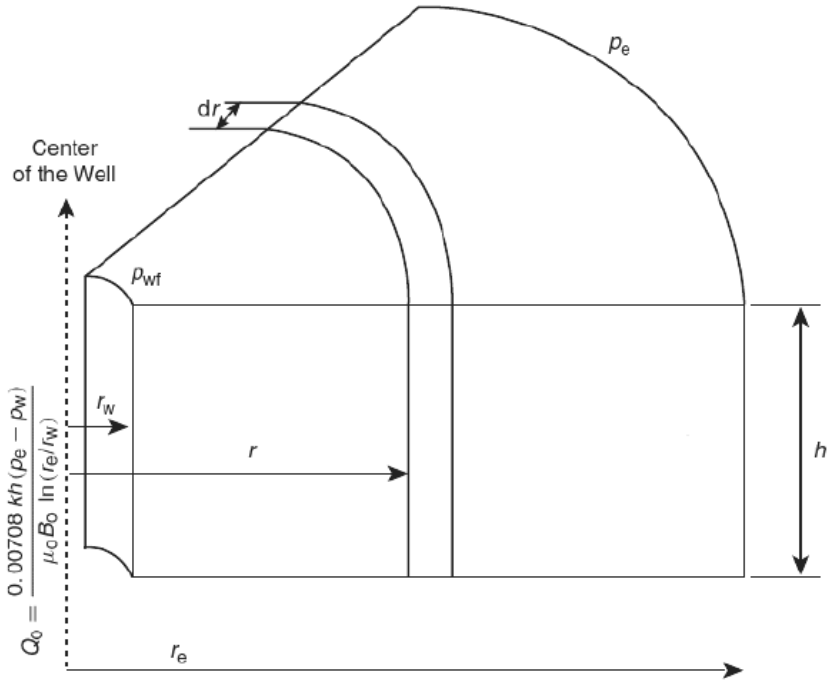

Figure 2.11 – Radial flow model (Ahmed and Meehan, 2011).

Because the fluid is incompressible, the flow rate q must be constant at all radii. Due to the steady-state flowing condition, the pressure profile around the wellbore is maintained constant with

time. Let p_c denote the external pressure at the drainage radius. Then Darcy's equation can be used to determine the flow rate at any radius r (Ahmed and Meehan, 2011):

$$v = \frac{q}{A_r} = 0{,}001127 \frac{k}{\mu} \frac{dp}{dr} \qquad (2.8)$$

where

v apparent fluid velocity (bbl/day ft^2)

q flow rate at radius r (bbl/day)

k permeability (mD)

μ viscosity (cp)

A_r cross-sectional area at radius r (ft^2)

Conversion factor here is equal 0,001127 and used to express the equation in field units. The minus sign is no longer required for the radial system because the radius increases in the same direction with the pressure. This means that as the radius increases by going away from the wellbore the pressure also increases (Ahmed and Meehan, 2011).

The above equations are valid for a single fluid only. In hydrocarbon reservoirs there is always connate water present, and commonly two fluids are competing for the same pore space (Jahn et al., 2008). The presence of different phases means that, since each fluid occupies only part of the pores, each flow rate can no longer be calculated just from the absolute permeability of the rock, because the fluids are "mutually hindered". Their flow is accordingly slower, especially that of the oil (Cossé, 1993). The permeability of one of the fluids is then described by its relative permeability, which is a function of the saturation of the fluid, as shown in Figure 2.12 (Jahn et al., 2008).

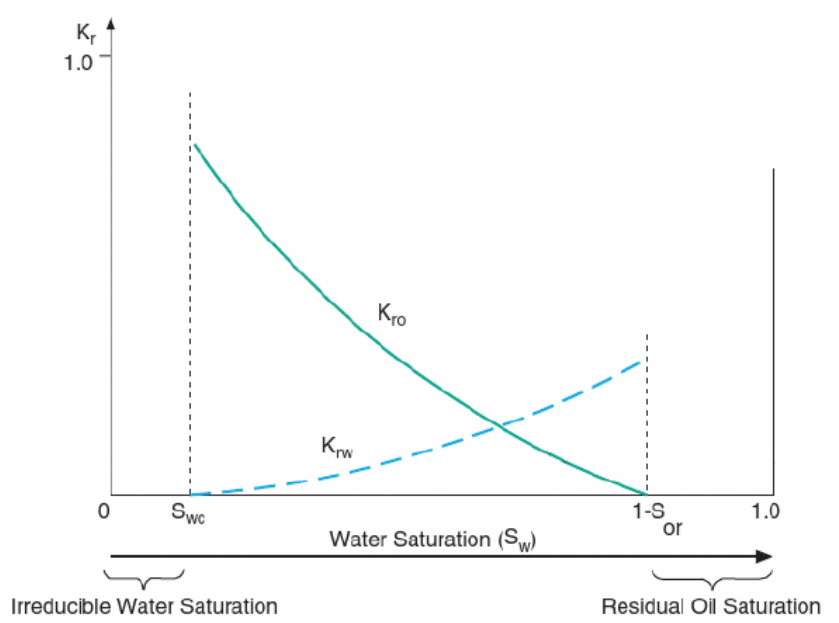

Figure 2.12 – Relative permeability curves for oil and water (Jahn et al., 2008).

For situations with several phases the concept of the effective permeability of each phase and the associated physical properties must be used in Darcy's equation. For a radial system, the generalized form of Darcy's equation can be expressed for oil, water and gas as follows (Ahmed and Meehan, 2011):

$$q_o = 0{,}001127\left(\frac{2\pi rh}{\mu_o}\right)k_o\frac{dp}{dr} \qquad (2.9)$$

$$q_w = 0{,}001127\left(\frac{2\pi rh}{\mu_w}\right)k_w\frac{dp}{dr} \qquad (2.10)$$

$$q_g = 0{,}001127\left(\frac{2\pi rh}{\mu_g}\right)k_g\frac{dp}{dr} \qquad (2.11)$$

where

k	absolute permeability (md)
k_o, k_w, k_g	effective permeability for oil, water, and gas (md)
μ_o, μ_w, μ_g	viscosity of oil, water, and gas (cp)
q_o, q_w, q_g	flow rates for oil, water, and gas (bbl/day)

The effective permeability can be expressed in terms of the relative and absolute permeability as (Ahmed and Meehan, 2011):

$$k_o = k_{ro}k \qquad (2.12)$$

$$k_w = k_{rw}k \qquad (2.13)$$

$$k_g = k_{rg}k \qquad (2.14)$$

where

k	absolute permeability (md)
k_{ro}, k_{rw}, k_{rg}	relative permeability for oil, water, and gas

2.4 Surface charge

To understand such complex problem as smart waterflooding in chalk it is first necessary to describe the surface chemistry of calcite and the mechanisms leading to dissolution of calcite mineral and wettability changing of its surface. This processes lead naturally to discussing of such terms as surface charge, double layer and zeta potential.

2.4.1 The origin of surface charge

Natural particles develop surface charge from isomorphic substitutions and structural disorder (including defects) in minerals, and from adsorption reactions with ionic species in aqueous solution (Sposito, 2004). The surface charge may be modified by altering the environment (electrolyte), for example by changing the pH or adding an ionic surfactant (Cosgrove, 2010). There are several mechanisms, by which an interface may acquire a charge, but it is important to know and there can be

more than one mechanism operating in our practical systems (Goodwin, 2009). Generally, there are four mechanisms by which a surface immersed in a liquid can gain a charge: ionization of surface groups, dissolution of ionic solids, ion adsorption, isomorphous substitution. These mechanisms are summarized on Figure 2.13 (Cosgrove, 2010).

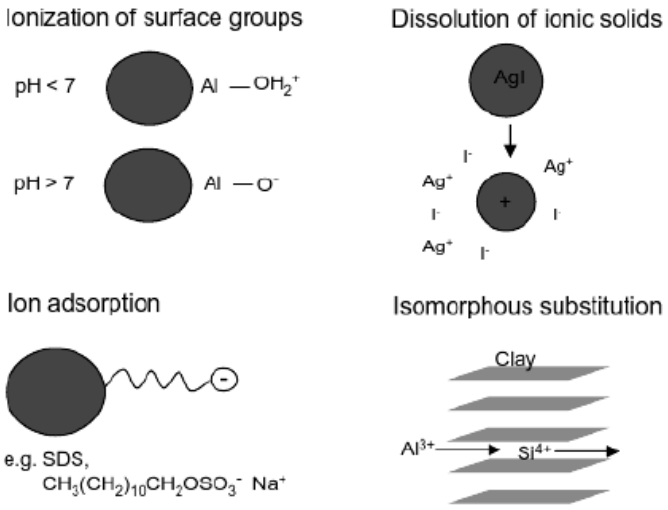

Figure 2.13 – The methods of charging a solid surface immersed in electrolyte (Cosgrove, 2010).

2.4.1.1 Ionization of surface groups

Particles that possess suitable chemical functionality may attain charge as a result of the ionization of their surface groups. In aqueous solutions pH is commonly used to control the degree and nature of such ionization. For example, metal oxides can gain charge as a result of the protonation or deprotonation of surface groups (Cosgrove, 2010). This is possible, because the surfaces of uncoated oxide particles have surface hydroxyl groups. At high pH, these can ionize to give $–O^-$ and at low pH the lone pair on the oxygen can hold a proton to give $—OH_2^+$ (Goodwin, 2009). For example, pH of the isoelectric point of titanium oxide is 5.8, i.e. at a pH of 5.8 the ζ potential of titania will be equal zero. At a pH less than 5.8 the titania has positive charge (Cosgrove, 2010). The process for titania can be summarized by the following equation (Goodwin, 2009):

$$\text{surface } TiOH_2^+ + H_2O \xleftarrow{H_3O^+} \text{surface } TiOH \xrightarrow{OH^-} \text{surface } TiO^- + H_2O \qquad (2.15)$$

2.4.1.2 Ion adsorption

If the bulk material cannot be ionized, ionic surfactants may be added to generate charge-stabilized suspensions. For example, particles of carbon black on which anionic surfactants are adsorbed may be suspended in water, and this is the basis of inks (Cosgrove, 2010). Another example is proteins adsorbing on hydrophobic surfaces and providing a hydrophilic charged outer layer, as it happens with fat droplets in milk, which are stabilized by casein. The charge here is negative as it results from the carboxyl groups on the protein (Goodwin, 2009).

2.4.1.3 Dissolution of ionic solids

When the colloidal particles are made up of sparingly soluble salts, dissolution occurs until the concentration of the ionic components in solution corresponds to the solubility product of the compounds (Goodwin, 2009). Silver halides are poorly soluble salts. If the dissolution of Ag^+ and I^- ions is unequal then at equilibrium the sol will contain charged silver iodide particles. Thus, in the presence of excess iodide ions the salt particles will have negative surface charge and with excess silver ions positive surface charge will be obtained (Cosgrove, 2010).

2.4.1.4 Isomorphous substitution

The replacement of one atom by another atom of similar size in a crystal lattice is called isomorphous substitution (Cosgrove, 2010). This is a common occurrence in clay minerals. The basic structure of a clay particle is an aluminosilicate layer lattice. As the clay is formed, it crystallizes with a layer of silicon atoms tetrahedrally coordinated to oxygen atoms (SiO_2 layer). The next layer of the lattice is aluminum with octahedrally coordinated oxygens (Al_2O_3 layer), some of which are shared with the tetrahedral silica layer (Goodwin, 2009). The tetrahedral–octahedral bilayers are bound together by a combination of van der Waals forces and hydrogen bonding (Cosgrove, 2010). This layer structure is repeated throughout the crystal. During the crystallization process, an occasional silicon atom (Si^{4+}) can be substituted by an aluminum atom (Al^{3+}) and more frequently an aluminum atom in by a magnesium atom (Mg^{2+}). A small amount of such substitution does not produce too much distortion of the lattice to stop it growing and it retains the same structure – hence the term isomorphism substitution (Goodwin, 2009).

2.4.2 Potential determining ions

When discussing the influence of ions with relation to surface chemistry, it is important to differentiate potential-determining ions from inert ions. Potential-determining ions are those ions which by virtue of their electron distribution between the solid and liquid phase determine the difference in potential between these phases. In the case of silver iodide sols, that was mentioned above, the potential changes with addition of silver or iodide ions. Therefore, for this system Ag^+ and I^- ions are potential-determining ions. With respect to metal oxides, protons are potential-determining ions and thus a change in pH will result in a change in the surface charge (Cosgrove, 2010).

For calcite Somasundaran and Agar (1967) and Lebell and Lindström (1982) have shown that at low pH the calcite surface becomes positively charged because of calcium ions, whereas at higher pH the higher concentration of CO_3^{2-} ions turns the calcite surface to be negatively charged. Thompson and Pownall (1989), Pierre et al. (1990), Schramm et al. (1991), and Besra et al. (2000)

suggested that dissolved Ca^{2+} and CO_3^{2-} ions are potential-determining ions for calcite (Gomari and Hamouda, 2006).

2.4.3 Electrochemical double layer

At any interface there is always an unequal distribution of electrical charges between the two phases. This unequal distribution causes one side of the interface to acquire a net charge of a particular sign and the other side to acquire a net charge of the opposite sign, giving rise to a potential drop across the interface and the so-called electrical double layer (Rosen, 2004). For example, if a positively charged surface is placed in an electrolyte containing inert ions then simple electrostatics indicates that cations will be repelled from and anions will be attracted to the interface. Electroneutrality will be attained when the electrolyte layer near the interface possesses a net negative charge of equal magnitude with the solid material surface charge. Potential drop depends on the concentration and nature of the ionic species (Cosgrove, 2010).

2.4.3.1 The Stern-Gouy-Chapman (SGC) model of the double layer

The Stern-Gouy-Chapman model divides the solution side of the double layer into two parts: a layer of strongly held counterions, adsorbed close to the charged surface on fixed sites, and a diffuse layer of counterions. According to this model, the electrical potential drops rapidly in the fixed portion (Stern layer) of the double layer and more gradually in the diffuse portion. Distribution of counterions and the potential drop is depicted in Figure 2.14 (Rosen, 2004).

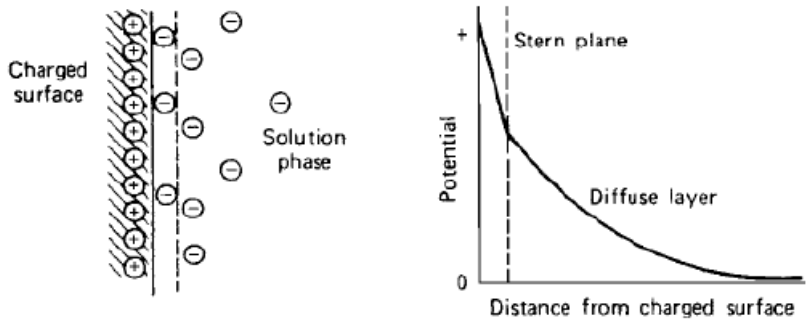

Figure 2.14 - Stern-Gouy-Chapman model of the electric double layer (Rosen, 2004).

The more complex model, including ions of both sign is shown in Figure 2.15. The model considers the solvent as a dielectric continuum and the ions as non-interacting point charges. In the absence of ions in direct contact with the surface, the surface charge of the solid material is counterbalanced by ions located across two distinctive regions, the Helmholtz and diffuse layers. The contribution of each of these two layers lo the total interfacial charge density depends on the concentration of the ions in solution and also on the relative permittivity of the solvent (Cosgrove, 2010).

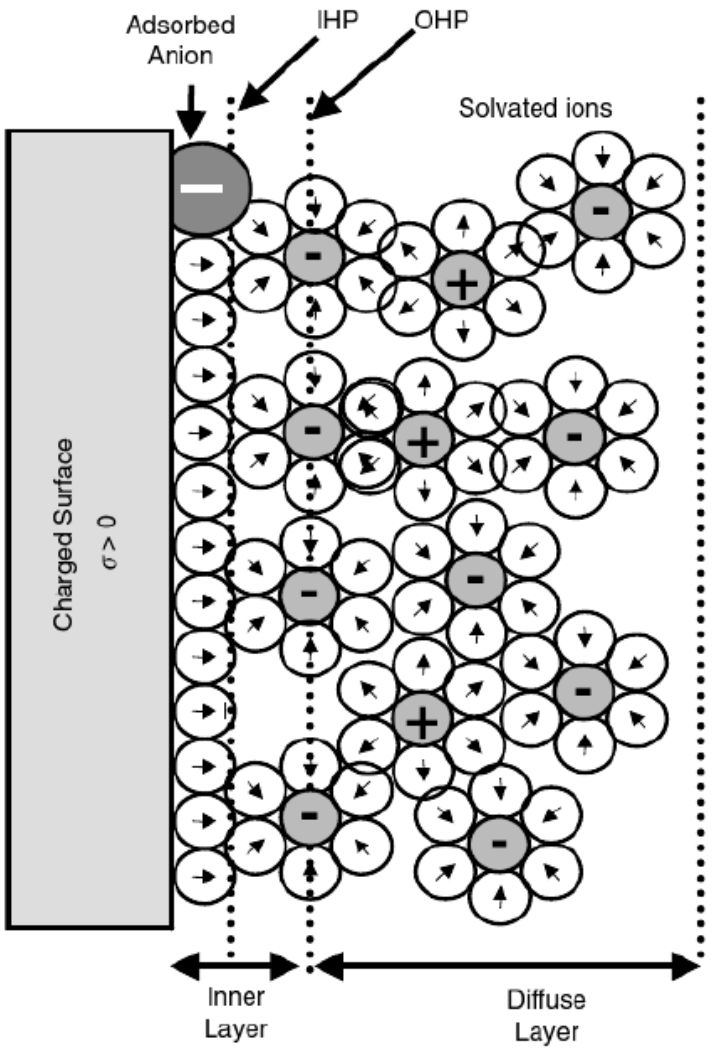

Figure 2.15 – Schematic representation of the double layer structure and the solid/electrolyte interface according to the SGC model (Cosgrove, 2010).

The Helmholtz layer (Stern layer) contains two planes, called the inner (IHP) and outer Helmholtz planes (OHP). The first one represents the plane in which specifically adsorbed species are located as well as solvent molecules in direct contact with the surface. Specifically adsorbed species are those molecules which possess a solvation layer that is affected by the interaction with the surface of the solid material. The OHP defines the plane of closest approach of the fully solvated ions (non-specifically adsorbed ions) (Cosgrove, 2010). There is a thermodynamic justification for differentiating between the surface charge ions (IHP) and the ions solvated in the Stern layer (OHP), but a more comprehensive reason is kinetic (ability to move). The surface charge ions are assumed to be fixed to the surface (immobile); they cannot move in response to external disturbances. In contrast, the OHP ions retain some degree of freedom, almost as high as ions of the diffuse layer (Dukhin and Goetz, 2002).

Beyond the OHP, the surface charge is counterbalanced by a dynamic ionic atmosphere called the diffuse or Gouy-Chapman layer (Cosgrove, 2010).

A term often associated with the electrical double layer, and one that is often misused, is the zeta potential. It is the potential of the charged surface at the plane of shear between the particle and the surrounding solution. Zeta potential is conveniently measured, and it is very tempting to place this plane of shear at the solution side of the Stern layer, since this is the boundary of the fixed ion layer and would give us an experimentally calculable value for the potential at that boundary. Unfortunately, the plane of shear is not necessarily at the solution edge of the Stern layer and is at some undetermined point somewhere farther out in the diffuse layer. The zeta potential is consequently smaller in magnitude than the Stern potential, but, unfortunately, exactly how much smaller is not known definitely (Rosen, 2004).

An example of overall interfacial potential drop including both the Helmholtz and the diffuse layers for various electrolyte concentrations is illustrated in Figure 2.16 (Cosgrove, 2010).

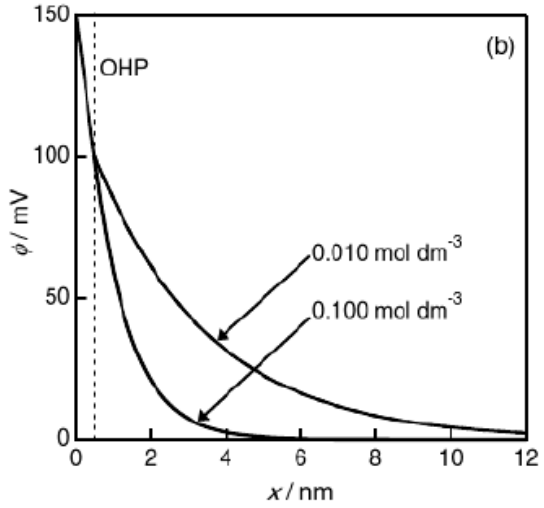

Figure 2.16 – Electrostatic potential distribution across the overall interfacial region for various electrolyte concentrations (Cosgrove, 2010).

2.5 Smart waterflooding in carbonates

Waterflooding was first practiced for pressure maintenance after primary depletion and has since become the most widely adopted IOR technique (Morrow and Buckley, 2011). Some of the reasons for the general acceptance of waterflooding are as follows: water is an efficient agent for displacing oil of light to medium gravity, water is relatively easy to inject into oil-bearing formations, water is generally available and inexpensive, and waterflooding involves relatively lower capital investment and operating costs that leads to favorable economics (Romero-Zerón, 2012).

Traditionally, a little attention has been given in reservoir engineering practice to the role of chemistry of injection water on displacement efficiency or its impact on oil recovery (Zahid, 2012). However, in recent years the impact of brine salinity and its ionic composition on oil recovery on chalk formations and to less extent in carbonate reservoirs have been investigated extensively due to the potential of extra oil recovery (Jabbar et al., 2013). The mechanisms associated to this processes

are still unclear, however, the favorable oil recovery in carbonates is attributed to wettability alteration and to interfacial tension reductions between the low salinity injected water and the oil. This waterflooding process requires more research in order to clearly establish the mechanisms involved and an understanding of the application boundaries based on the type of reservoir formation to avoid adverse effects on reservoir permeability caused by the injection of water that could negatively interact with the formation water and the formation rock (Romero-Zerón, 2012).

In this chapter the surface chemistry of calcite is discussed, its wettability alteration and also the proposed mechanisms behind smart waterflooding and low-salinity waterflooding in carbonate reservoirs.

2.5.1 The surface chemistry of calcite

The surface chemistry of calcium carbonate represents a rather complex case. It is generally accepted that calcite exhibits a basic character in nonaqueous systems, while a surface charge exists in aqueous media, caused by the dissolution of ions from the $CaCO_3$ surface (Plank and Bassioni, 2007).

Calcite dissolution results in enrichment of the water with calcium ions and carbonate alkalinity. Alkalinity of water-calcite system is described by the following equation (Lehmann et al., 2013):

$$\text{Alkalinity} = 2[CO_3^{2-}] + [HCO_3^-] + [OH^-] - [H^+] \qquad (2.16)$$

Dissolution of calcite in water can be expressed by the following equation (Hansen et al., 2000):

$$CaCO_3 + H_2O \rightarrow Ca^{2+} + HCO_3^- + OH^- \qquad (2.17)$$

Carbonate ions CO_3^{2-} are the most basic species of the carbonate weak-acid system, whose equilibrium reactions are shown in following two equations (Lehmann et al., 2013):

$$H_2CO_3 \leftrightarrow HCO_3^- + H^+ \qquad K_{C1} = 10^{-6,35} \qquad (2.18)$$

$$HCO_3^- \leftrightarrow CO_3^{2-} + H^+ \qquad K_{C2} = 10^{-10,33} \qquad (2.19)$$

where

K_{C1}, K_{C2} thermodynamic equilibrium constants for different carbonate species

So the actual carbonate species distribution is mainly a function of pH. For example, at pH values below 6.35 at least 50% of the sum of carbonate system species appears in the form of H_2CO_3 (Lehmann et al., 2013). pH values lower than 9, Ca^{2+}, HCO_3^- and OH^- ions were found in the aqueous phase. At pH above 9, CO_3^{2-} appears in addition to these ions and reaches the highest concentration of all ions present (Plank and Bassioni, 2007).

At low pH, the calcite surface becomes positively charged because of calcium ions, whereas at higher pH the higher concentration of CO_3^{2-} turns the calcite surface to be negatively charged (Gomari

and Hamouda, 2006). Thus, the partial dissolution of calcium carbonate has influence on its surface charge, its colloidal properties and its interaction with other substrates. The results of numerous investigations on the adsorption of small organic anions such as salicylate and of succinic, phthalic and maleic acid on $CaCO_3$ have been published, and for these species surface complexation occurs between the carboxylate groups of these molecules and hydrated calcium atoms located on the $CaCO_3$ surface exposed to the liquid phase (Plank and Bassioni, 2007).

High ionic strength of the brine leads to increased dissolution of calcite. Water temperature also affects the solubility of calcite. The dissolution reaction is exothermic, i.e. an increase in the solution temperature results in decreased calcite solubility (Lehmann et al., 2013).

2.5.2 Wettability alteration of calcite

Acidic components in crude oil influence the mineral wettability through their effect on electrostatic interactions with the mineral surfaces (Fathi et al., 2010). The presence of asphaltene and natural polar components (acids and bases) soluble in the crude oil and their interaction at solid surface alters solid surface wettability to more oil-wet and enhances retention of crude oil in reservoir rock pores (Tabrizy et al., 2011). In order to obtain a hydrophobic surface of calcite in the modification method, monocarboxylic acids with aliphatic hydrocarbon chain (also known as fatty acids and their salts) are most frequently used as the surfactants. By adsorption of such surfactants on calcite, its hydrophilic surface becomes hydrophobic (Mihajlović et al., 2013). The analysis of crude oil samples from Norwegian continental shelf showed that carboxylic acids with carbon number ranging from 16 to 20 are the most abundant acids in the crude oil. Thus they can play a critical role in oil recovery by water flooding (Tabrizy et al., 2011).

2.5.2.1 The model for wettability changing of calcite surface to oil-wet

According to previous studies the oil-water interface, negatively charged (due to the presence of carboxylic acids), interacted with the positive (due to pH<9) water-rock interface. The water film became unstable and the carboxylic group adsorbed on the calcium carbonate surface altering it to oil-wet (Martavaltzi et al., 2012). In the following example of calcite wettability alteration stearic acid is chosen as an adsorbent.

The bond between the calcium and the carbonate group in $CaCO_3$ molecule is not as strong as the internal bond of CO_3, that's why in presence of hydrogen ions calcite breaks down (Ahr, 2008). Dissolution of calcite in water can be expressed by the following equation (Hansen et al., 2000):

$$CaCO_3 + H_2O \rightarrow Ca^{2+} + HCO_3^- + OH^- \qquad (2.20)$$

As indicated by the above equation, the result of the dissolution is a localized increase of the solution alkalinity (Hansen et al., 2000). In this reaction Ca^{2+} ions are formed as the primary center for adsorption (Mihajlović et al., 2013).

Ionization of stearic acid is taking place in the n-decane–water interface (Hansen et al., 2000):

$$RCOOH \rightarrow RCOO^{-} + H^{+} \qquad (2.21)$$

Following the increase of the pH, ionization of the stearic acid occurs hence the tendency of the anionic group [$CH_3(CH_2)_{16}COO^{-}$] to dissolve in the water increases. These stearic ions reach the calcite surface where a chemisorption reaction occurs at the surface of the calcite and the calcium stearate is formed. These interactions convert the calcite surface to a strong oil-wet (Hansen et al., 2000). The chemical adsorption provides the strongest bond between the adsorbates and adsorbents (Mihajlović et al., 2013). The stability of water film and the presence of dissociated acids and Ca^{2+} and CO_3^{2-} ions at interfaces govern the adsorption of acid species on the calcite surface, and therefore wettability alteration (Gomari, 2009).

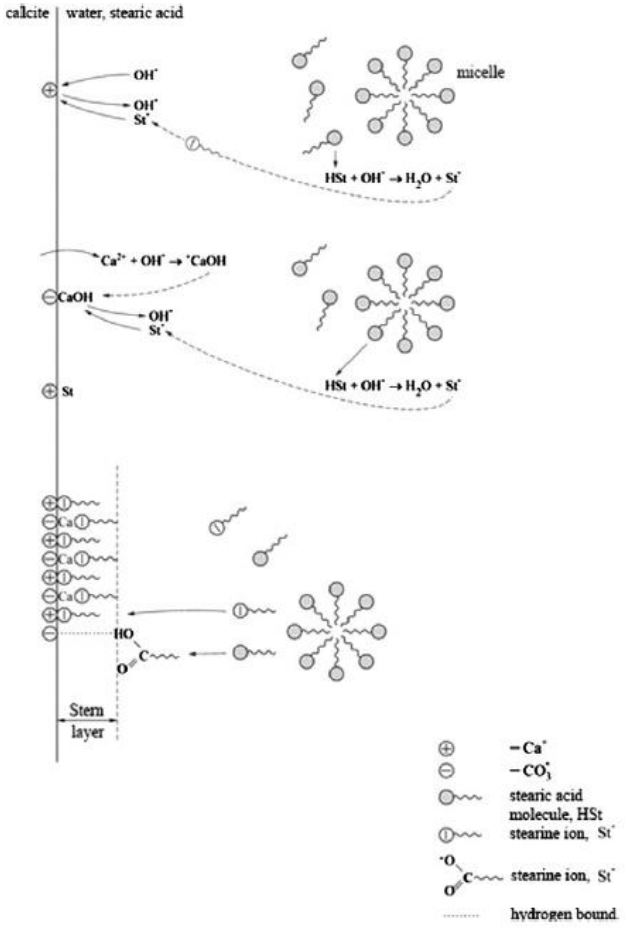

Figure 2.17 - The assumed mechanism of interaction in the system calcite/water, stearic acid and structure of the Stern layer (Mihajlović et al., 2013).

Figure 2.17 shows the boundary between calcite surface and aqueous media. Due to the solubility of calcite in water, Ca^{2+} ions exist in the solution and a calcium hydroxide CaOH is formed in very basic media that is chemisorbed on the primary surface center of the carbonate ion CO_3^{2-}. Also adsorption of OH^{-} ions may occur on the primary center Ca^{2+} due to very basic media. Subsequently, secondary surface centers are formed that can participate in the interaction of ions with stearic ions,

formed by stearic acid dissociation. Stearic ions can be chemisorbed either on the primary centers with Ca^{2+} ions or participate in the ion exchange reaction with OH^- ions from the secondary surface centers (Mihajlović et al., 2013).

In many cases, however, the adsorption is of a mixed nature (i.e. partly chemical and partly physical). It is created by formation of multilayers. The first layer is built on the basis of strong chemical forces, with the following layers physically adsorbed over the chemisorbed layer (Mihajlović et al., 2013). Gomari and colleagues performed several experiments with adsorption of stearic acid on calcite surface. In all pH values between 3 and 10, during the contact angle measurements, calcium stearate deposition occurred during interaction of calcite with stearic acid. At high pH values, a thicker layer is observed. At low pH a thinner layer appears, however, it is harder to remove. This may be due to the ability of the protons to penetrate into the calcite lattice, which promotes the formation of surface attached Ca^{2+} where chemisorption of stearic acid onto the surface takes place (Gomari and Hamouda, 2006).

Stipp (1999) suggested a model for the calcite surface in contact with aqueous solution: at the calcite surface a chemi-bonded layer of H^+ and OH^- groups are formed to satisfy local charge imbalance from the bulk dangling bonds of Ca^{2+} and CO_3^{2-}. This hydrolysis layer located at $x = 0$ in the Stern adsorption model, while the potential-determining ions (Ca^{2+} and CO_3^{2-}) are at $x = \delta$ where the potential at Stern layer ψ_δ represent ζ potential. As discussed above, calcium stearate formed on the surface, where at low pH the deposited layer is much firmer and harder to remove, whereas at high pH the deposited layer can be easily removed. These observations may support the above mechanism based on the modified electrical double layer model (Stipp, 1999). At low pH stearic ions are adsorbed to surface Ca^{2+} ($x = 0$) and they are hard to remove. At high pH, the dissociation of the stearic acid increases, where the carboxylate ions become more stable and may react with the available Ca^{2+} present in Stern layer ($x = \delta$), hence they become less adhered to the calcite terminal surface (Gomari and Hamouda, 2006).

2.5.2.1 The influence calcite-water-oil system parameters on adsorption

For small organic anions on a given positive surface, the adsorbed amount and the ratio between adsorbed and dissolved substrate (adsorption equilibrium) in general case depends on the type and number of the functional groups responsible for adsorption and the stereochemistry of the substrate molecule. The adsorption of salts of carboxylic acids on calcite surface is strongly influenced by the number of carboxylate functions in the molecule. High numbers of carboxylate groups in each molecule require smaller molar amounts of the organic anions to achieve charge compensation on the $CaCO_3$ surface, as shown by zeta potential measurements (Plank and Bassioni, 2007).

Even though the strength of the bonding of carboxylic material onto the calcite surface is mostly dictated by the carboxylic group, the organic structure of the carboxylic material will also influence the wettability alteration process (Fathi et al., 2010). Hamouda and colleagues performed a

study on wettability alteration of calcite with four fatty acids with long and short chains, two naphthenic acids with one and two saturated rings, quinoline and 5-indanol. The selected types of substances were based on their abundance in oils from North Sea reservoirs. Advancing and receding contact angle measurements have shown that oil soluble fatty acids play an important role in the wettability alteration of the calcite surfaces, with wettability end result greatly influenced by the structure of the fatty acids. Long chain fatty acid (stearic acid), in presence of water film, alters the calcite wettability to strongly oil-wet at low pH, where reaction between stearic acid and Ca^{2+} ions occurs (Gomari and Hamouda, 2006). The study of wettability using vapor adsorption isotherm show that, the number of adsorbed water layers decreases after modification for calcite, whereas the n-decane vapor adsorption shows an increase in the number of adsorbed layers at a given pressure. The results of adsorption enthalpy for both modified and unmodified samples show conversion of a fully hydrophilic calcite surface to partially hydrophilic due to the adsorption of fatty acids on the surface. This behavior was explained based on the decrease in the number of active sites on the calcite surface for interaction with the water vapor (Gomari et al., 2006).

Hamouda and colleagues in series of work with calcite-water-oil system revealed that the adsorption of long chain fatty acids on the calcite surface depends on several factors, namely chemical structure of fatty acid, pH, brine composition and temperature. They have also shown a synergistic effect between asphaltene and fatty acids for alteration of chalk surface to more oil-wet (Tabrizy et al., 2011). The presence of water enhances the adsorption of fatty acids on calcite (Gomari et al., 2006).

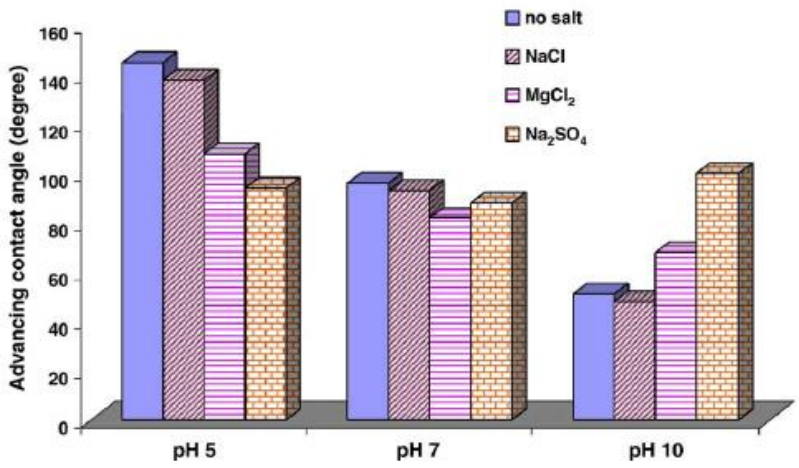

Figure 2.18 - Advancing contact angles of n-decane/calcite system, measured at distilled water interface. The calcite is pre-wetted with different salts (NaCl, $MgCl_2$ and Na_2SO_4) and at different pH (Gomari and Hamouda, 2006).

Naphthenic acid containing two rings (decahydronaphthelen-pentanoic acid) has greater effect on changing the wettability of calcite surface than naphthenic acid containing only one ring (cyclohexane-pentanoic acid). Presence of Na^+ ions has inconsiderable effect on wettability of calcite in presence of stearic acid. However, the presence of Mg^{2+} and SO_4^{2-} ions converts the calcite to more water-wet in the range of pH values below 7. Above pH 7, presence of sulfate converts the surface to

slightly more oil-wet, on contrary to the presence of magnesium where it increases the water-wetness. The measured contact angles at the modified calcite surface at different pH are shown in Figure 2.18. (Gomari and Hamouda, 2006).

In summary, potential determining ions for calcite are proved, in literature, to be Ca^{2+} and CO_3^{2-}, which, together with the chemical structure, determine the extent of the adsorption of fatty acids at specific pH. Zeta potential measurements showed how much the electrical properties of pure calcite surface are changed from positively charged surface (-15.03 mV) to more negatively charged surface (-2.03 and -0.67 mV) in presence of fatty acids (namely PODA and SA, respectively). This is also reflected by contact angle measurements, indicating less water-wet surface. The surface properties of the modified calcite may again be transferred to less negative/positive surface potential in presence of inorganic ions such as SO_4^{2-} and Mg^{2+}, which is also reflected by contact angle showing increasing of water-wettability. Magnesium ions are shown to convert the calcite surface to more water-wet than that for SO_4^{2-} ions. Both ions have affinity to adsorb onto calcite surface, both ions raised the pH, however, sulfate has changed the solution with the modified calcite surface to a higher pH 9.25 compared to 8.48 in presence of magnesium ions. Increasing of pH may have partly contributed to the alteration, however, doesn't explain the higher water-wetness of the calcite surface in case of presence of Mg^{2+} than SO_4^{2-}. At the relatively high concentration of Mg^{2+} ions (0.1M), compared for example to seawater (0.06M), may have induced exchange reaction with surface Ca^{2+}, hence renewal of the calcite surface. Also the presence of Mg^{2+} ions has effect on the calcite stability (Gomari et al., 2006).

Chromatographic wettability tests and SI (spontaneous imbibition) confirmed that cores saturated with oil depleted in water-soluble acids were somewhat more water-wet. This indicates that water-soluble acids may affect the stability of the initial water film between the rock and oil. In a SI experiments by wettability alteration using SW, both the rate and ultimate oil recovery were systematically higher for those cores, which were saturated with oil depleted in water-soluble acids (Fathi et al., 2010).

As the temperature increases, calcite surface becomes more water-wet. The trend of decrease in contact angles with temperature follows the same trend as IFT and distribution coefficients, specifically if one divides acids to saturated and unsaturated separately. Zeta potential measurements of calcite surface at different temperatures demonstrate that increasing temperature reduces surface charge to less positive. This may enhance the repulsive forces between dissociated acids and calcite surface. Due to this change in surface charge, the adsorption of acids on the surface becomes less effective at higher temperatures; therefore wettability of the calcite surface tends to be more water-wet (Hamouda and Gomari, 2006).

2.5.3 Smart Waterflooding in Carbonates: a review of previous studies

Traditionally, a little attention has been given in reservoir engineering practice to the influence of the chemistry of the injected water on displacement efficiency. However, over the last decade a

considerable amount of studies has shown that composition of injected water can influence crude oil/brine/rock interactions in a favorable way to improve oil recovery (Zahid, 2012).

Carbonate oil reservoirs have neutral to oil-wet character. Based on an evaluation study for the wetting state of 161 carbonate reservoirs, it indicated that 15% were strongly oil-wet. 65% were oil-wet, 12% were in the intermediate class and 8% were water-wet. It is documented that close to 50% of the world proven petroleum reserves are located in carbonates, which usually show low oil recovery factor (less than 35%). mainly due to wettability and the fractured nature of these reservoirs' which makes EOR a huge potential to boost oil recovery in carbonates (Jabbar et al., 2013).

Seawater flooding in high temperature chalk reservoirs and low salinity waterflooding in sandstone reservoirs are two examples of smart waterflooding. Most recently, low salinity waterflooding has also been implemented in carbonates (Zahid, 2012).

2.5.3.1 Seawater flooding in chalk reservoirs

Spontaneous imbibition of water into low permeability matrix blocks of a fractured chalk reservoir is considered to be an important method for optimal secondary oil recovery from this type of oil reservoir (Standnes and Austad, 2000). One of the most important factors, which decrease the oil recovery from carbonate reservoirs, is that most of them tend to be intermediate-wet to oil-wet. This tendency is due to such aspects, as high Zeta potential of the rock, and also the oil and brine composition (e.g. presence of asphaltenes, high formation brine salinity etc.). Stronger tendency towards oil-wet makes improved oil recovery by using waterflooding less efficient (Martavaltzi, 2012). Both laboratory experiments and field tests have shown that water-wet and mixed-wet chalk material appears to imbibe water quite well due to the large positive capillary pressure. However, under oil-wet conditions the value of the capillary pressure is low (negative or slightly positive), so the water does not imbibe in small pores (Standnes and Austad, 2000).

Carbonate wettability is dictated by the surface chemistry related to stability of the water film between the oil phase and the rock surface. It has been verified, both in the field and laboratory, that seawater is an excellent injection fluid to enhance the oil recovery from fractured chalk (Zhang et al., 2007).

As an example of a very successful waterflooding, Ekofisk oilfield case can be mentioned. It was initiated in 1987 and contributed to the significant increase in oil production rates. The primary depletion recovery factor with gas reinjection was initially estimated to be 18% of the original oil in place. The current oil recovery estimate from Ekofisk field is more than twice times higher – 38% of the original oil in place. Figure 2.19 shows the dramatic increase in historical oil production rate from a low of 70,000 BOPD in 1987 to the current production level of 290,000 BOPD, which has been a result of waterflooding (Hermansen et al., 2000).

However, waterflooding in chalk reservoirs can also cause some amount of problems. Many chalks show remarkable weakening when water is injected, leading to water-enhanced compaction.

Such effects are well known from the Ekofisk and Valhall fields in the North Sea, where 10 meters subsidence occurred after implementing water injection for EOR purposes (Liteanu et al., 2013).

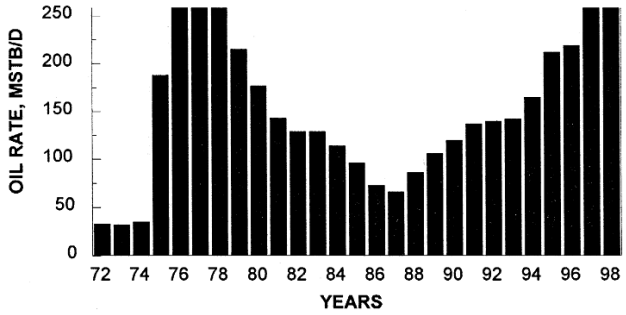

Figure 2.19 – Ekofisk oil production (Hermansen et al., 2000).

Historically the salinity of water used for flooding has not been considered as an important factor in determining the amount of recovered oil. Over the last decade, a significant number of studies have shown that waterflooding performance is dependent on the composition of the brine injected. Extensive laboratory research has been performed in order to understand the mechanism of improved oil recovery from chalk using surfactant solutions and later on using the modified sea water. The researchers suggested wettability alteration towards more water-wet as the reason for improvement in oil recovery (Zahid, 2012). Austad and coworkers in several of experiments with carbonate rocks showed that seawater with a salinity of about 33 000 ppm acts as a wettability modifier. It was experimentally verified that the interaction between Ca^{2+}, Mg^{2+}, and SO_4^{2-} at the chalk surface will displace adsorbed carboxylic acids and increase the water wetness (Fathi et al., 2010).

The affinity of SO_4^{2-} and Ca^{2+} towards the surface of chalk together with the impact of temperature has been studied chromatographically. Spontaneous imbibition experiments have also been carried out in order to understand the effects of sulfate and calcium ions on the wettability modifying process. The mechanism was suggested, according to which sulfate from seawater, which is not present in the initial brine, will adsorb onto the positively charged water-wet sites on the chalk surface and will lower the positive surface charge. Due to less electrostatic repulsion between the chalk surface and the calcium ions from seawater, more Ca^{2+} will adsorb onto the chalk to create excess of Ca^{2+} close to the chalk surface. Ca^{2+} ions can then react with carboxylic groups bonded to the chalk surface and thus release some of the adsorbed organic carboxylic materials. It is well known that among the organic molecules present in crude oil, carboxylic materials have functional groups, which are most strongly bonded to the $CaCO_3$ surface. It is further known that at high temperatures Mg^{2+} ions can substitute Ca^{2+} at the chalk surface. Because Mg^{2+} is able to displace Ca^{2+} from the chalk lattice close to the surface, it must also be able to replace Ca^{2+} linked to carboxylic groups on the chalk surface. Based on data from experiments, a chemical mechanism for the wettability modification of calcite surface is suggested, it is illustrated on Figure 2.20. At low and high temperature Ca^{2+} may react with the adsorbed carboxylic material, thus releasing it from the surface. At high temperature, Mg^{2+} may displace the Ca^{2+}–carboxylate complex, and the fact that the wettability modification using

Mg^{2+} and SO_4^{2-} is only active at high temperatures strongly supports the suggested mechanism. It is hard to believe that the small and strongly solvated Mg^{2+} is able to substitute Ca^{2+} in a Ca^{2+}–carboxylate complex by a similar mechanism as suggested on Figure 2.20 (A), not to mention the fact that the Ca^{2+}–carboxylate bond is normally stronger than the Mg^{2+}–carboxylate bond. Neither Ca^{2+} nor Mg^{2+} will increase spontaneous imbibition of water into a chalk core without the presence of SO_4^{2-} in the imbibing fluid, and SO_4^{2-} also is not active without the presence of either Ca^{2+} or Mg^{2+}. Ca^{2+} is able to modify the wetting conditions at low and high temperature, but Mg^{2+} is only active at high temperatures (Zhang et al., 2007).

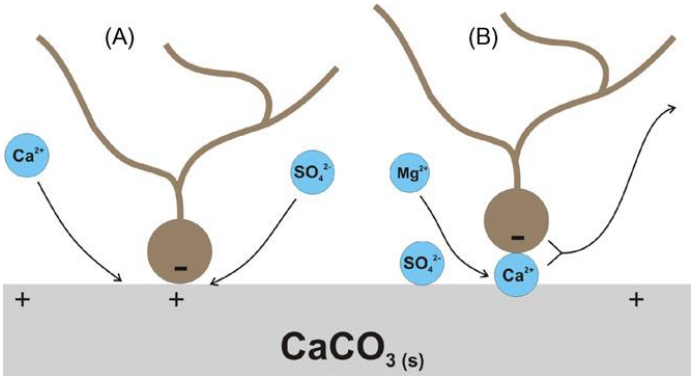

Figure 2.20 - Schematic model of the suggested mechanism for the wettability alteration induced by seawater. (A) Proposed mechanism when Ca^{2+} and SO_4^{2-} are active at lower and high temperature. (B) Proposed mechanism when Mg^{2+} and SO_4^{2-} are active at higher temperatures (Zhang et al., 2007).

2.5.3.2 Modified seawater. Potential determining ions

Over the last decade, a number of studies have indicated SO_4^{2-}, Ca^{2+} and Mg^{2+} as the potential determining ions for the chalk, which may be added to the injected brine for improving oil recovery by waterflooding in chalk reservoirs. However, the mechanism itself that leads to an increase in oil recovery is still not clear understood (Zahid, 2012). Besides, these ions (SO_4^{2-}, Ca^{2+} and Mg^{2+}) are suggested to be responsible for surface wettability alteration and the way it works only in chalk, and it is really not clear if that is the case with other carbonates or only chalk since most experimentation are not done on surface analysis level. Several questions still need to be answered and more amount of controlled research work should be conducted. What level of alteration these potential determining ions can cause? What is the range of the injected water salinity is necessary? Is it just individual ion we are looking at, or a ratio as suggested by some researchers? How does reservoir temperature and pressure affect the recovery process using this technique? Do the type of polar species in crude oil and its acidity play an important role in the efficiency of wettability alteration and the recovery process? Too many question still need to be answered (Jabbar et al., 2013). Following are presented several works by different authors on potential determining ions for wettability changing in carbonates, and the proposed mechanisms for smart water flooding.

Austad and coworkers proposed that enhanced spontaneous imbibition of water into weakly water-wet chalk can be obtained if the capillary forces are increased, which can be done if the injected

brine can increase the water-wetness of the chalk. A wettability alteration mechanism was proposed, according to which sulfate will adsorb onto the chalk surface and lower the net positive charge to facilitate some desorption of negatively charged polar components (carboxylic material). Adsorption of sulfate ions onto the chalk surface is enhanced as the temperature increases. Experimental data showed that the concentration ratio $[SO_4^{2-}]$ / $[Ca^{2+}]$ is also important: seawater appeared to be an excellent injection fluid in fractured chalk at weakly water-wet conditions because of the ratio $[SO_4^{2-}] \sim 2[Ca^{2+}]$. The effluent from the cores was strongly depleted in SO_4^{2-} ions partly because of adsorption onto the chalk surface. Because of that, if produced water is injected into the chalk, it will probably have a negative effect on the oil recovery (Austad et al., 2005).

Karoussi investigated extreme cases with ion-free water and water containing Mg^{2+} or SO_4^{2-}. Modified carbonate rocks with stearic acid that was initially saturated with ion-free water followed by an imbibition process with fluids containing Mg^{2+} or SO_4^{2-}, at the same concentration as the injected seawater, shows the highest oil recovery when Mg^{2+} is present in the imbibing fluids (Karoussi and Hamouda, 2008).

Zahid performed flooding experiments on the core plugs from Stevns Klint outcrop chalk, which were saturated with three different oils: North Sea crude oil, Latin American crude oil, Middle East field crude oil. The initially saturated cores without any aging were put into the Hassler core holder with a confining pressure of 30 bars. Flooding experiments were performed using combinations of the different injection rates, temperatures, crude oil types, core plugs and compositions of the injected brine. According to the results, increment in oil recovery with the aid of sulfate ions cannot be explained just by the rock wettability alteration. Injection of brine rich in sulfate ions may lead to additional recovery even under completely water-wet conditions. The oil recovery is dependent upon the sulfate concentration and increases as the sulfate concentration increases. Furthermore, effectiveness of sulfate itself increases with increase of the temperature. Crude oil composition type plays a dominant role in the effect that brine composition can have on recovery increment. Injection rate also affects the recovery (Zahid, 2012).

The reference limestone sample, which was only equilibrated in formation brine and was not exposed to any aging in oil proved to be weakly water-wet (contact angle is equal 51°). Aging with the model oil for 10 days affected the wettability: contact angle was increased to 138°. Immersion in 0.01M Ca^{2+} decreased the contact angle from 138° down to 34°, while Mg^{2+} brine of the same salinity only reduced it down to 104°. The rest of the studied brines (higher $CaCl_2$ salinities and Na_2SO_4) not only did not alter the wettability of the sample to water-wet but some of them turned the limestone sample to more oil-wet. High salinity sulfate brine increased the contact angle up to the value of 168°. All of the measurements were performed at the ambient temperature and therefore, the effect of higher temperatures on wettability was not considered in this study (Martavaltzi et al., 2012).

Al-Attar presented his work with flooding of carbonate core samples taken from Bu Hasa field in Abu Dhabi. These results were used to evaluate the effect ionic composition on the possible

interactions of limestone rock/ brine/ and oil system and to identify the oil recovery mechanism. The field injection water was first diluted to different salinities and the optimum salinity was determined to be 5000 ppm, and second it was modified by varying the sulfate and calcium ion concentrations. Wettability alteration was determined by contact angle measurements. Increasing the Ca^{2+} concentration in the injected brine resulted in decreased ultimate oil recoveries. Increasing the SO_4^{2-} concentration in the injected brine tends to change the wettability to more intermediate levels and resulted in improved ultimate oil recoveries (Al-Attar et al., 2013).

This experimental study investigates the wettability alteration of calcite crystal and carbonates outcrop rock surface aged in model oils of total acid number of 2 and then treated with different brine solutions. Model oils were prepared by mixing toluene with short chain (Heptanoic acid) and long chain (Stearic acid) carboxylic acids. The investigated brine solutions composed a range of different salinities and were aimed on study the effect of individual ions such as SO_4^{2-}, Ca^{2+} and Mg^{2+}. The results of experiments showed that the long chain fatty acid (stearic acid) strongly adsorbs onto the calcite surface compared to the short chain (heptanoic acid). It was confirmed by the measured contact angles. Twice dilution of Arabian Gulf seawater has been found to be a less efficient EOR fluid for wettability alteration in comparison with undiluted Arabian Gulf seawater. This was also confirmed by the changes in the measured contact angles toward more water-wet for aged calcite in heptanoic acid model oil and aged calcite in stearic acid model oil. It was indicated also that significant wettability alteration was observed for the twice diluted Arabian Gulf seawater with higher concentrations of SO_4^{2-} and Mg^{2+} ions (Jabbar et al., 2013).

Zahid studied the crude oil/seawater ions interaction at different temperatures, pressures and sulfate ion concentrations. Results of these experiments showed that sulfate ions may help decrease the crude oil viscosity when brine is contacted with oil under conditions of high temperature and pressure. Also during the experiment was observed formation of an emulsion phase between brine and oil, which appeared with the increase in sulfate ion concentration at high temperature and pressure. In addition to this, sulfate ions can reduce interfacial tension between oil and water. It was proposed that the decrease in viscosity and formation of an emulsion phase could be the possible reasons for the observed increase in oil recovery with sulfate ions at high temperature in chalk reservoirs besides the mechanism of the rock wettability alteration (which has been reported in most previous studies) (Zahid, 2012).

2.5.3.3 Low salinity waterflooding in chalk reservoirs

The low salinity water injection method has become one of the important research topics in the oil industry because of its enormous possible advantages (Shalabi et al., 2014). Evidence from laboratory studies, supported by some field tests targeting mainly sandstones, has distinctly shown that injecting low-salinity water has a significant impact on oil recovery (Yousef et al., 2011).

The effect of low salinity water injection on carbonate has not been thoroughly investigated in contrast to sandstone rocks because wettability alteration by low salinity water is related to the presence of clay, which is not the case in carbonate rocks. No field scale pilots have been conducted so far to investigate the effect of low salinity water injection on carbonate rocks. Some work was done at laboratory scale on the effect of low salinity water injection on oil recovery from carbonate rocks (Shalabi et al., 2014). Although the potential for carbonates has not been thoroughly investigated, some reported studies have excluded carbonates from this effect (Yousef et al., 2011). However, some other recent studies also highlighted that low salinity water can increase oil recovery in carbonate reservoirs (Alotaibi et al., 2010).

The oil recovery from chalk cores by spontaneous imbibition and forced displacement was investigated by comparing the oil recovery using ordinary seawater and modified seawater. It has been stated that, unlike for sandstones, improved oil recovery by low-salinity flooding is not possible for carbonates because the chemical mechanism for wettability modification is different. Modified seawater, with regard to both salinity and composition, has been compared as a wettability modifier to seawater during a spontaneous imbibition and forced displacement process at temperatures between 100 and 120°C. Based on the experiments results following two conclusions were made. (1) Both the imbibition rate and ultimate oil recovery increased relative to seawater when it was depleted in NaCl. The effect was more significant at high temperatures. (2) Diluted seawater decreased the oil recovery drastically, when used as imbibing fluid (Fathi et al., 2010).

Alotaibi run coreflood experiments with dolomite cores, which were saturated and flooded with oil at high temperature. In first sequence, dolomite core plug was water flooded with aquifer water as well as diluted aquifer water (1:1 and 1:10). Oil recovery was 21.7% after injecting aquifer water for more than two pore volumes. Diluted aquifer water at two different ratios, 1:1 and 1:10, were injected but no additional oil was recovered. Second dolomite core plug was flooded with seawater, aquifer water and then 1:1 diluted aquifer water. Seawater injection as a secondary mode in dolomite rock showed more recovery than aquifer. In this test, oil recovery was 35.5% after injecting seawater for 2.5 pore volumes. Then, it was switched to aquifer water and 8.9% additional oil was recovered. Moreover, 1:1 diluted aquifer water added 1.7% more oil recovery (Alotaibi et al., 2010).

Al-Harrasi investigated the impact of low-salinity water on oil recovery by conducting coreflood and spontaneous imbibition experiments at 70 °C using core samples from a carbonate reservoir, crude oil and synthetic brine which was mixed with distilled water in four proportions twice, 5 times, 10 times and 100 times dilution brines. Moreover, both crude oil brine interracial tension measurements (IFT) and ionic exchange experiments were carried out. The results of the study show higher oil recovery as a result of reducing injected water salinity in both coreflood and spontaneous imbibition experiments. Coreflood experiments showed an increase in oil recovery by 3 to 5 % of OOIP, while spontaneous imbibition experiments showed an increased by 16 to 21 %. The additional oil recovery was attributed to wettability change (Al-Harrasi et al., 2012).

Al-Attar performed flooding tests on selected carbonate core samples taken from Bu Hasa field in Abu Dhabi. These results were used to evaluate the effects of brine salinity and ionic composition on the possible interactions of limestone rock/ brine/oil system and to identify the oil recovery mechanism. The experimental results revealed that a significant improvement in the oil recovery can be achieved through alteration of the injection water salinity. Reducing the salinity of injection water from 197.362 ppm to 5000 ppm resulted in an improvement of oil recovery from 63% to 84.5% of OOIP. Contact angle measurements indicated that lowering the solution salinity could shift the wettability of the system towards intermediate wettability levels. Results also indicated that there is no clear correlation between the improvements in oil recovery and interfacial tension and the pH of the studied systems (Al-Attar et al., 2013).

Saudi Aramco reported on a new recovery method/process for carbonate reservoirs, tagged "smart waterflooding." It is aimed to improve or enhance oil recovery by means of altering the salinity and ionic composition of injection water. The method was demonstrated using composite cores from one of the Saudi Arabian carbonate reservoirs. The experimental parameters and procedures were well designed to reflect reservoir conditions and current field injection practices, including such parameters as reservoir pressure, reservoir temperature, initial reservoir connate water (salinity of 200,000 ppm), and synthetic brines for injection seawater (56,700 ppm). The method represents an injection sequence of various diluted versions of regular seawater. The additional oil recovery was approximately 7 to 8.5% with twice-diluted seawater, approximately 9 to 10% with 10-times-diluted seawater, and approximately 1 to 1.6% with 20-times-diluted seawater (all the results are in in terms of the OOIC). The results revealed an existence of a substantial potential to obtain additional incremental oil recoveries by altering the salinity of injection seawater. Figure 2.21 shows results on one of the composite cores (Yousef et al., 2011).

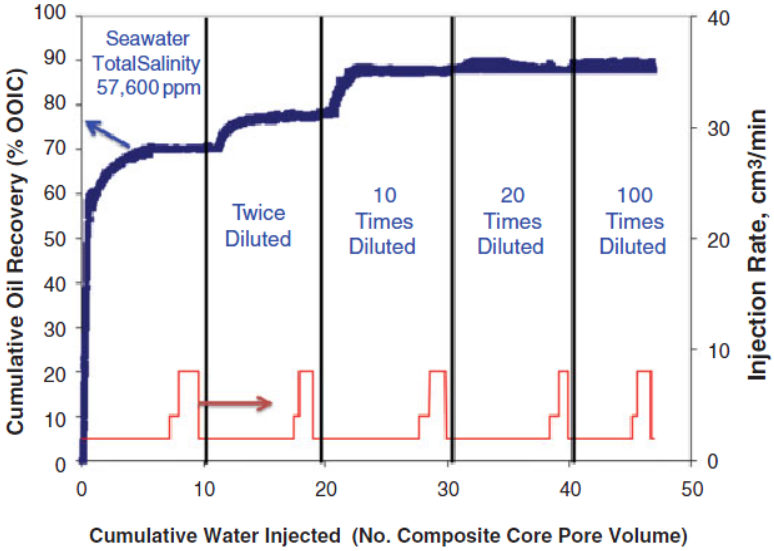

Figure 2.21 - Oil-recovery curve of the first coreflood experiment. The blue curve represents the amount of oil produced in terms of OOIC through all injected salinity slugs of seawater, and the red curve represents the injection-rate profile implemented during the coreflood experiment (Yousef et al., 2011).

3 Experiments

Experimental part include flooding of several chalk cores with synthetic sea water (SSW) and low salinity water (LSW), measuring of such parameters as recovery, pH of initial brines and effluents, pressure drop, absolute and relative permeability, interfacial tension (IFT) and ion chromatography.

3.1 Materials

3.1.1 Oil

For flooding experiments synthetic oil was used. The oil is a mixture of n-decane and stearic acid. Here n-decane is used as a bulk phase. The concentration of stearic acid in n-decane is 0.005 mole/l. N-decane was supplied by Chiron AS at 99% purity. Stearic acid was supplied by Aldrich at 98.5% purity.

It is assumed that the additive (SA) does not have any significant influence on the properties of the oil, since its concentration is low (0.005 mole/l) (Hamouda et al., 2014). Physical properties of synthetic oil are given in Table 3.1, which are actually the properties of bulk phase (n-decane).

Table 3.1 – Synthetic oil properties.

Property	**Value at 20 °C**	**Value at 50 °C**	**Value at 70 °C**
Density (g/ml)	0,73	0,705	0,67
Dynamic viscosity (cP)	0,92	0,61	0,41

3.1.2 Brines

During experiments synthetic sea water (SSW) was used for initial saturation and as an injection fluid in flooding. Also diluted versions of SSW were used in flooding experiments. SSW was prepared by dissolution of different salts in distilled water. LSW brines were acquired by dilution of prepared SSW with distilled water in following concentrations: 5 times diluted SSW (LSW 1:5), 10 times diluted SSW (LSW 1:10), 15 times diluted SSW (LSW 1:15), 20 times diluted SSW (LSW 1:20), 25 times diluted SSW (LSW 1:25). Ion concentrations of brines are given in Table 3.2.

The ionic strength of a solution is a measure of the concentration of ions in that solution. It is a function of the concentration of all ions present in that solution (Wikipedia, Ionic strength):

$$I = \frac{1}{2}\sum_{i=1}^{n} c_i z_i^2 \qquad (3.1)$$

where

c_i molar concentration of ion i (mole/l)

z_i charge number of ion i

Table 3.2 – Ion concentration of SSW and LSW brines.

Ion	SSW (mole/l)	LSW 1:5 (mole/l)	LSW 1:10 (mole/l)	LSW 1:15 (mole/l)	LSW 1:20 (mole/l)	LSW 1:25 (mole/l)
HCO_3^-	0.002	0.0004	0.0002	0.00013	0.0001	0.00008
Cl^-	0.525	0.105	0.0525	0.035	0.02625	0.021
SO_4^{2-}	0.024	0.0048	0.0024	0.0016	0.0012	0.00096
Mg^{2+}	0.045	0.009	0.0045	0.003	0.00225	0.0018
Ca^{2+}	0.013	0.0026	0.0013	0.00087	0.00065	0.00052
Na^+	0.45	0.09	0.045	0.03	0.0225	0.018
K^+	0.01	0.002	0.001	0.00067	0.0005	0.0004
TDS (ppm)	33388	6678	3339	2226	1669	1336
Ionic strength	0.657	0.1314	0.0657	0.0438	0.03285	0.02628

Physical properties of SSW and LSW brines are given in Table 3.3.

Table 3.3 – Physical properties of SSW and LSW brines.

Brine	Density at 20 °C (g/cm^3)	Density at 50 °C (g/cm^3)	Density at 70 °C (g/cm^3)	Viscosity at 20 °C (mPa*s)	Viscosity at 50 °C (mPa*s)	Viscosity at 70 °C (mPa*s)
SSW	1.024	1.012	1.002	1.073	0.592	0.440
LSW 1:5	1.003	0.993	0.983	1.015	0.555	0.411
LSW 1:10	1.001	0.991	0.980	1.008	0.551	0.407
LSW 1:15	1.000	0.990	0.979	1.006	0.550	0.406
LSW 1:20	1.000	0.989	0.979	1.005	0.549	0.406
LSW 1:25	0.999	0.989	0.979	1.004	0.548	0.405

The density was calculated by means of Water Density Calculator (Water Density Calculator, 2011). The calculator is created with assistance of the University of Michigan and the NOAA. The density of pure water is 1 g/cm^3. There are two main factors which influence the density of ocean water – the first is the temperature of the water and the other is the salinity of the water. So the calculator finds the density of salt water as a function of these two factors (Water Density Calculator, 2011).

The actual value of SSW and LSW densities for room temperature were checked on the PAAR DMA46 densitometer and the values correspond with those gotten by means of the calculator. The densitometer is shown on Figure 3.1.

Figure 3.1 – PAAR DMA46 densitometer.

Water viscosity was calculated by means of Water Properties Calculator (Water Properties Calculator, 2010). The calculator is based on MATLAB algorithms, which take into consideration different correlations of thermophysical properties of seawater. The calculation of viscosity is made as a function of salinity and temperature of brine (Water Properties Calculator, 2010).

3.1.3 Porous media

For the experiments Stevns Klint outcrop chalk cores were used. Seven similar cores were made out of the same piece of chalk to get more comparable results. The parameters for cores were measured during preparation for flooding procedure. Absolute permeability for three cores was measured by means of flooding the core, completely saturated with SSW, with the same SSW brine at three different flowrates. The actual value of absolute permeability was calculated using Darcy law as an average for three flowrates. The results for three different cores showed almost identical value, so the same absolute permeability for each core was taken as a basis. The parameters for the cores are given in Table 3.4.

In general, specific surface area of Stevns Klint chalk from quarry nearby Copenhagen, Denmark, is comparable with that of reservoir chalk. This outcrop chalk cores may constitute suitable substitution for reservoir chalk with respect to flooding properties, provided that porosity and permeability of reservoir chalk are both comparable to outcrop samples (Hjuler and Fabricius, 2009). For comparison, Ekofisk chalk formation has porosities ranging from 30% to 48% (Hermansen, et al., 2000). Outcrop Stevns chalk is highly porous (45-50%), low-permeable (2-5 mD), and has a specific surface area of about 2.0 m^2/g (Fathi et al., 2010). The matrix material properties and petrophysical behavior of Stevns Klint outcrop chalk resemble closely those of reservoir chalk, although there are important differences in depositional processes and diagenetic history (Frykman, 2001).

Table 3.4 – Parameters of Stevns Klint chalk cores.

Core number	Diameter, cm	Length, cm	Pore volume, ml	Porosity, %	Permeability, mD
#1	3,81	7,38	40,7	48,3	3,9
#2	3,815	7,335	39,5	47,2	3,9
#3	3,81	7,77	44,2	50,0	3,9
#4	3,81	6,98	39,2	49,2	3,9
#5	3,81	7,455	40,1	47,2	3,9
#6	3,8	7,3	41,1	49,7	3,9
#7	3,805	7,35	39,9	47,8	3,9

Stevns Klint chalk compares stratigraphically to the interval including the uppermost Tor formation and lower Ekofisk formation in the North Sea chalk reservoirs, which is shown in Figure 3.2. For a large amount of the fields in the southern North Sea, the uppermost Maastrichtian chalk forms the main producing interval (Frykman, 2001).

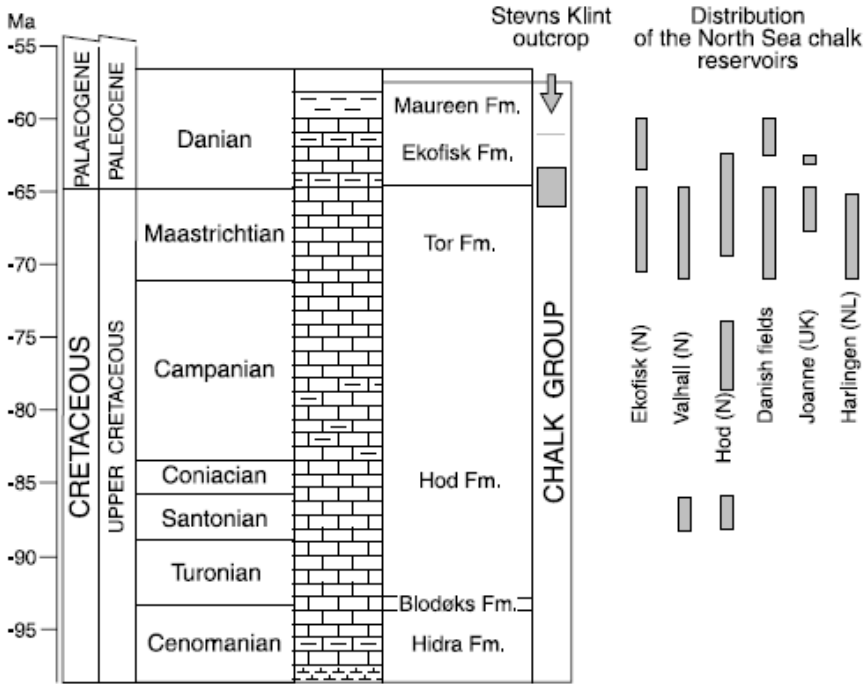

Figure 3.2 – Stratigraphic distribution of the North Sea chalk reservoirs and the outcrop at Stevns (Frykman, 2001).

3.2 Equipment

3.2.1 Preparation of SSW, LSW and synthetic oil

To create SSW the salts in appropriate proportions were mixed with distilled water and steered on magnetic steerer for 1 day to get proper dissolution. Then the SSW was filtered through 0.22 µm

Millipore filter to remove any undissolved salts or any other particles, which can plug the core pores. The magnetic steerer and filtration setup are pictured on Figure 3.3. The LSW was obtained by dilution of SSW with distilled water in different proportions.

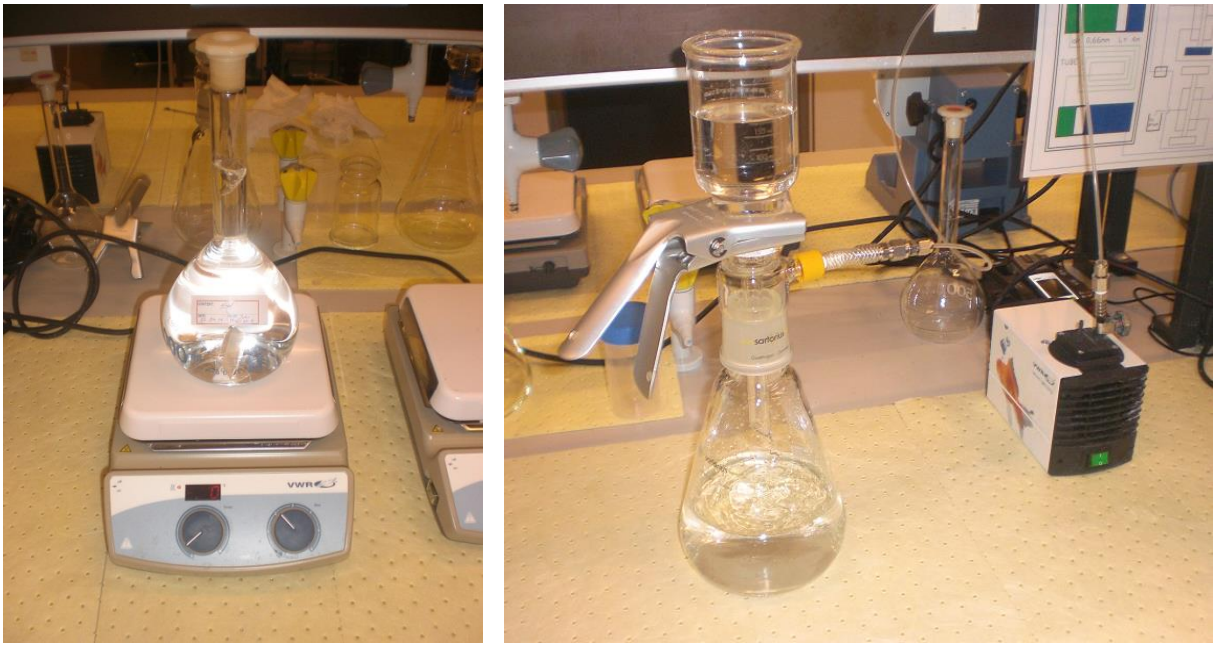

Figure 3.3 – Magnetic steerer (left picture) and filtration setup (right picture).

In experiments with waterflooding synthetic oil is used instead of crude oil. This is done because crude oil contents a vast amount of different chemical components, so the substitution by synthetic oil can reduce the number of uncertainties, make results more comparable and simplify the interpretation process. Synthetic oil was prepared by mixing normal decane (n-decane) with stearic acid (SA). For this procedure magnetic steerer was also used.

Gomari and Hamouda, 2006 studied the effect of different acids, which were found in abundance in North Sea reservoirs, on the wettability of calcite. From them SA, which presents in itself the long chain fatty acid, was found to be able to modify calcite surface to strongly oil-wet.

3.2.2 Preparation of cores

Before the flooding procedure the cores were dried in oven, saturated with water and oil and aged. The aging procedure is made to change wettability of the calcite from initially water-wet to oil-wet, which creates the conditions close to reservoir.

The chalk cores were first dried in the oven at 100 °C for several days to remove all the water that could contain in pore space. To check that the cores are completely dried the weight of the cores was measured each day. The weighing-machine is shown on Figure 3.4. When the weight stopped decreasing, the cores were ready for saturation.

Figure 3.4 – Measuring weight of the core by weighting-machine.

The length and diameter of dried cores were measured, and from these values the volume of the cores was calculated. The cores then were saturated 100% with SSW using vacuum setup, which is pictured on Figure 3.5. Here vacuum pump is used to create vacuum in glass bowl. SSW is placed in the plastic container. The valve is used to drop the water slowly on the top of the core. The water is imbibed in the core and the air is removed from pore space by vacuum.

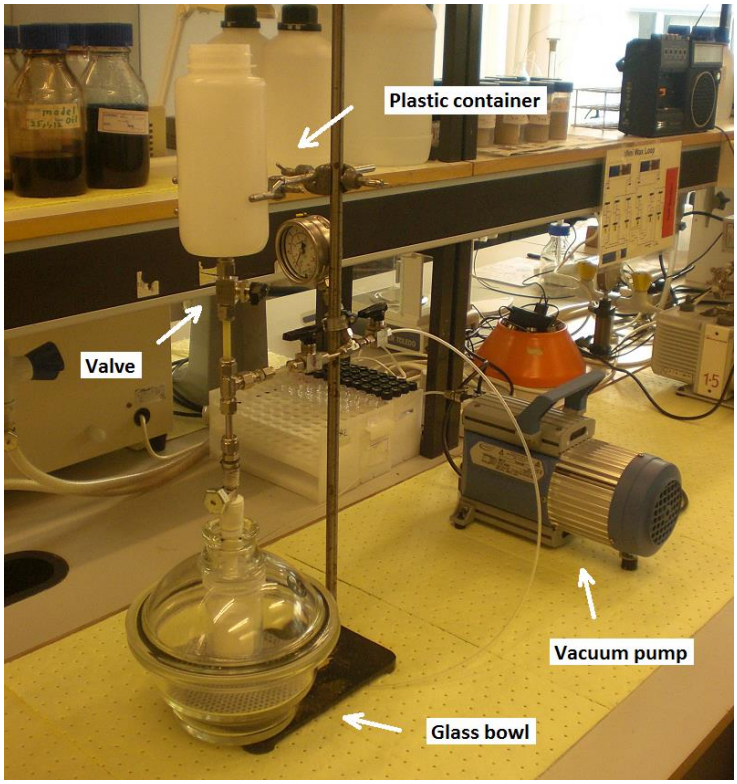

Figure 3.5 – Vacuum setup.

After that the weight of the core with water inside was measured again, and the pore volume was calculated, using the following equation:

$$PV = \frac{m_{sat} - m_d}{\rho_{ssw}} \qquad (3.2)$$

where

PV pore volume

m_{sat} weight of the core with SSW inside

m_d weight of dried core

ρ_{ssw} SSW density

After that the cores were prepared for saturation with synthetic oil. Firstly, each core was wrapped in Teflon tape to exclude any possible evaporation of fluids during process. Then the plastic cover was put over the core. This is done because in previous experiments it was noticed that the rubber sleeve, which is installed over the core, inclined to some amount of decomposition at high temperatures. So the plastic cover prevents rubber particles from penetrating inside the core.

The core was then put in Hassler core holder. Synthetic oil was placed inside the cylinder. The core holder and the cylinder were placed inside the oven and connected to each other, to pumps and to manometers (Figure 3.6). The scheme of flooding setup is shown on Figure 3.7.

The temperature for initial water saturation (IWS) procedure was set to 50 °C. The confining pressure was set to value 25 bar. For this Tellus oil was used, which was pumped by Gilson pump #1 in the space around rubber sleeve. Gilson pump #2 was used to pump synthetic oil inside the core and displace SSW from pore space. The amount of water flooded from the core was measured by checking effluent in test-tube, aiming to stop the process when the IWS was about 20%. The real IWS for different cores is shown in Table 3.5.

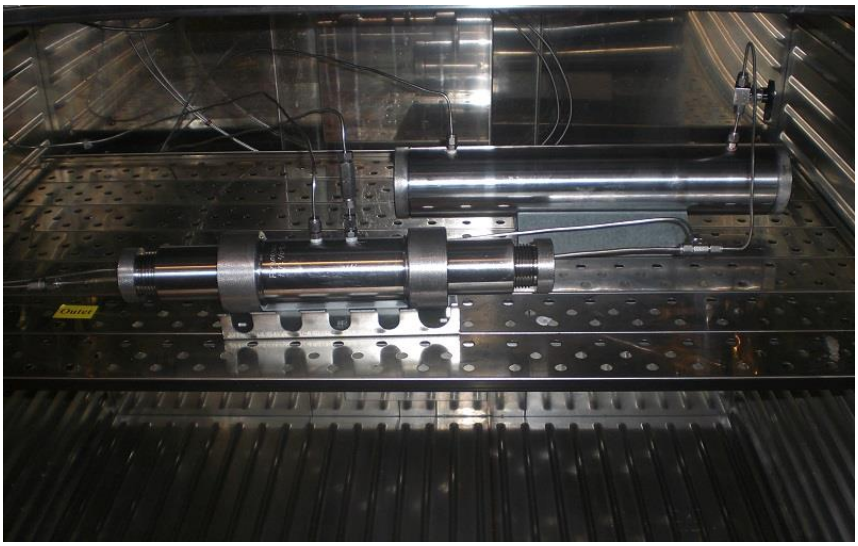

Figure 3.6 – Oven with Hassler core holder and cylinder.

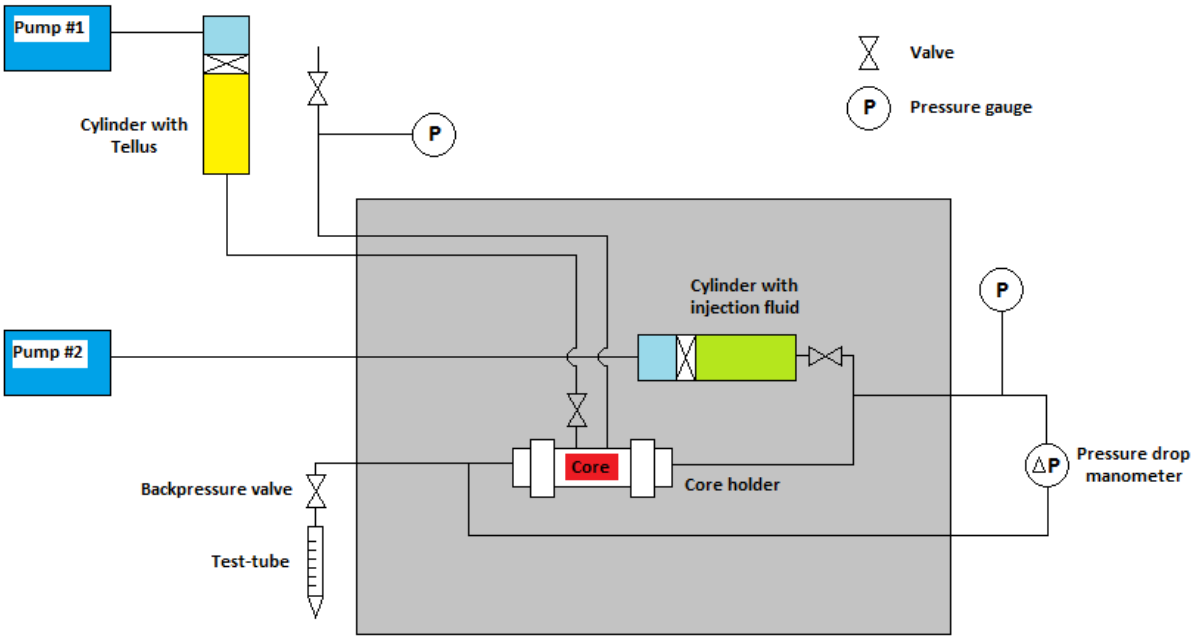

Figure 3.7 – Scheme of flooding setup.

Table 3.5 – IWS for cores.

Core number	IWS
#1	20,1
#2	20,0
#3	20,9
#4	20,9
#5	20,0
#6	20,4
#7	20,1

The core was then placed inside aging cell (which was filled with synthetic oil), put in the oven and aged for 2 weeks at 50 °C.

Chukwudeme and Hamouda, 2009 studied the effect of aging time on recovery from chalk cores and suggested that 2 weeks aging of cores is relatively enough for laboratory studies, because aging for more time shows no difference in oil recovery.

3.2.3 Flooding of the cores

After the cores were aged for 2 weeks and wettability changed from water-wet to more oil-wet, the cores were flooded with brines of different salinities. Each core was again wrapped in Teflon paper, had a plastic cover and was put into Hassler core holder. The cylinder was filled with different brine for each core, as shown in Table 3.6.

Table 3.6 – Brines used for flooding.

Core number	Brine
#1	LSW 1:5
#2	SSW
#3	LSW 1:10
#4	LSW 1:15
#5	LSW 1:20
#6	LSW 1:25
#7	SSW, then LSW 1:10

The connection of the core holder, cylinder, pumps and manometers is analogues to the saturation procedure. The confining pressure was set to 25 bars. The temperature was set to the value 70 °C. The backpressure valve was installed on the outlet line from the core to prevent the boiling of liquids at high temperature. The outlet pressure was set to the value 10 bar, for this compressed nitrogen was used. Each core was flooded for at least 4 PV on the low flowrate 4 PV/day, and then 4 PV at the high flowrate 16 PV/day. The change of flowrate is made to make sure that all possible recovery from the core is acquired and only what is called "residual oil" is left inside. The oil recovery was continuously measured by looking at the amount of fluid in test-tube. The pressure-drop across the core is measured by the manometer and the data is transferred to the computer and saved on the computer by Labview program. The pH values of the effluent were measured continuously by means of Mettler Toledo pH meter, which is pictured on Figure 3.8. Before the measurements the pH meter was calibrated using buffering solutions with known pH (4, 7 and 10). The effluent was collected from the test-tube and immediately measured to prevent the interaction with CO_2 from air, which can change pH of the water-based brine.

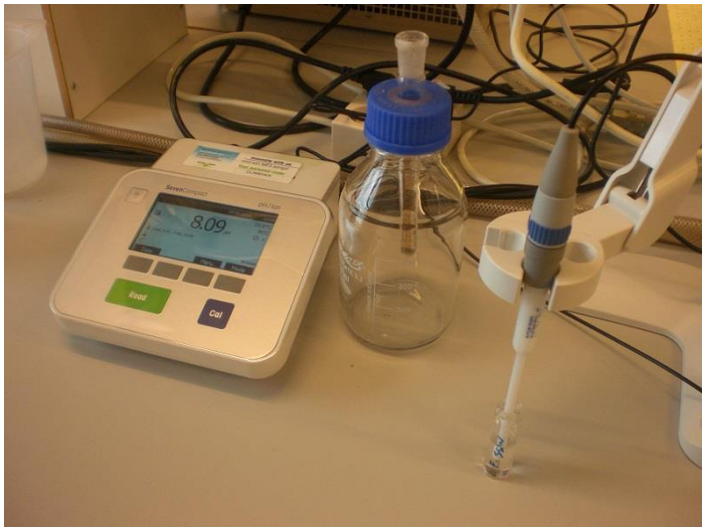

Figure 3.8 – Mettler Toledo pH meter.

Absolute permeability was measured on the same flooding setup. Core completely filled with SSW was flooded with SSW at three different flowrates, and absolute permeability of the core was calculated using Darcy's law.

3.2.4 Ion chromatography

The amount of anions and cations in the effluent was measured by means of Dionex ICS-3000 chromatograph, which is shown on Figure 3.9. Due to high salinity of the effluent, the SSW samples were diluted 200 times and LSW samples 50 times. They were then filtered with 0.2 μm filter to remove solid particles, which could be flooded out of the core. The data were processed manually after the analyses, using the program Chromeleon 7. In this program the area of each peak was adjusted to reduce the error. The SSW samples with known concentration of ions were used as the basis for interpretation.

Figure 3.9 – Dionex ICS-3000 chromatograph.

4 Results and discussion

Waterflooding with SSW and different LSW brines was performed to study the effect of injection fluid salinity on recovery in chalk cores. Cores with similar parameters, saturated with the same initial brine (SSW) and synthetic oil, were used for experiments. All flooding parameters were kept at the same value. So the only difference between experiments is the injection brine salinity. By performing such kind of study we can be relatively sure, that the difference in recovery will be dependent on the properties of the injection brine, which in turn depends on salinity.

4.1 The difference in recovery for cores flooded with brines of different salinity

On the following graph (Figure 4.1) you can see the recovery during flooding process for SSW and five LSW. The vertical axis represents the recovery in percent of original oil in core (OOIC). Horizontal axis shows the amount of injected fluid in PV. The vertical black line indicates the time, when the flowrate was switched to 16 PV/day.

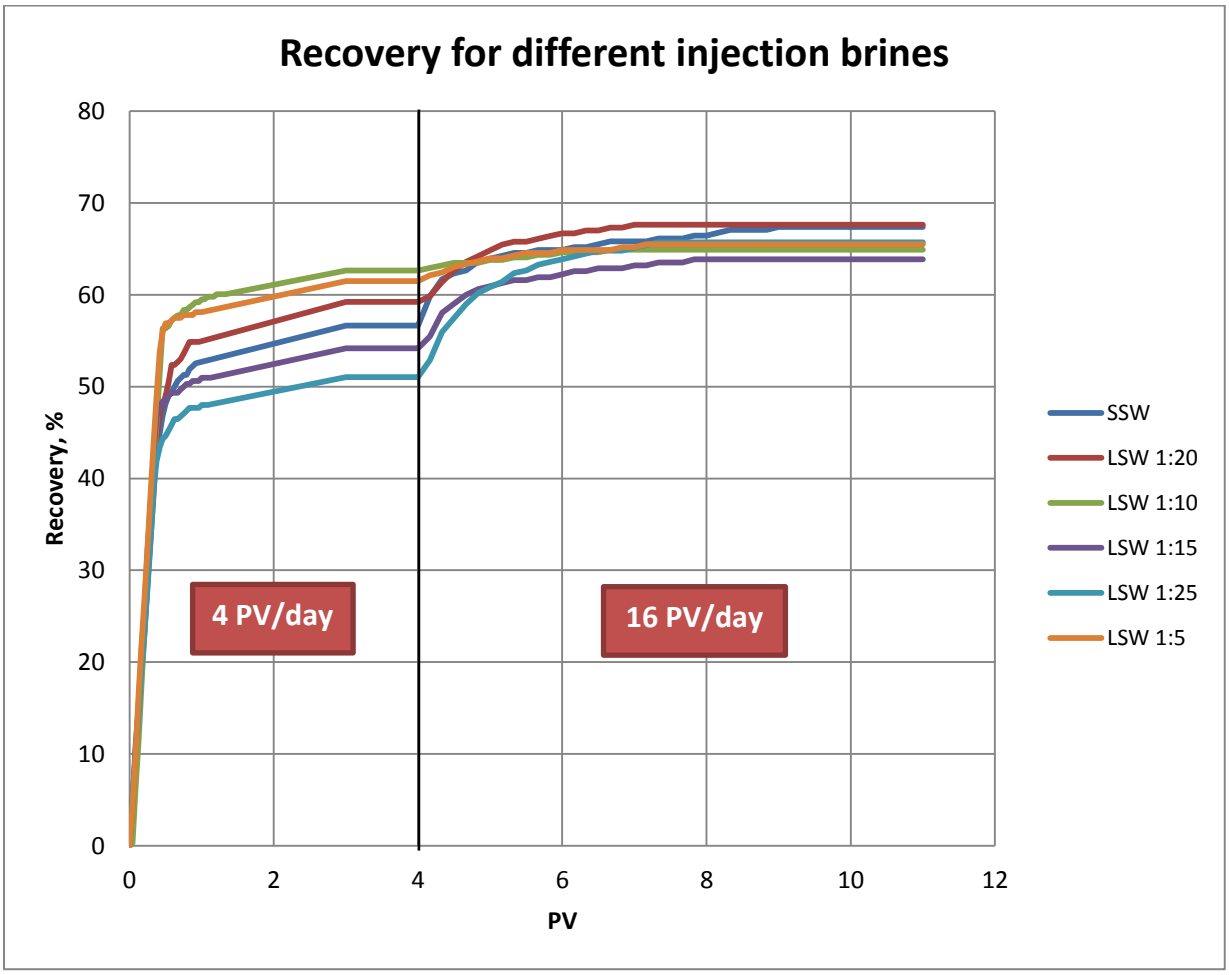

Figure 4.1 – The recovery during flooding with SSW and LSW brines.

From the graph it is clear that there is a difference in recovery for flooding with brines of different salinities. Moreover, the difference exists on both flowrates, where higher recovery on low flowrate doesn't necessary mean the higher total recovery on both flowrates.

On Figure 4.2 you can see maximum recovery acquired on low and high flowrate for different injection brines. Here the blue dots show the total recovery on low flowrate (the values are indicated on left vertical axis). The red dots show the recovery increment, when the flowrate is switched to 16 PV/day (the values are indicated on right vertical axis). Horizontal axis shows a salinity of injection brine.

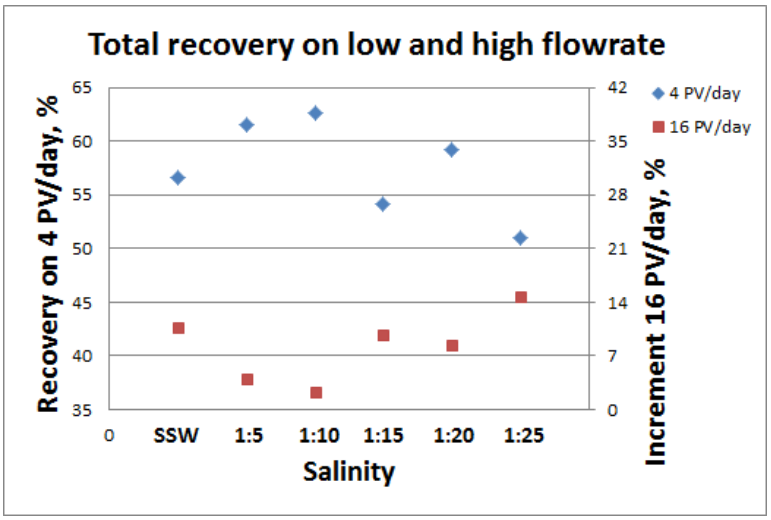

Figure 4.2 – Total recovery for two flowrates and different salinities.

Several interesting things can be noticed on the above graph. First of all, high recovery on 4 PV/day corresponds with low recovery increment on 16 PV/day. Second is that recovery here follows some kind of trend. If for now we will exclude the results for LSW 1:15, we will see that, when the salinity of injection brine is decreasing, the recovery on low flowrate first increase, reach the maximum value (LSW 1:10) and then decrease. The recovery on high flowrate follows opposite trend. The deviation in the trend due to LSW 1:15 can be either because of error, or maybe trend does follow the results and we should have two peaks instead of one. The recovery from core actually depends on many parameters, some of which are injection fluid parameters. In order to explain the results, we need to discuss the data for each salinity flooding.

4.2 Flooding with LSW 1:5

Core #1 was flooded with 5 times diluted SSW at 4 PV/day (0.113 ml/min) flowrate. The recovery here was high enough compared to other cases (61.5%). When the amount of injected fluid reached 4 PV, and it was clear that there will be no more recovery increment, the flowrate was switched to 16 PV/day (0.452ml/min). The recovery increment was low compared to other cases (4%). Total recovery from this core reached the value 65.5%. The recovery with LSW 1:5 compared to brines of other salinities you can see on Figure 4.3.

Under the conditions of flooding with low flowrates capillary forces may dominate the flow and oil production will be strongly affected by capillary end effect, especially for non-water-wet rock (Al-Harrasi et al., 2012). For this reason all the experiments in this work are done at two flowrates. And, as we can see, due to switching to high flowrate, the flooding of core #1 brought plus 4% more of oil.

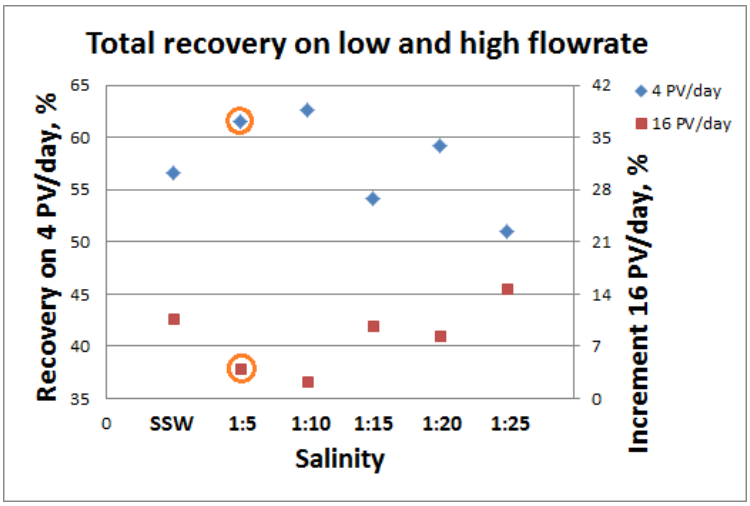

Figure 4.3 – Recovery for core #1 flooded with LSW 1:5 at two different flowrates, compared to other cases.

On the Figure 4.4 you can see the recovery during the flooding process on both flowrates and pH of effluent and inlet brine. Left vertical axis indicates recovery in percent from OOIC. Right axis indicates pH value. Horizontal axis shows the amount of injection fluid flooded through the core in PV. Vertical black line indicates switching of flowrate from 4 PV/day to 16 PV/day. For pH trend the space between 1 PV and 3 PV has only one measurement, because at that time equipment was left for a night. So the measurement for 2 PV was actually taken in the morning and represents the average pH value for the effluent between 1 PV and 3 PV. The same applies for recovery trend – you can see a straight line between 1 PV and 3 PV.

Figure 4.5 represents interpretation of ion chromatography for effluent samples, taken during flooding process. The vertical axis indicates the concentration of ions in the effluent relative to injection brine in logarithmic scale. Horizontal axis indicates the amount of injection fluid flooded through the core. For 16 PV/day the amount of samples, for which ion chromatography was made, is about two times less than those, for which pH measurements were made. The reason that not all samples were put to the chromatography is that the process is time consuming – one measurement for cations takes about 30 minutes.

Figure 4.6 shows the pressure drop values during flooding of the core #1. The vertical axis indicates pressure drop in bars and the horizontal axis the amount of injection fluid flooded through the core.

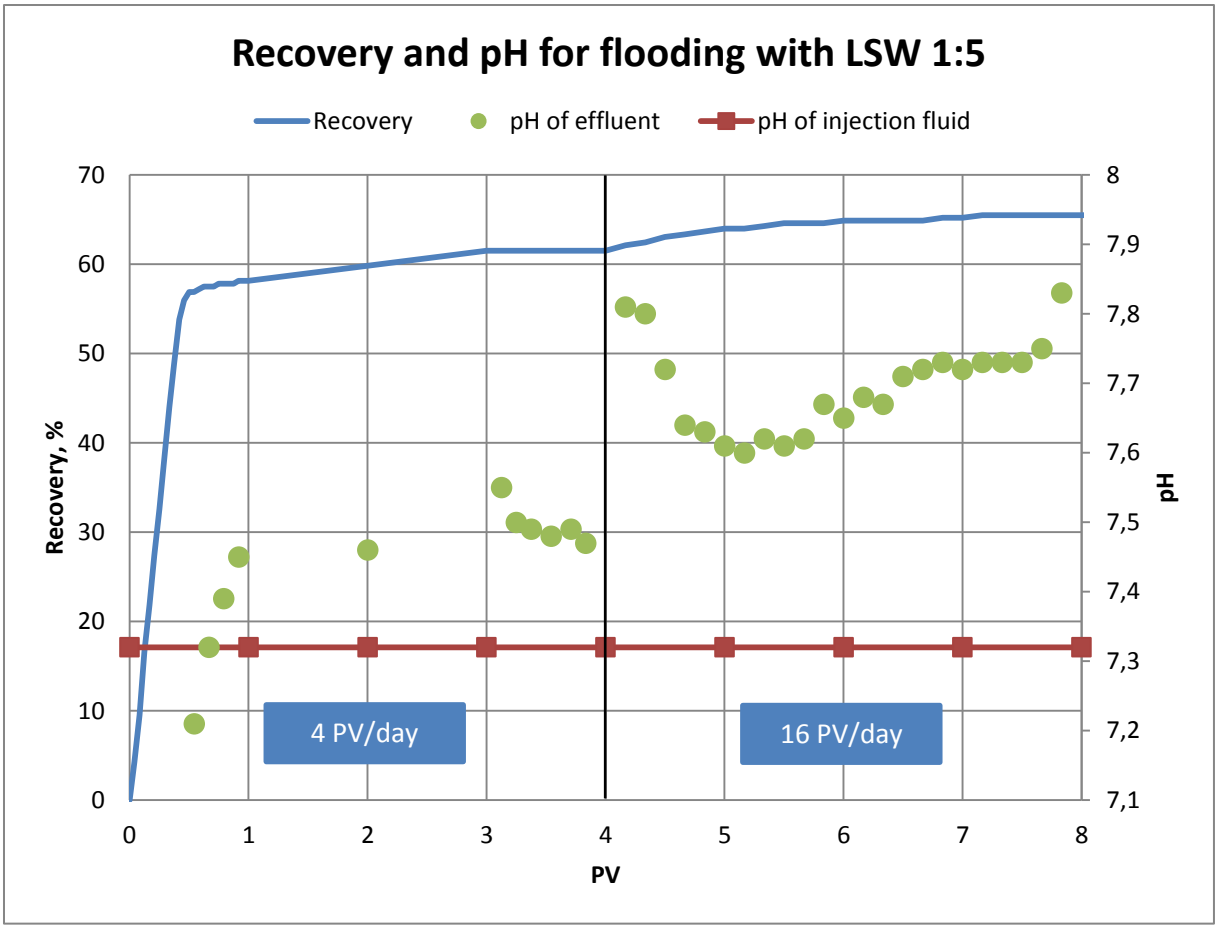

Figure 4.4 – Recovery and pH values during flooding with LSW 1:5.

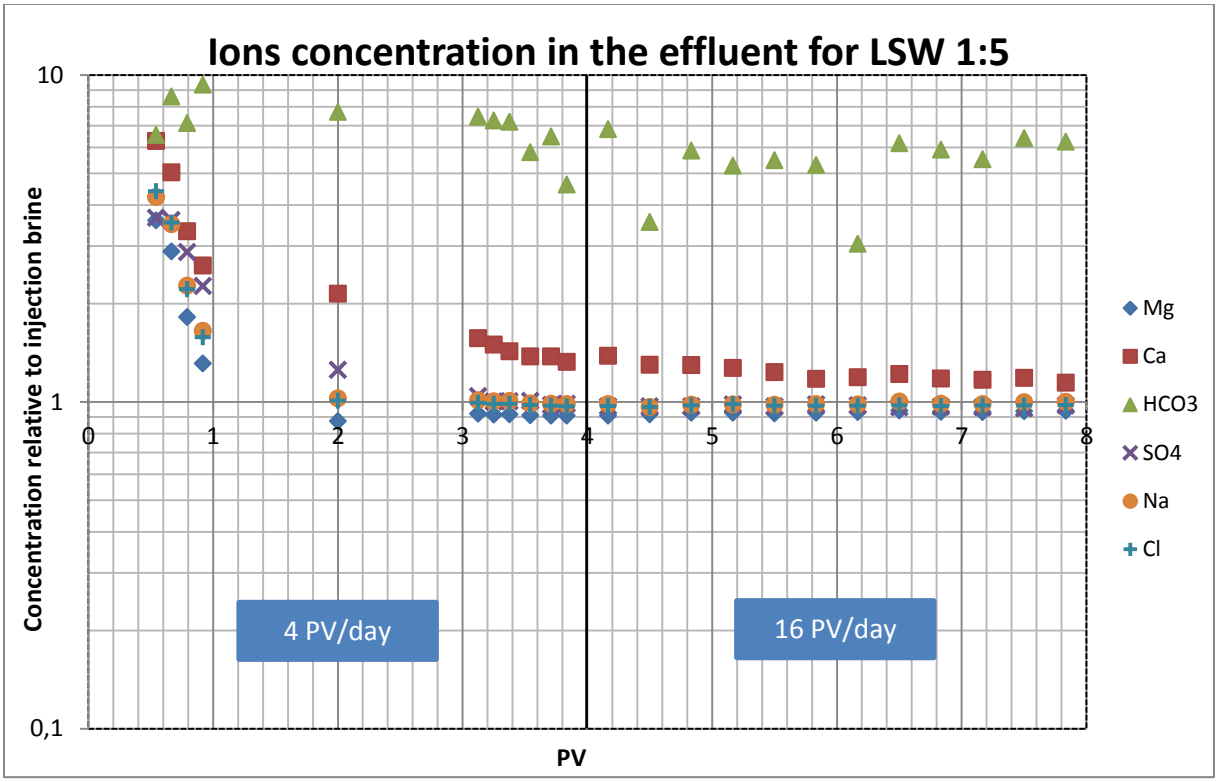

Figure 4.5 – Concentration of ions in the effluent samples, taken during flooding with LSW 1:5.

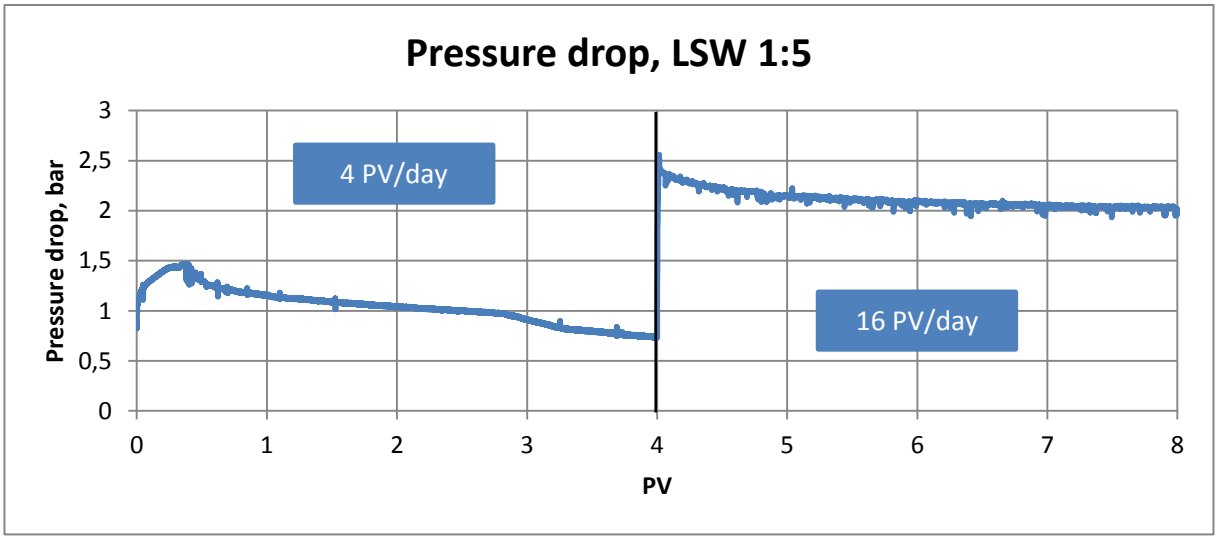

Figure 4.6 – Pressure drop across the core during flooding with LSW 1:5.

Now let's look more closely at the data and try to understand the processes which are going on during flooding. The recovery on the 4 PV/day flowrate is high compared to other cases. We also have late water breakthrough. The pressure drop graph has a high peak in the beginning of the flooding process. Before this peak the pressure drop values increase and after that decrease and stabilize at the level of 1 bar. This building up of pressure in the beginning can mean that we have some restrictions of the flow (possibly due to fine migration).

From ion chromatography we have the analysis of three cations – calcium, magnesium and sodium, and three anions – bicarbonate, chloride and sulfate. Fathi et al., 2010 indicated in his work, that neither sodium nor chloride is regarded as a potential determining ion toward the chalk surface, which means that these ions are not part of the inner Stern layer. This means that the concentration of these ions shouldn't change during the flooding process and we can take them as the base trend for comparing other ions. From the chromatography graph you can see that the relative concentration of these ions in the effluent first about three times higher than in the injection brine and then drops smoothly to the concentration equal to injected LSW 1:5. Higher values in the beginning are gotten because the core initially is saturated with SSW, so the effluent in the beginning is a mixture of SSW and LSW 1:5. The stabilizing of Na^+ and Cl^- at the relative concentration equal 1 confirms that those ions do not interact with calcite surface.

If we will look at calcium, we can see that from the beginning its concentration is higher than it is supposed to be. The high amount of calcium ions in the effluent is most probably connected to the dissolution of calcite surface. Dissolution of calcite in water can be expressed by the following equation (Hansen et al., 2000):

$$CaCO_3 + H_2O \rightarrow Ca^{2+} + HCO_3^- + OH^- \qquad (4.1)$$

Calcite dissolution results in enrichment of the water with calcium ions and carbonate alkalinity. Alkalinity of water-calcite system is described by the following equation (Lehmann et al., 2013):

$$\text{Alkalinity} = 2[CO_3^{2-}] + [HCO_3^-] + [OH^-] - [H^+] \qquad (4.2)$$

We can actually see the confirmation of this from the ion chromatography and pH graphs. The values for pH are increasing from the beginning of the flooding and keep at value higher than that of the injection fluid (7.46 in the effluent compared to 7.32 in the injection brine at 2 PV). We can also see increased amount of bicarbonate in the effluent – about 7.5 times more than in the injection fluid. Its trend does not exactly correspond with the pH trend. But the bicarbonate amount in the water based solution represents quite a complicated system. The actual carbonate species distribution is a function of pH. For example, at pH values below 6.35 at least 50% of the sum of carbonate system species appears in the form of H_2CO_3 (Lehmann et al., 2013). Moreover, the water that has been exposed to air becomes more acidic. This is because water absorbs carbon dioxide from the air, which is then slowly converted into bicarbonate and hydrogen ions (essentially creating carbonic acid), as indicates the equation below (Wikipedia, pH):

$$CO_2 + H_2O \leftrightarrow HCO_3^- + H^+ \qquad (4.3)$$

So the amount of bicarbonate from chromatography analysis does not represent the exact amount of this ion in the effluent samples, because: 1) the interaction of the effluent with the air, 2) the dilution of effluent samples with distilled water during preparations for ion chromatography, 3) the dependence of the system on pH of the solution.

Other thing that should be indicated about pH is that pH values represent first of all the concentration of H^+ ions in the effluent. They are relatively trustworthy, because the measurements of pH for the effluent samples were made right after taking water sample from the test-tube in order to exclude possible interaction with air. The water in the test-tube has synthetic oil above it, which is acquired during flooding process. The synthetic oil is located above the water because of density difference, and it keeps water from interacting with air. The increasing of pH can actually correspond with the idea that we have dissolution of calcite. In common the value of pH is higher for the effluent than for inlet brine, which corresponds with higher amount of bicarbonate. But the average value of bicarbonate gives more or less smooth line, which also correspond with calcium trend. So the increasing of pH (not the overall high value, but the trend itself) during flooding process should be connected to something else. Gomari and Hamouda, 2006 mentioned about the ability of hydrogen to penetrate into the calcite lattice. This maybe exactly the same process what we see here. For example let's look at the first pore volume of flooding. We have low enough pH level of the injection fluid, which can promote the above mentioned process. At first fluid flows through the channels with undissoluted calcite. The more dissolution we have, the more calcium we lose. So the surface becomes

more exhausted with respect to calcium ions (which are bearing the positive charge). Then the penetration of hydrogen in crystal lattice of calcite begins and the more fluid we flood, the more pH level increase.

The other process which can follow the dissolution of calcite is the losing of integrity of calcite surface. The dissolution itself doesn't explain the idea of fine migration, by which we try to explain high recovery and pressure drop peak. But the losing of integrity can lead to peeling off calcite particles from the surface. These particles then block the pore throats and this leads to increasing of sweep efficiency.

The other possible source of fines is the precipitation of salts, such as $CaSO_4$. This salts can also stuck the pore throats and influence sweep efficiency. But if we look at the trend for sulfate ions and compare it to the base trend for sodium and chloride, we will see that during the beginning of flooding the relative amount of SO_4^{2-} is at higher level than Na^+ and Cl^-. This actually means that we do not precipitate SO_4^{2-} ions with Ca^{2+}, but rather get sulfate from some dissolution process. This can be from the dissolution of mineral $CaSO_4$, which was located in the core pore space before flooding. Also, the ion chromatography for the very first effluent sample shows lower relative amount of SO_4^{2-}, than for the base trend. Gomari and Hamouda, 2006 wrote about the affinity of SO_4^{2-} ions to react with the available Ca^{2+} ions during aging process. So the reduced amount of sulfate in the first effluent sample can be due to this reaction.

The relative amount of magnesium ions during flooding process is lower than a base trend. Especially it is noticeable for the first pore volume of injected fluid. Hamouda et al., 2014 reported about the decreased amount for Mg^{2+} during beginning of the flooding, where it corresponds with the increased amount of Ca^{2+} ions. He also reported that this is online with observations made from Ekofisk field. So this lost amount of magnesium in the effluent can be explained by the affinity of this ion to the calcite surface.

Another interesting thing with the calcium ions is that after 3 PV its amount drops again and we can see a new trend. Its amount then stabilizes at a new level of 0.26 relative to SSW (the stabilization level before 3 PV was about 0.42 relative to SSW). In the following cases the amount of calcium will always be compared relative to SSW, because the graphs are made relative to the injection brine and comparing the concentration of calcium on the basis of inlet brine can bring misleading conclusions. The new trend for calcium ions corresponds with the decreasing pressure drop at this time. It can mean flooding out of some restrictions (the permeability for water increases and we can see lower pressure drop).

So let's now look at 16 PV/day flowrate. The pressure drop values here are higher, than for the low flowrate, which is in accordance with the Darcy law. In the beginning we can see that the peak for pressure drop is low and the pressure drop decreases to the stabilization level fast enough. This can mean that the injection fluid mostly flows through the existing channels, which are dissolute enough.

So we do not increase sweep efficiency very much, and as a result the recovery increment after changing of flowrate is low (+4%).

Amount of calcium is still higher than in the LSW 1:5, but it is decreasing. It can be connected to the fact that channels, through which water flows, are very dissolute. The amount of bicarbonate ions is still on the high level and has big deviations from average value for different effluent samples. Other ions keep at the concentration of LSW 1:5, with the exception of magnesium, where its concentration is slightly lower than in the injection fluid.

The interesting observation here is the shape of pH trend, where after 4 PV the pH value is high, then it decreases fast, and then slowly increases again. The possible explanation for this phenomenon will be given later, because it should be compared with the other cases.

4.3 Flooding with LSW 1:10

Core #3 was flooded with LSW 1:10 first at low flowrate 4 PV/day (0.123 ml/min) and then after 4 PV, when the recovery stopped increasing, the flowrate was switched to 16 PV/day (0.492 ml/min). This is the case of the highest recovery on low flowrate (62.6%) and the lowest recovery increment on high flowrate (+2.3%). The total recovery from this core amounts 64.9%. The recovery for LSW 1:10 compared to other cases is shown on Figure 4.7.

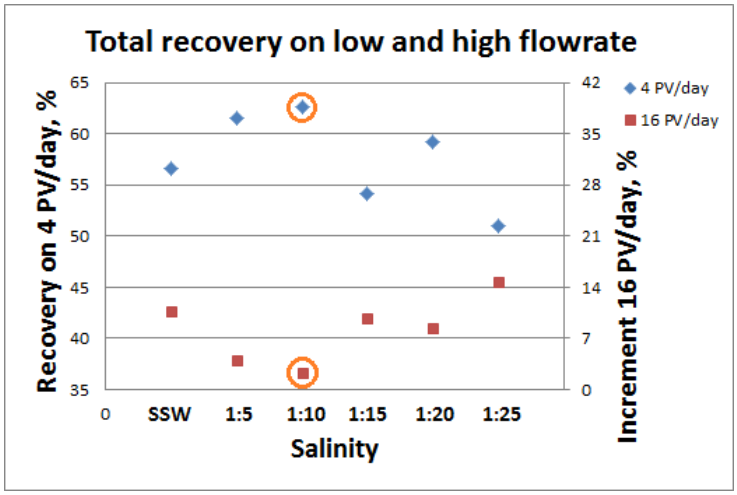

Figure 4.7 – Recovery for core #3 flooded with LSW 1:10 at two different flowrates, compared to other cases.

On the Figure 4.8 you can see the recovery during flooding with LSW 1:10 on both flowrates and pH values both for the effluent samples and the injection brine. The same conditions according to axis as in previously described case apply for this graph. All other graphs for all other cases are also made in the same way as for LSW 1:5. Figure 4.9 represents the ion chromatography analysis for LSW 1:10 effluent samples. Figure 4.10 shows the pressure drop values during flooding of core #3.

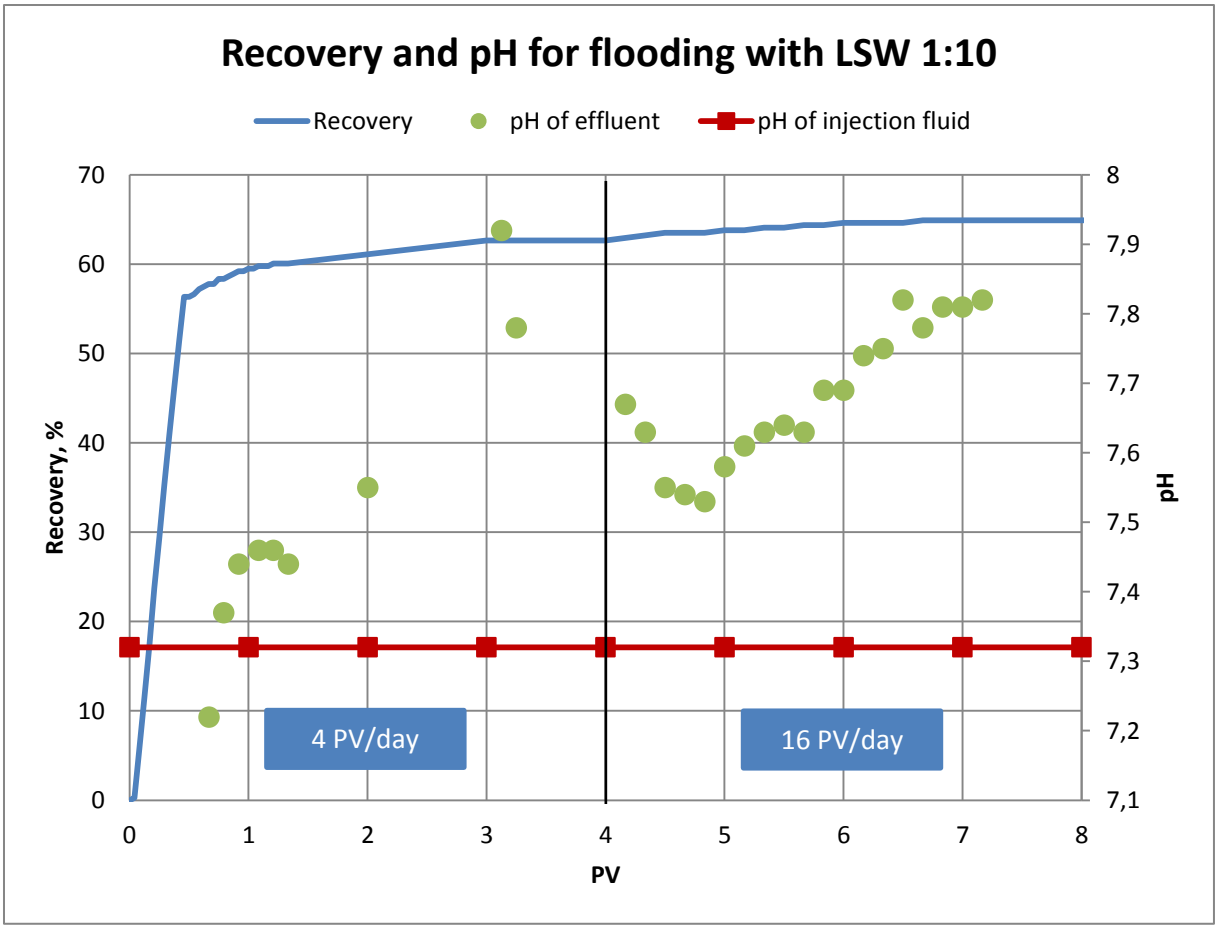

Figure 4.8 – Recovery and pH values during flooding with LSW 1:10.

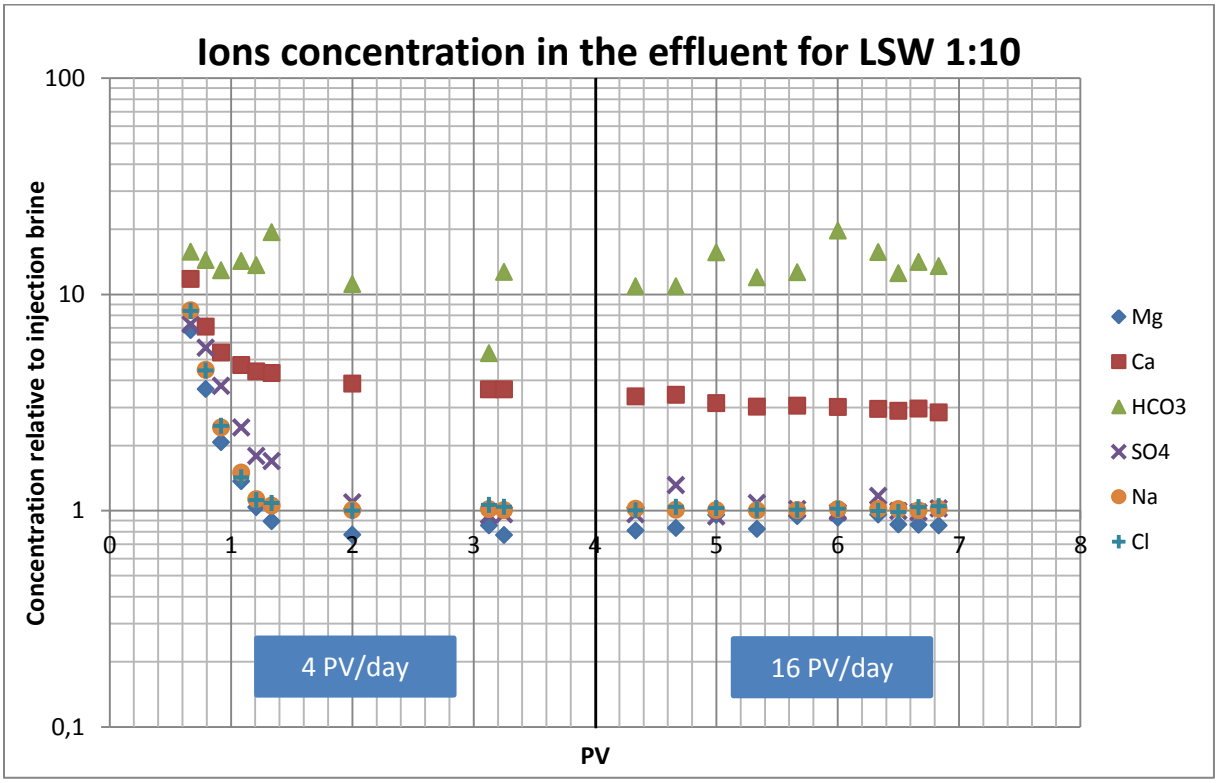

Figure 4.9 – Concentration of ions in the effluent samples, taken during flooding with LSW 1:10.

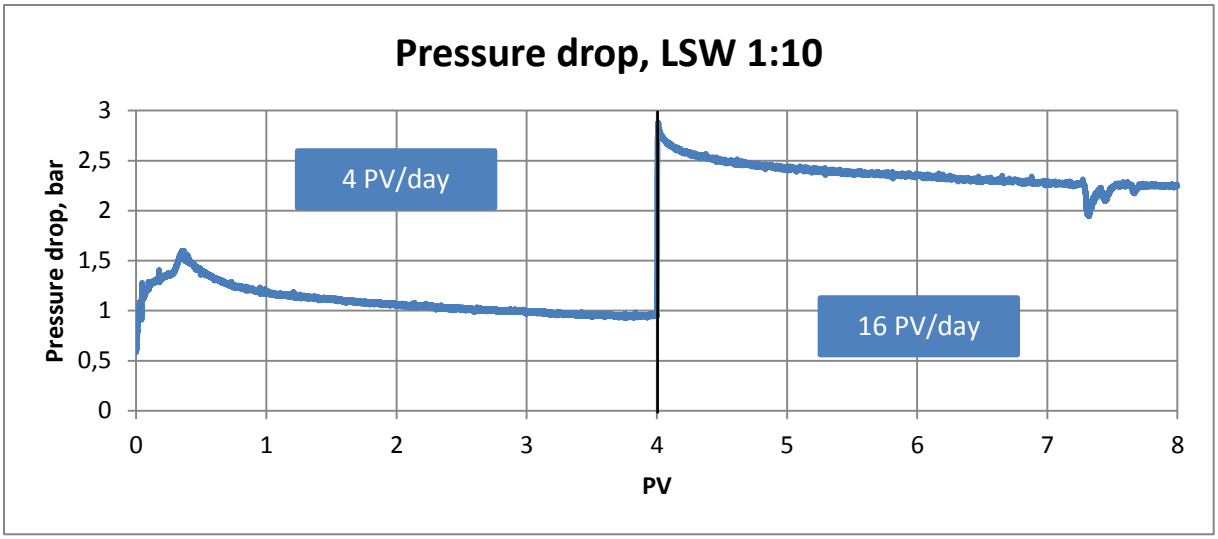

Figure 4.10 – Pressure drop across the core during flooding with LSW 1:10.

If we will take a look at the trends for ions, they look the same as in previous case with LSW 1:5, but the actual values are different. We again have sodium and chloride as a base trend to compare other ions with. The amount of calcium at 4 PV/day stabilizes at the value 0.39 SSW. It is less than in previous case and seems not to correspond with our idea of dissolution and fine migration, because here the recovery is higher. But the amount of calcium ions in the injection fluid in case of LSW 1:10 is two times less than in LSW 1:5. So the actual difference in calcium between the effluent and influent here is higher (0.29 SSW in LSW 1:10 versus 0.22 SSW in LSW 1:5). This can mean that during flooding with LSW 1:10 we do have more fine migration than in previous case. To get any confirmation of this idea we should look at the pressure drop graph.

The pressure drop peak in the beginning of the flooding with LSW 1:10 is higher than in LSW 1:5 case. The peak is located on the graph at the same value of injected fluid (about 0.35 PV) as in previous case, which also corresponds with the fact that water breakthrough happened about the same time as in previous cases. The water breakthrough actually happens a little bit later than pressure drop begins to reduce. It can be explained by the fact that the pressure drop is measured by the program Labview every 5 seconds, and the recovery is measured by looking at the effluent in the test-tube every 15 minutes. Moreover the core and the test-tube are connected by the line. So the actual water breakthrough happens earlier than we observe it.

So, according to the pressure drop graph, we do have in this case more fine migration and as a result more flow restrictions. If we compare the pressure drop trends before 3 PV for these two cases, we will see that they stabilize at the same value of about 1 bar, but the difference between the peak and stabilization level is higher for LSW 1:10. This indicates better sweep efficiency and as a result slightly more recovery.

The amount of sulfate here again is higher than a base line during first 2 PV of waterflooding, and the chromatography for the first effluent sample gives again lower result than for a base line. This

can indicate that we observe here the same processes regarding precipitation and dissolution of $CaSO_4$ salts as in case with LSW 1:5. The amount of magnesium ions is lower than a base line, which can mean the substitution of some of calcium ions (which went from the calcite surface into the brine during dissolution) with magnesium. The amount of bicarbonate is higher than in the influent, which correspond with the idea of dissolution of calcite.

The pH level on first PV again reaches the value close to 7.45, and the lost hydrogen ions can be explained partly by the higher amount of bicarbonate in the effluent and partly by penetration of hydrogen in the calcite lattice. Both of these processes are going on due to dissolution of calcite surface. If we compare the pH values for this experiment with LSW 1:5 after 3 PV of flooding, we will see that for LSW 1:10 the pH values are higher (7.8-7.9 as compared to 7.5 in case of LSW 1:5). But for previous case we observed the dropping of pressure drop level and calcium concentration in the effluent. We connected it to the fact, that some of the restrictions are flooded out. So this should mean that water flows through new less dissolute channels, which were previously stuck with fines. That's why the pH level is lower than in present experiment with LSW 1:10 – we flood less dissolute channels, so hydrogen ions penetrate the crystal lattice worse. In the experiment with LSW 1:10 we do not remove any restrictions after 3 PV, channels are very dissolute and hydrogen penetrate crystal lattice better. As a result pH level increases to higher values.

At 16 PV/day we have a low peak for pressure drop in the beginning, which corresponds with low recovery increment. The stabilization level for pressure drop and the actual value for the peak are higher in this case, but we should remember that for LSW 1:5 flooding we had decreasing of pressure drop between 3 PV and 4 PV. We also observe some deviations from the stabilization level for pressure drop values between 7 PV and 8 PV. It can mean fine migration.

The calcium concentration keeps first on the same level as was before switching of flowrate and then drops slowly. This corresponds with previous case, where we observed the same behavior for calcium ions. The amount of bicarbonate is on the high level, which is again can be due to dissolution of calcite. Magnesium ions have some relative concentration values, which are lower than the base line. This can mean substitution of Ca^{2+} with Mg^{2+}. The values for SO_4^{2-} ions are sometimes higher than the base line, which can mean dissolution of $CaSO_4$ salts.

The effluent samples pH has the same trend as for LSW 1:5, but there are differences in exact values. The next case with LSW 1:15 have the difference in recovery on 16 PV/day flowrates from the two cases which are already described. So we can compare it later and try to understand what's happening with pH.

4.4 Flooding with LSW 1:15

Flooding of core #4 was made with LSW 1:15 brine. The core was first flooded on low flowrate 4 PV/day (0.11 ml/min) for 4 PV, and then the flowrate was switched to 16 PV/day (0.44 ml/min). The recovery on low flowrate was 54.2%; on high flowrate the recovery increment of 9.7%

was observed. Total recovery for this core is 63.9%. The comparison of recovery on both flowrates for this experiment with other cases you can see on the Figure 4.11.

You can see from the figure below that the recovery increment on low flowrate for flooding with LSW 1:15 brine was considerably lower than in comparison with previous two cases. However, the recovery increment after switching of flowrate is much higher. To explain this difference, we should take a look at other data, which we got for this experiment. Figure 4.12 shows the recovery during flooding with LSW 1:15 and also pH values both for effluent samples and injection fluid. Figure 4.13 shows the ions concentrations in the effluent relative to the concentration in LSW 1:15 brine. Figure 4.14 has on it the pressure drop graph.

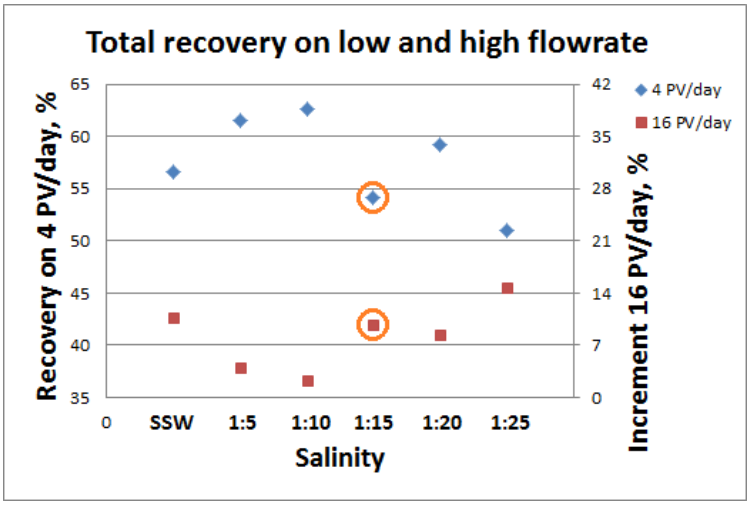

Figure 4.11 - Recovery for core #4 flooded with LSW 1:15 at two different flowrates, compared to other cases.

The first important difference from the previous two cases is the amount of calcium ions in the effluent. It is higher than a base line (like in previous cases), but the actual stabilization level is much lower, where the concentration of Ca^{2+} ions is about 0.25 relative to SSW. If we connect it to the idea of dissolution, happening during flooding of the core, then it should mean, that in case of LSW 1:15 the dissolution is much lower than in previous cases. Lower amount of dissolution, in turn, means that integrity of calcite surface is higher, and as a result we should have lower amount of fine migration. This can be the reason why the recovery on 4 PV/day is low here in comparison with LSW 1:5 and LSW 1:10. The confirmation for the lower amount of restrictions for the water flow can be found on pressure drop graph, so let's look at it. We can see on figure 45, that the peak of pressure drop in the beginning of the flooding is lower, than for previous two cases (1.3 bar in comparison with about 1.5 bar in previous cases).

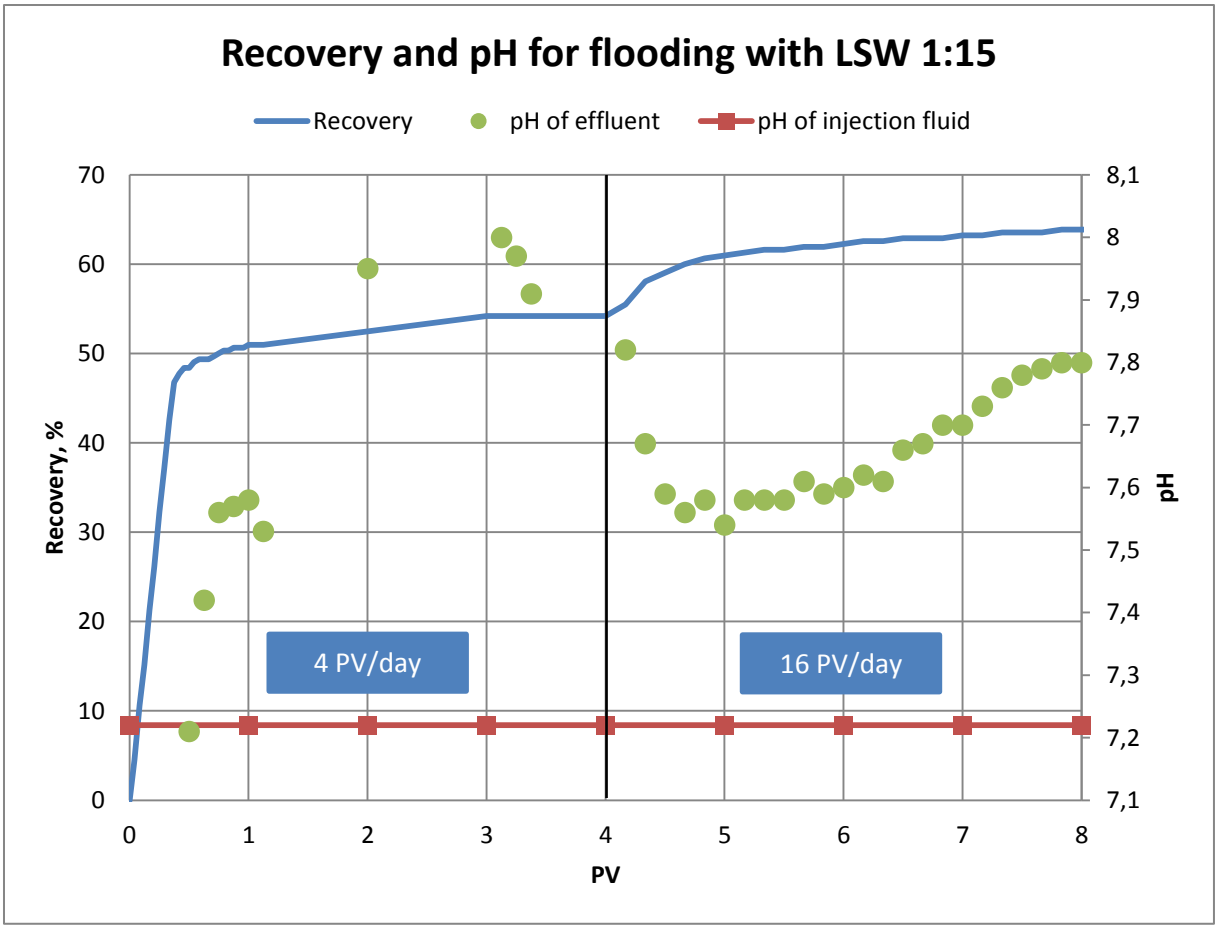

Figure 4.12 – Recovery and pH values during flooding with LSW 1:15.

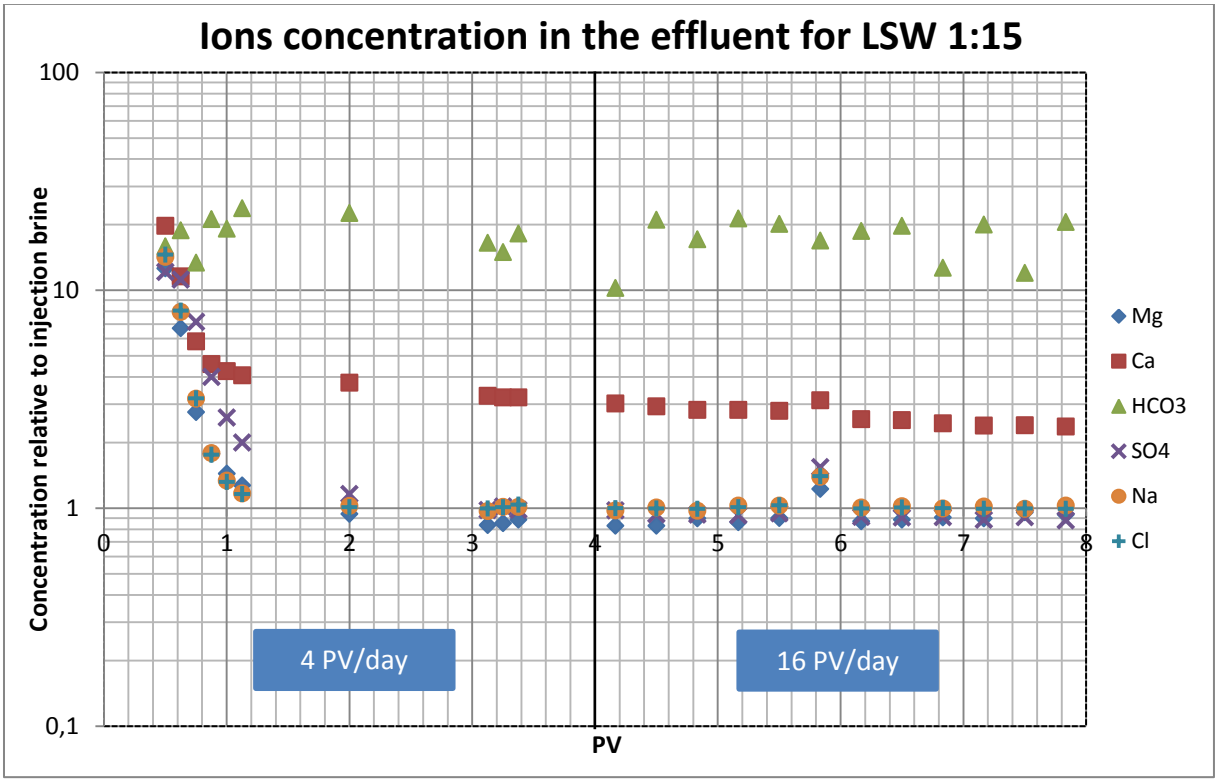

Figure 4.13 – Concentration of ions in the effluent samples, taken during flooding with LSW 1:15.

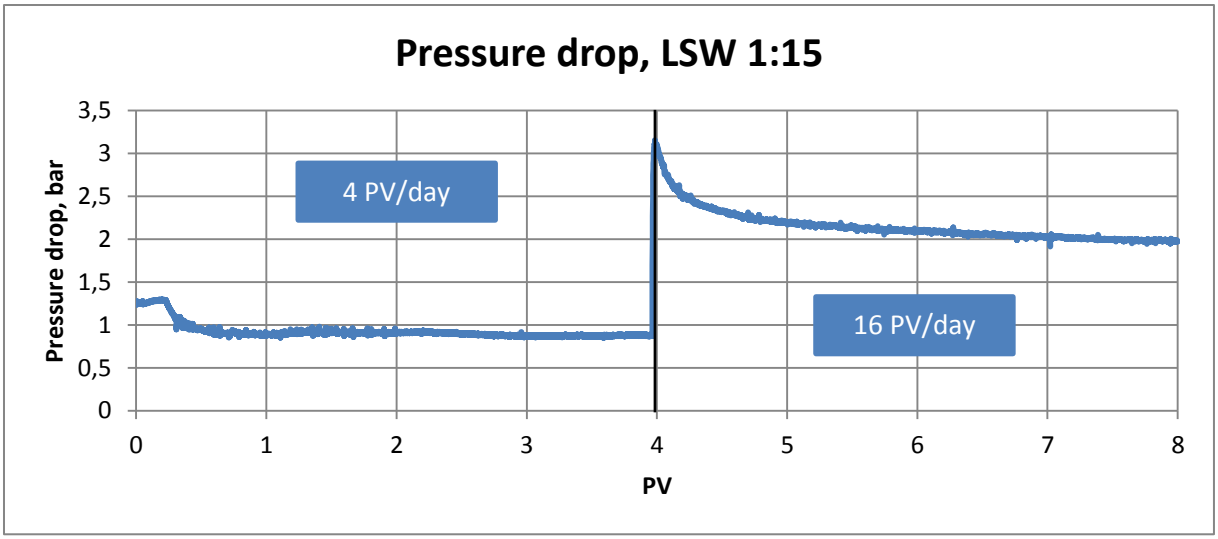

Figure 4.14 – Pressure drop across the core during flooding with LSW 1:15.

Another interesting phenomenon with a pressure drop graph is that stabilization level is lower, than in previous cases. Its value is equal to about 0.9 bar, and it is 0.1 bar lower, than for LSW 1:5 and LSW 1:10. The stabilization level should mainly be dependent on two parameters: absolute permeability of the core and the viscosity of the injection brine. As it was indicated in part 3.1.2 Table 3.3, the dynamic viscosity of all LSW brines is very similar, it changes in the range from 0.405 cP to 0.411 cP. So the explanation for difference in pressure drop should be searched in absolute permeability of different cores. As it was mentioned before, all cores were made out of the same piece of rock, and absolute permeability was measured for two cores. These cores where not used in flooding experiments, because the procedure of measuring absolute permeability includes pumping of the water through the core at different flowrates, which can damage the core (because of dissolution and channeling). As it was expected, the measurements gave the same result. But even if the cores are made out of the same piece of rock, it is still possible that they have different absolute permeability. Absolute permeability can also be changed during flooding experiment itself because of channeling.

The pH values during first PV of flooding reach the value of about 7.55. It is higher than in previous two cases, where pH reached the value 7.4. If we suppose that higher pH means that more amount of hydrogen penetrate crystal lattice of calcite, it actually corresponds with the sweep efficiency. In this case of flooding with LSW 1:15, sweep efficiency is worse, which means that the injection liquid flows through less amount of pore space. This leads to higher dissolution of the surface of these channels, which enable hydrogen ions to penetrate the calcite in higher amount. As a result, pH increases more.

The other ions trends look similar to those which we already saw in previous cases. Sodium and chloride we can take as a base line, because their concentration is equal for that of injection brine. First high values of these ions are due to mixing of LSW 1:15 with IWS brine. Bicarbonate level is high again and has big deviations from its average value. Sulfate amount is higher than in the injection

brine during first two PV of flooding, but the very first effluent sample has the value lower, then influent. Average magnesium relative concentration is less than for the injection brine, but the difference is not so pronounced, as in previous cases. This corresponds with lower amount of calcium, so if we accept the supposition that magnesium ions substitute calcium in crystal lattice of calcite, the lower difference between Ca^{2+} and the base line should lead to lower difference between Mg^{2+} and the base line.

The recovery increment after switching of flowrate to 16 PV/day is higher than in previous cases (+9.7% in present case against +2.3% and +4% in flooding with LSW 1:10 and LSW 1:5 respectively). There are also differences in other data, which can explain this phenomenon. If we will take a look at the pressure drop graph, we will see that the peak after switching to 16 PV/day is higher than in previous cases. Also the difference between the peak and the stabilization level constitutes here 1 bar, where in cases with LSW 1:10 and LSW 1:5 it was about 0.5 bar. The higher peak can mean that we observe here flooding out of some amount of fines, and higher difference between the peak value and the stabilization level can mean greater increasing of permeability due to reduced amount of fines sticking pore throats. One problem which we can see with this explanation is that we suppose that amount of dissolution (and as a result fine migration) is lower in case of LSW 1:15. But this also can mean that in cases with LSW 1:10 and LSW 1:5 the pores are stuck so severely with fines, that we cannot flood them out by means of increasing the flowrate. Another possible explanation for the behavior of pressure drop lies in the amount of pores, through which the injection brine flew on low flowrate. It was supposed before that higher amount of dissolution leads to the improvement of sweep efficiency through fine migration. If we do have in case of flooding with LSW 1:15 worse sweep efficiency, the brine flows through less amount of pore volume (this can be confirmed by lower recovery on 4 PV/day). When we switch to higher flowrate, this amount of pore space will not be enough for flooding. That's why the water penetrate new pores and we see on the pressure drop graph both high peak in the beginning and high difference between this peak and stabilization level. This increased sweep efficiency leads to higher recovery increment than in previous cases. If we now try to connect this with previous cases, we can suppose, that LSW 1:10 and LSW 1:5 already had high sweep efficiency on low flowrate, and switching to 16 PV/day does not make the injection fluid to penetrate much amount of new pores.

The second difference on 16 PV/day between LSW 1:15 and two experiments described before lies in pH trend. If we will take a look at it we will see that the shape of pH graph looks the same for all three cases, but pH for LSW 1:15 increases after 6 PV, and for LSW 1:10 and LSW 1:5 it increased after 5 PV. It can actually be a very good confirmation of the greater increase of sweep efficiency in present case. If we will recall the connection between hydrogen ions penetrating the crystal lattice of dissolute channels of calcite and the increase in pH values, it will tell us that in case of LSW 1:15 we flood more amount of new pores. The surface of these pores is undissoluted in the beginning of flooding on 16 PV/day and we see decreasing of pH values. The amount of these pores is

higher than in previous cases, it takes more time for dissolution, that's why we observe the increase of pH not after 5 PV but after 6 PV.

The values for calcium relative concentration keep more or less on the same level before 6 PV, but begin slowly to decrease after. This can also be the confirmation of dissolution of new pore space, where before 6 PV the surface of these pores undergoes the dissolution process and after 6 PV pores are already dissolute enough, and the amount of Ca^{2+} ions in the effluent samples drops.

For other ions we can see the same trends as in previous cases. The chromatography for the samples just before 6 PV gave strange results, where the amount of all ions in the effluent is higher in comparison with overall trend. This can be an error of chromatograph, but the chromatography is made separately for anions and cations (different columns are used for it). So the most probably this error happened during the preparation for chromatography, when samples were diluted 50 times with deionized water. The higher values for all ions in this sample maybe due to the error of dilution machine, where it could for some reason dilute sample less than 50 times. The magnesium and sulfate ions trends show the same behavior as before. Bicarbonate again keeps on high level.

4.5 Flooding with LSW 1:20

For core #5 the flooding experiment was made with LSW 1:20 brine. Firstly, the core was flooded on low flowrate of 4 PV/day (0.11 ml/min). The recovery was equal 59.2% and it is the third highest result after LSW 1:10 and LSW 1:5. After 4 PV of flooding the flowrate was switched to 16 PV/day (0.44 ml/min). The recovery increment of 8.4% was gotten, which is also high enough compared to other cases. The total recovery for flooding with LSW 1:20 brine is 67.6%. You can see the comparison of recovery on both flowrates on Figure 4.15. Figure 4.16 shows the recovery trend during flooding process and pH values for effluent samples and influent. Figure 4.17 shows ions concentrations for the effluent samples relative to LSW 1:20. Figure 4.18 has on it the pressure drop trend for this case.

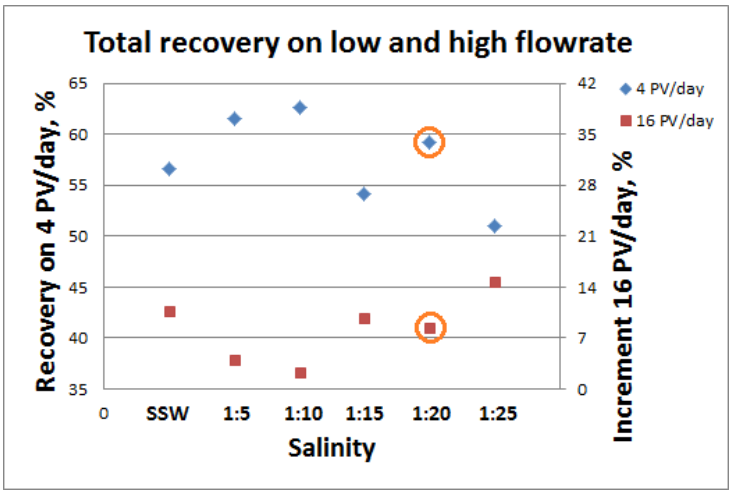

Figure 4.15 – Recovery for core #5 flooded with LSW 1:20 at two different flowrates, compared to other cases.

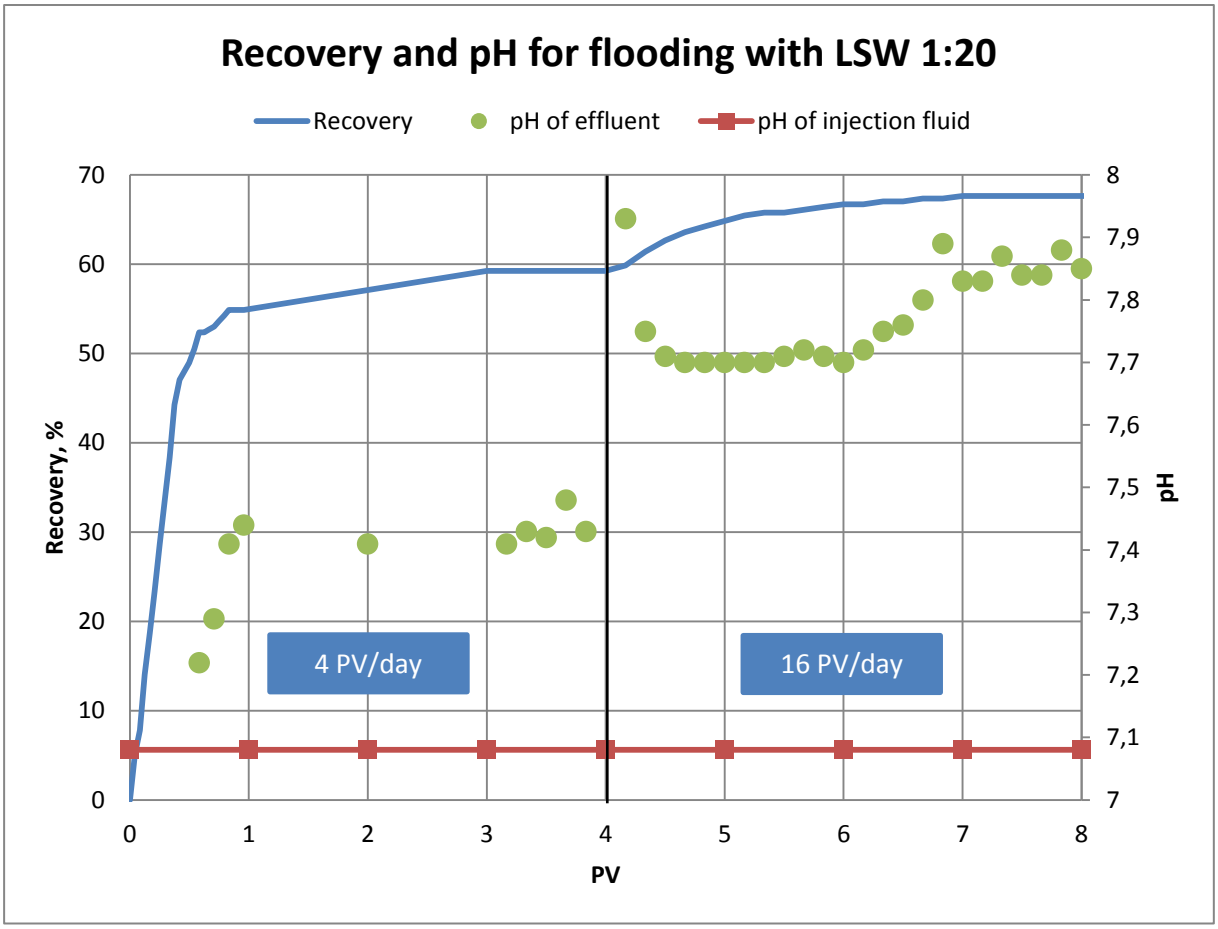

Figure 4.16 – Recovery and pH values during flooding with LSW 1:20.

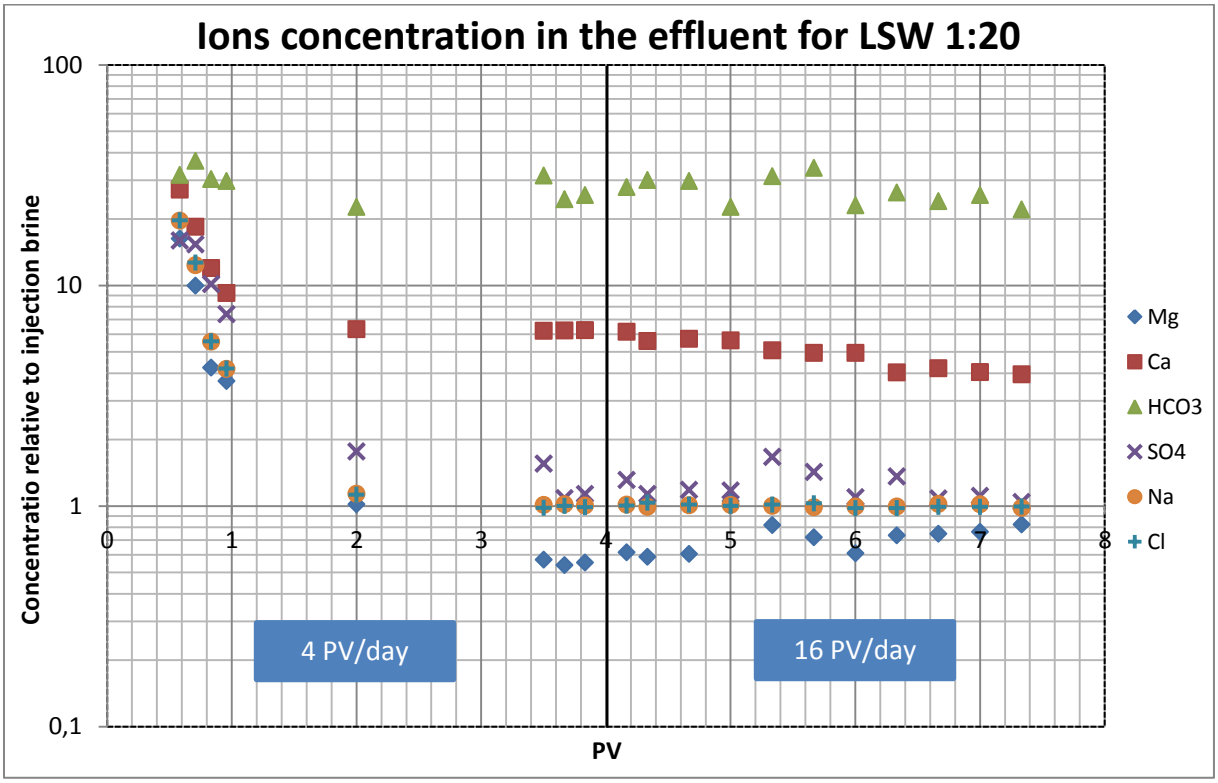

Figure 4.17 – Concentration of ions in the effluent samples, taken during flooding with LSW 1:20.

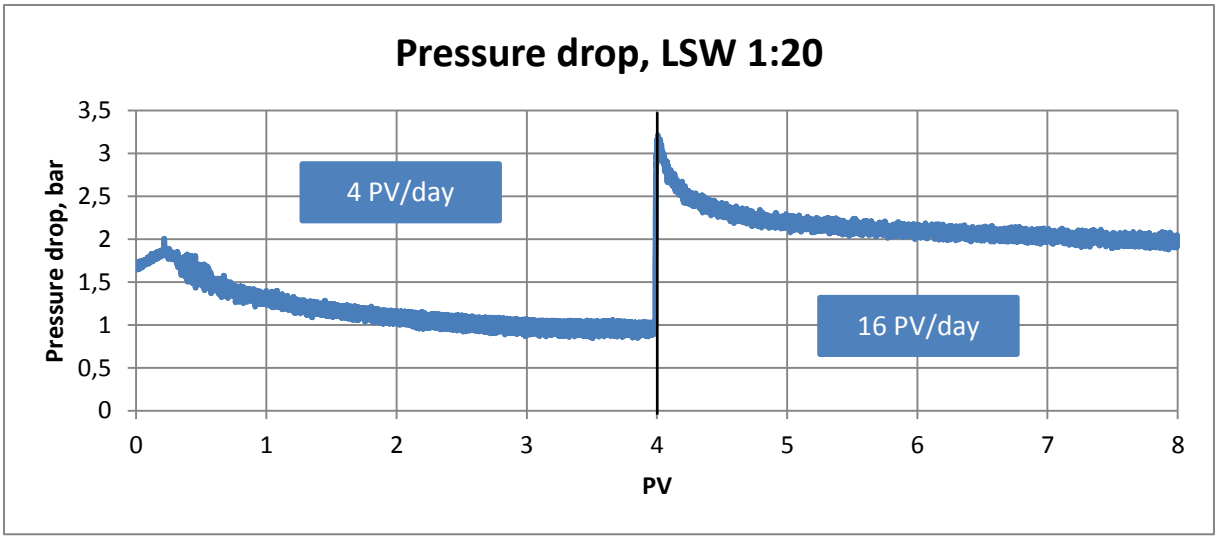

Figure 4.18 – Pressure drop across the core during flooding with LSW 1:20.

High enough recovery on low flowrate corresponds again with high pressure drop peak in the beginning of the flooding. The actual value of the peak is even higher than in flooding with LSW 1:10 and LSW 1:5, where we had greater recovery. But this experiment was made on the other equipment due to limited capacity of the laboratory and other people working there. You can see that deviations from average value for pressure drop are much higher for this experiment (in previous experiments the line was much thinner). This observation indicates that sensitivity for pressure drop manometer on this equipment is much lower. The higher value of the peak can be because of the error of manometer or due to some other reason. The important thing here is that stabilization level for pressure drop in this experiment is the same with LSW 1:5 and LSW 1:10, which indicates the reliability of acquired data.

The amount of calcium during flooding on 4 PV/day is high again and the concentration is equal to 0.32 SSW. This can mean high amount of dissolution and fine migration, which leads to increase of sweep efficiency. The bicarbonate concentration keeps again on high level which can be the confirmation of calcite dissolution.

High values of sulfate in the effluent can mean dissolution of $CaSO_4$ salts. They could be deposited as minerals inside the core and therefore existed before flooding experiment, or could precipitate during flooding itself. The first effluent sample has the reduced concentration for SO_4^{2-} ions which can confirm the precipitation of $CaSO_4$ salts.

Now let's take a look at pH trend. At first PV pH values rise to 7.44, which is similar with LSW 1:5 and 1:10, where we also had high recovery and high peak for pressure drop. The difference we can see in interval between 3 PV and 4 PV, where the values are not rising. Before it was proposed that the rising of pH means penetration of hydrogen ions in the calcite lattice, when channels are very dissolute. Here we should also have dissolute channels, but pH does not rise. But on ions chromatography we can see the data, which can explain this phenomenon. If we will look at the values for relative concentration of magnesium, we will see that they are much lower than the base line. It can

mean that for some reason the dissolute calcium here is substituted by magnesium ions. As a result hydrogen does not penetrate calcite in so large amount as in cases of LSW 1:5 and LSW 1:10, and pH level does not increase so sharply.

After switching the flowrate to 16 PV/day the pressure drop graph shows a peak, which looks similar to the one in case of LSW 1:15. There we also had high recovery increment after increase of flowrate, so the results seem to correspond. It should be mentioned, that the high peak here can be either due to fines, sticking the pore throats, or just due to shortage of pore space, through which injection fluid can flow. Both of these processes in the end lead to increase of sweep efficiency and also high recovery increment, which was observed.

As it was mentioned before, under the conditions of flooding with low flowrates capillary forces may dominate the flow and oil production will be strongly affected by capillary end effect, especially for non-water-wet rock (Al-Harrasi et al., 2012). It can be supposed, that the amount of recovery increment on high flowrate in our case is only due to capillary end effect, where the low recovery on 4 PV/day correspond with high recovery increment on 16 PV/day and vice versa. But then the total recovery should be equal for all experiments, and the real data show that it's different for the four cases described before. Therefore, it means that the recovery increment on the high flowrate depends also on some other processes, which are going on inside the core during flooding, such as dissolution and fine migration.

The other parallel between this experiment and LSW 1:15 is the pH trend for high flowrate. Here it has the same tendency to increase after 6 PV and not after 5 PV as in case of LSW 1:10 and LSW 1:5. This can be the confirmation of better sweep efficiency, where the injection fluid flows through more amount of undissoluted channels and it takes more time for pH values starting to increase.

The ions chromatography gives similar results, as in previous cases. The Ca^{2+} ions concentration decreases slowly during flooding on 16 PV/day flowrate. After 6 PV the relative concentration of this ion drops slightly, which can be the indication, that channels are very dissolute, and pH values begin to increase at the same time. Bicarbonate concentration is high, which corresponds with calcite dissolution.

The amount of sulfate here is higher than in the injection brine in some cases, which can be due to the dissolution of $CaSO_4$ salts. Magnesium ions show lower values, than for the base line, which can be due to substitution of dissolute calcium with magnesium. This tendency is more pronounced than in all previous cases, but we should not forget, that we suppose that dissolution here is also high on both flowrates. This corresponds also with the total recovery, which is the highest from all four described cases, and recovery itself depends on the sweep efficiency. The more pronounced difference in magnesium on the graph is also partly due to the fact, that the values are relative to the injection brine, and here the salinity is lower.

4.6 Flooding with LSW 1:25

The flooding experiment for core #6 was made with LSW 1:25 brine. First of all the core was flooded on 4 PV/day flowrate (0.115 ml/min) for 4 PV, than the flowrate was switched to 16 PV/day (0.46 ml/min). The flooding on low flowrate brought 51% OOIC recovery. After switching of flowrate additional 14.7% recovery was acquired. The total recovery from this core is 65.7% OOIC. The comparison of recovery on both flowrates for LSW 1:25 with other experiments you can see on Figure 4.19.

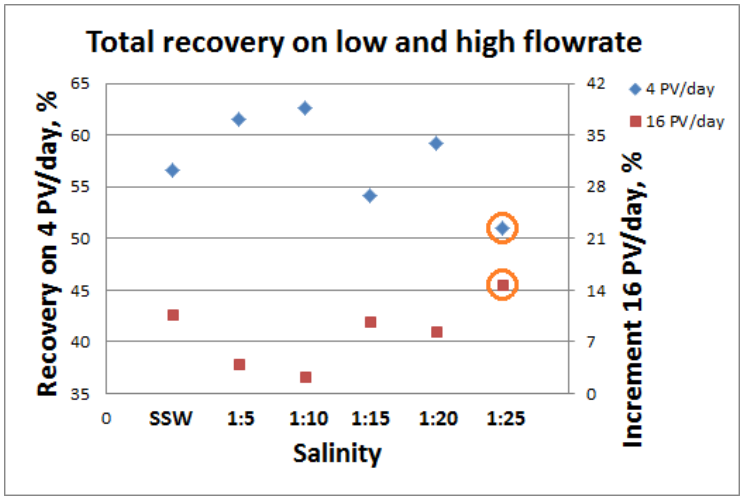

Figure 4.19 – Recovery for core #6 flooded with LSW 1:25 at two different flowrates, compared to other cases.

As you can see from the graph above, the recovery on low flowrate for LSW 1:25 experiment represents the lowest value from all six cases. However, on high flowrate the recovery increment is the highest from all experiments. Let's now take a look at the other data acquired during experiment with LSW 1:25 brine, and see if they correspond with our previous ideas. On the Figure 4.20 you can see the recovery trend during flooding process and pH values of effluent samples and the injection brine. Figure 4.21 shows relative ions concentration for the effluent samples with respect to the concentration in the injection brine. Figure 4.22 shows the pressure drop trend during the flooding process.

As the chromatography analysis shows, the calcium concentration stabilizes at level 0.16 relative to SSW. This is much lower than in all previous cases. According to the discussion that was performed before, the low amount of Ca^{2+} ions in the effluent should mean less dissolution, which in its turn leads to lower amount of fine migration. The waterflow meets fewer restrictions on its way and sweep efficiency does not increase much. As a result the recovery should be low, as in fact is observed. The confirmation for this theory should be found on pressure drop graph. If we will take a look at it, we will see that the peak is shifted much to the left in comparison with previous cases. This corresponds with earlier water breakthrough and low recovery.

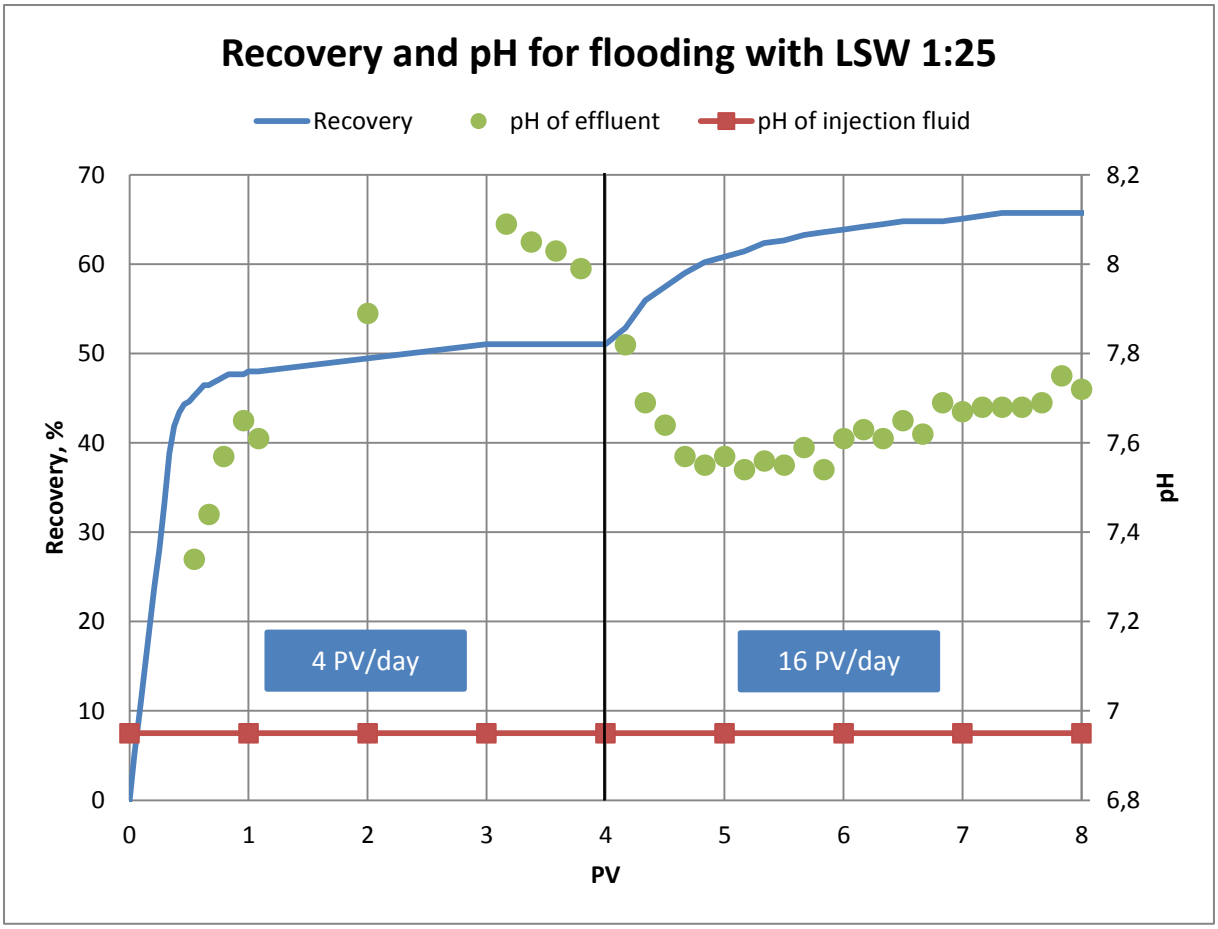

Figure 4.20 – Recovery and pH values during flooding with LSW 1:25.

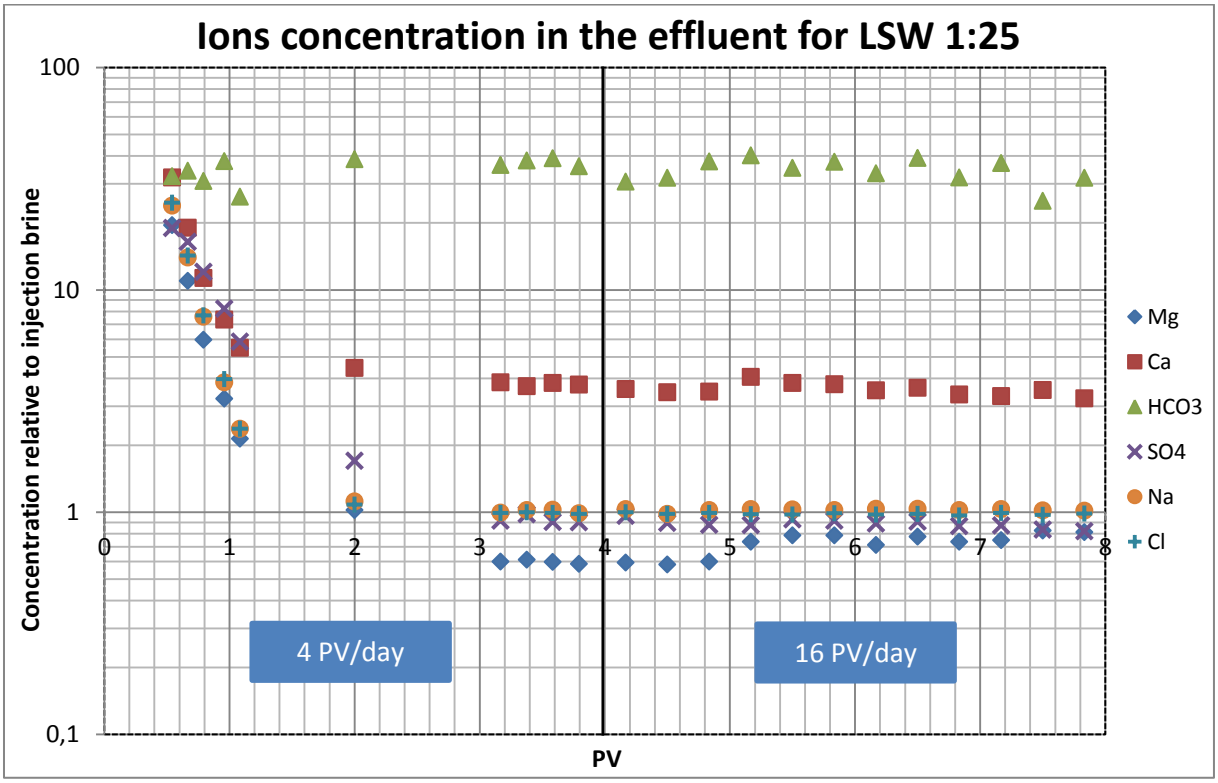

Figure 4.21 – Concentration of ions in the effluent samples, taken during flooding with LSW 1:25.

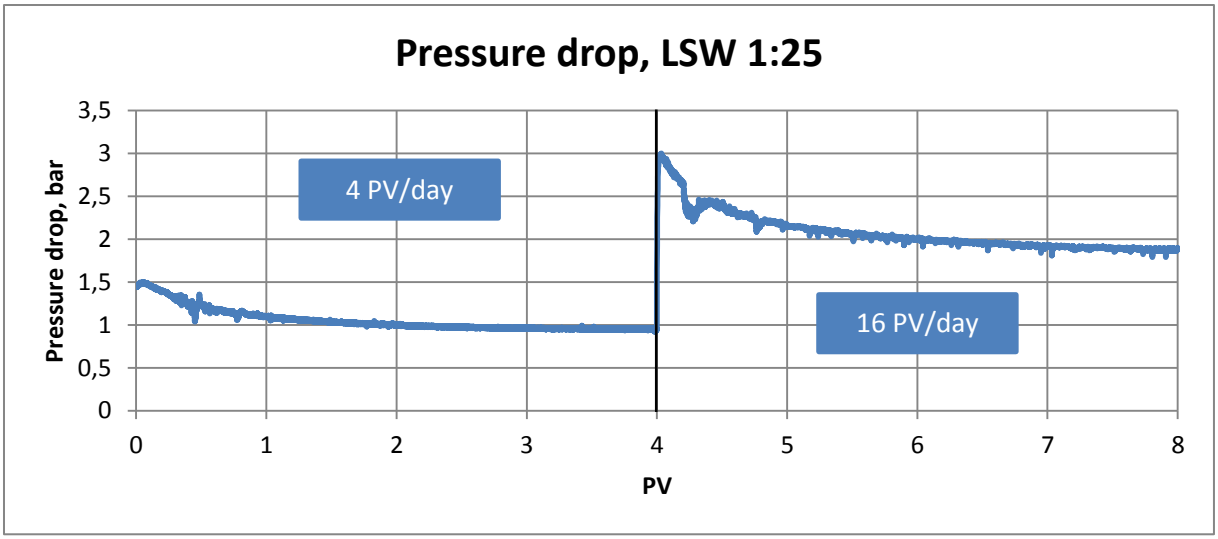

Figure 4.22 – Pressure drop across the core during flooding with LSW 1:25.

The value of the pressure drop peak itself is almost the same with LSW 1:5 and a little bit lower than LSW 1:10, but we do not see here long building of pressure drop as in those two cases, which can be the indication of shortage of flow restrictions.

The pH values during first PV of flooding rise to 7.65. It is much higher than in cases of LSW 1:5 and LSW 1:10, and it is even higher than in case of LSW 1:15, where also the low recovery was observed. It can be the indication of the low sweep efficiency, and that channels through which the injection fluid flows are very dissolute. As the flooding proceeds, the pH values rise higher and the maximum detected point here is equal to 8.09, which is the highest from all described cases. Again it can be the indication of the very dissolute channels.

The trend for sodium and chloride ions we can use again as the base line for comparison with the other ions both during mixing zone (where the concentrations are higher due to initial saturation with SSW) and during the stabilization level (when the effluent is not anymore influenced by the SSW). We can observe the similar behavior for bicarbonate, where the relative concentration values deviate very much from the average and overall keep at the high level (can be the indication of calcite dissolution). Sulfate amount is higher than the base line during first 2 PV of flooding, with the very first point lower than the base line, as we already observed for all described cases. Magnesium ions values are lower than the base line. This difference is noticeable especially between 3 PV and 4 PV of flooding maybe due to the fact, that channels are very dissolute and we observe here the substitution of dissolute Ca^{2+} ions with Mg^{2+}. Also this difference is so pronounced partly due to the fact that the values are relative to LSW 1:25, which is the lowest salinity from all experiments.

After switching to 16 PV/day flowrate the pressure drop peak is high and looks similar to LSW 1:15 and LSW 1:20, where we also observed high recovery increment on high flowrate. The difference between stabilization level and the peak value is about the same as in previous cases, but recovery increment is 1.5 times higher. This can be due to the fact, that recovery on low flowrate was

the lowest from all described cases, which means that at the moment when the flowrate was switched to 16 PV/day a lot of oil was left inside the pore space of the core.

The pH trend is comparable to those of LSW 1:15 and LSW 1:20 experiments. The pH values begin to increase after 6 PV as in before mentioned two cases. This can be a confirmation that the sweep efficiency is increased better than in experiments with LSW 1:5 and LSW 1:10, and the injection fluid floods more amount of undissoluted pore space. We can also see, that pH increase between 6 PV and 8 PV is equal to about 0.1-0.12 versus 0.15-0.2 in case of LSW 1:15 and LSW 1:20. It also corresponds with ion chromatography results, where it is shown that the decreasing of the amount of calcium in the effluent is not so pronounced as in those two cases. It correlates with 1.5 higher recovery increment for LSW 1:25 in comparison with the recovery data for LSW 1:15 and LSW 1:20 because of better improvement of sweep efficiency.

Bicarbonate and magnesium ions look similar with what we observed before with other experiments. Sulfate here shows concentrations lower than for the base line. The same phenomenon can be noticed in case of flooding with LSW 1:15 on 16 PV/day and also in case of some samples with other salinities, so here the difference is more pronounced due to low salinity of LSW 1:25 brine. These results can indicate some amount of precipitation of $CaSO_4$ salts during flooding process.

4.7 Flooding with SSW

The flooding with SSW is described the last after all cases of flooding with brines of low salinity. The reason for this is that both the pH and the ion chromatography graphs are comparable for LSW fluids. SSW, however, represents a very different case mainly due to three factors: 1) High ions concentrations in SSW injection brine 2) The initial water saturation made with SSW itself in all cases, which means that the mixing zone will look different here in comparison with LSW flooding 3) Higher pH of SSW brine. That's why it is more convenient to describe SSW after all LSW flooding experiments and not vice versa.

The core #2 was flooded first on 4 PV/day flowrate (0.11 ml/min) for 4 PV. Then the flowrate was switched to 16 PV/day (0.44 ml/min). The recovery on low flowrate is equal 56.6%. The recovery increment after switching of flowrate is 10.8%. The total recovery form this core is 67.4%. The comparison of recovery on both flowrates with brines of other salinities you can see on Figure 4.23.

If we will compare the recovery with all other experiments, we can see that on 4 PV/day the recovery is relatively low and on 16 PV/day the recovery increment is high. On the Figure 4.24 you can see the recovery during flooding experiment with SSW and also the pH for effluent and injection fluid. You can see that for core #2 it took more time to achieve residual oil saturation than for previous cases (9 PV versus less than 8 PV respectively). Figure 4.25 shows relative ion concentration for the effluent samples (SSW injection brine concentrations are taken as a reference here). The difference between the effluent and the reference is less pronounced because of high concentrations of ions in the injection brine. Figure 4.26 shows pressure drop trend during flooding experiment.

If we will take a look at pH values of the effluent, we will see that they are lower than for injection brine. Hamouda et al., 2014 observed the same phenomenon during flooding of chalk and sandstone cores with SSW brine. It was also indicated in his work, that the decrease in pH during flooding with SSW brine is consistent with the observations by other researchers. Hamouda and Valderhaug, 2014 proposed that the pH reduction may be due to hydration of magnesium ions.

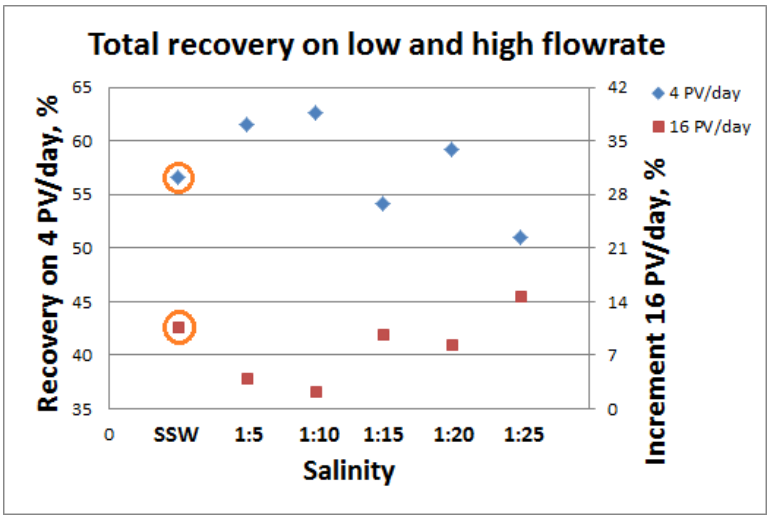

Figure 4.23 – Recovery for core #2 flooded with SSW at two different flowrates, compared to other cases.

Overall the shape of pH graph is similar to that of flooding with LSW brines. We can see here the increase of pH from about 7.05 in the beginning to 7.25 after 3 PV. Then pH drops in the interval between 3 PV and 4 PV. After switching to 16 PV/day pH first drops just after 4 PV and then increase again after 6 PV. This similarity between the shape of pH graphs for SSW and LSW brines can indicate that the same processes are going on inside the core during flooding. However, the values are different for SSW and LSW brines, so it's difficult to compare the amount of interaction by pH graphs. Besides in case of SSW the deviations in pH values are higher. This can be due to the fact that in case of SSW the pH values are influenced by two processes – lowering of pH due to high salinity of the injection brine and increasing due to the dissolution of calcite.

The pressure drop trend in the beginning of the flooding has a peak, similar to what we noticed before with other salinities. We can compare its value to the LSW 1:20 brine, because these two experiments were done on the same equipment. The peak value for SSW is lower, than for LSW 1:20. This corresponds with lower recovery in present case. It can mean that in the case of SSW the amount of fine migration is lower, sweep efficiency therefore is worse and as a result the recovery is also worse.

Another interesting observation with the pressure drop on the low flowrate is that the stabilization level for SSW is equal to about 1.1 bar, which is higher than in all previous cases. It can be explained by higher viscosity of SSW brine in comparison with LSW.

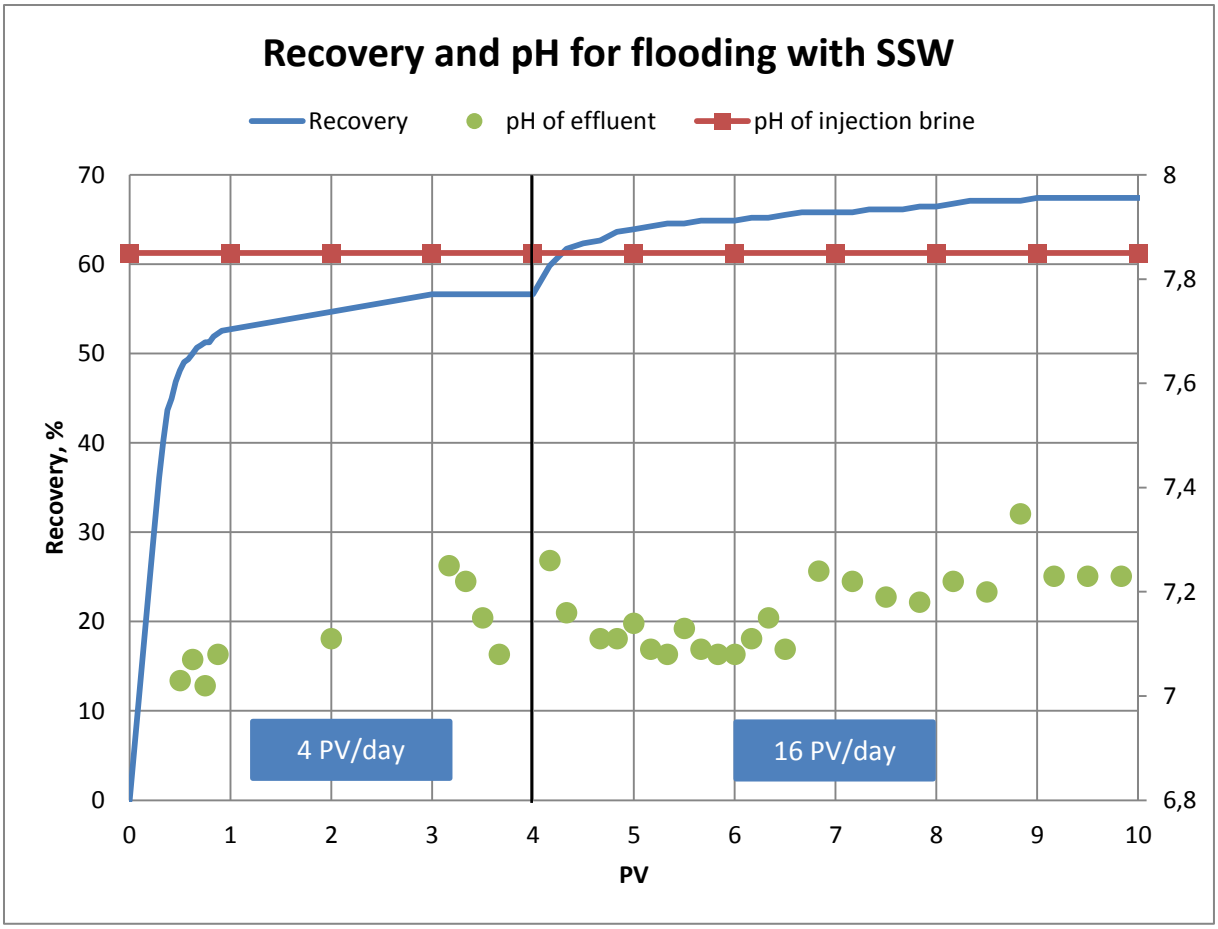

Figure 4.24 – Recovery and pH values during flooding with SSW.

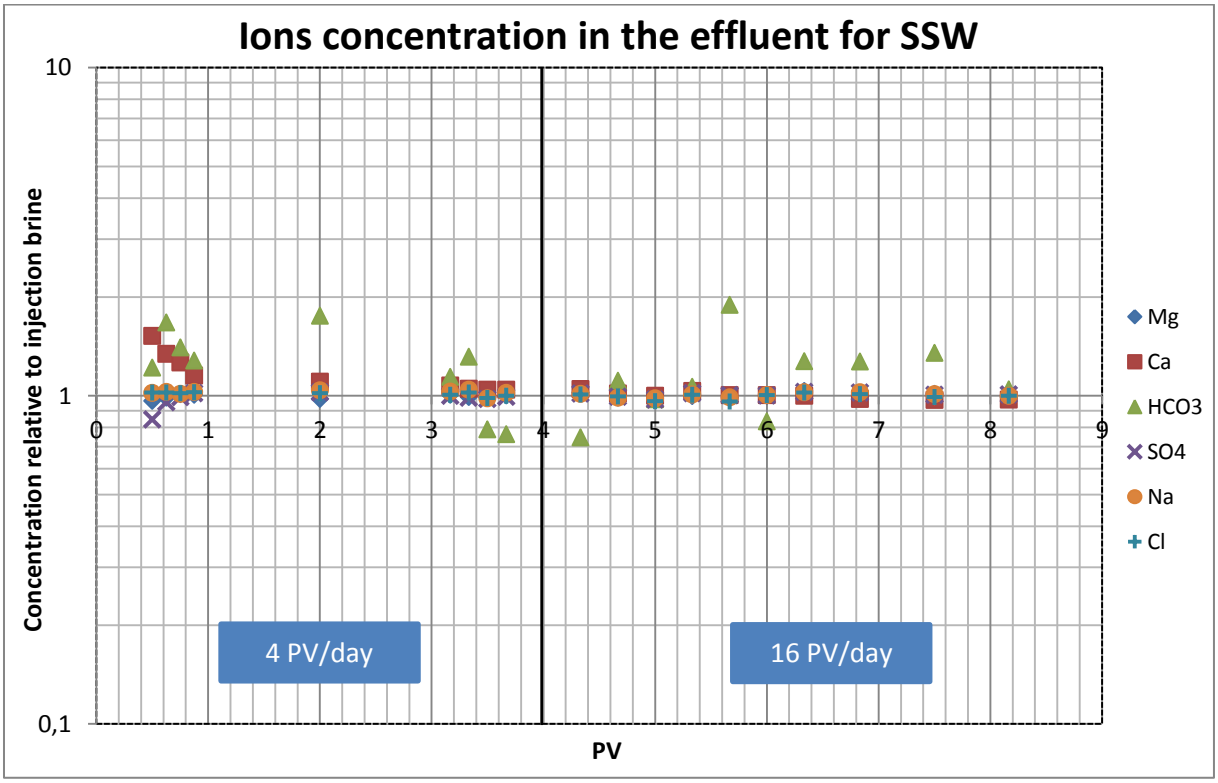

Figure 4.25 – Concentration of ions in the effluent samples, taken during flooding with SSW.

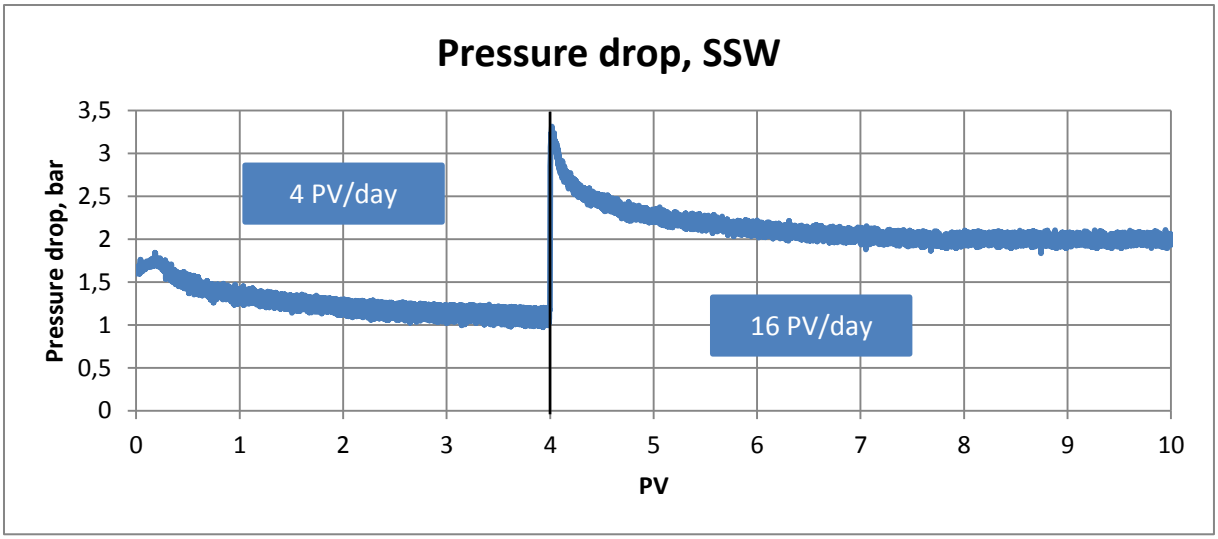

Figure 4.26 – Pressure drop across the core during flooding with SSW.

Ions concentration graph shows, that the amount of sodium and chloride keeps on the level equal to the injection brine during flooding. This can be the confirmation that these two ions do not interact with the calcite. Some values are deviating slightly from the SSW concentration, but it can be just because of the errors of chromatography process and the 200 times dilution procedure.

The amount of calcium in the beginning of flooding is higher than for the base line and then slowly decreases, but the values are higher during all time of flooding on 4 PV/day. The amount of magnesium is lower than the base line in the beginning, but then stabilizes at the level equal to SSW injection brine. These opposite trends for Ca^{2+} and Mg^{2+} during first PV of the flooding correspond with the results of work, done by Hamouda et al., 2014, where he observed the same phenomenon during flooding of chalk cores. It was also noticed that the results are online with observations made from Ekofisk field.

The relative concentration of sulfate ions in the beginning of the flooding is lower than for the base line, which can be explained by $CaSO_4$ salts precipitation. The amount of bicarbonate is deviating much from the average value, but the average value itself is higher than a base line. This can be again the confirmation of calcite dissolution.

After switching of flowrate we can observe the peak of the pressure drop, which is high and corresponds with high recovery. Between the peak value and the stabilization level the same difference of about 1 bar is observed, as in cases with LSW 1:15, LSW 1:20 and LSW 1:25. In those cases we also noticed the high recovery increment. The pH values also begin to increase after 6 PV, as in those cases. It can be the indication that the same process of increasing sweep efficiency is going on in case of SSW.

From ions chromatography we can see that the relative concentration of calcium between 4 PV and 6 PV is higher than the base line, but then drops on the level lower than the base line. This decreasing of the Ca^{2+} amount lower than the SSW injection concentration could be an indication of

some precipitation of $CaSO_4$ salts, but if we will look at the sulfate relative concentration, we will see that it keeps on the level of the base line. It could also be the indication of precipitation of $CaCO_3$ from the solution. However, the difference between the base line and the calcium amount is not so big, and therefore it could also be within the limit of chromatography analysis error. You can see for example that the sodium and chloride values are also deviating slightly; even so they are supposed not to participate in brine/rock interaction.

Bicarbonate level on the 16 PV/day flowrate has again large deviations and the average value is higher than the base line. Magnesium ion relative concentration is on the level of the base line.

4.8 Pressure drop comparison on 4 PV/day for different salinities

As it was discussed before, the trend for pressure drop across the core can be an important indication of the processes which are going on during flooding. The higher value of the peak can indicate more amount of fine migration and flow restrictions. The location of the peak more to the left on the pressure drop graph can indicate earlier water breakthrough and lower recovery. The stabilization level value can tell us about the absolute permeability of the core. You can see the pressure drop trends on 4PV/day flowrate for experiments with different salinities on Figure 4.27.

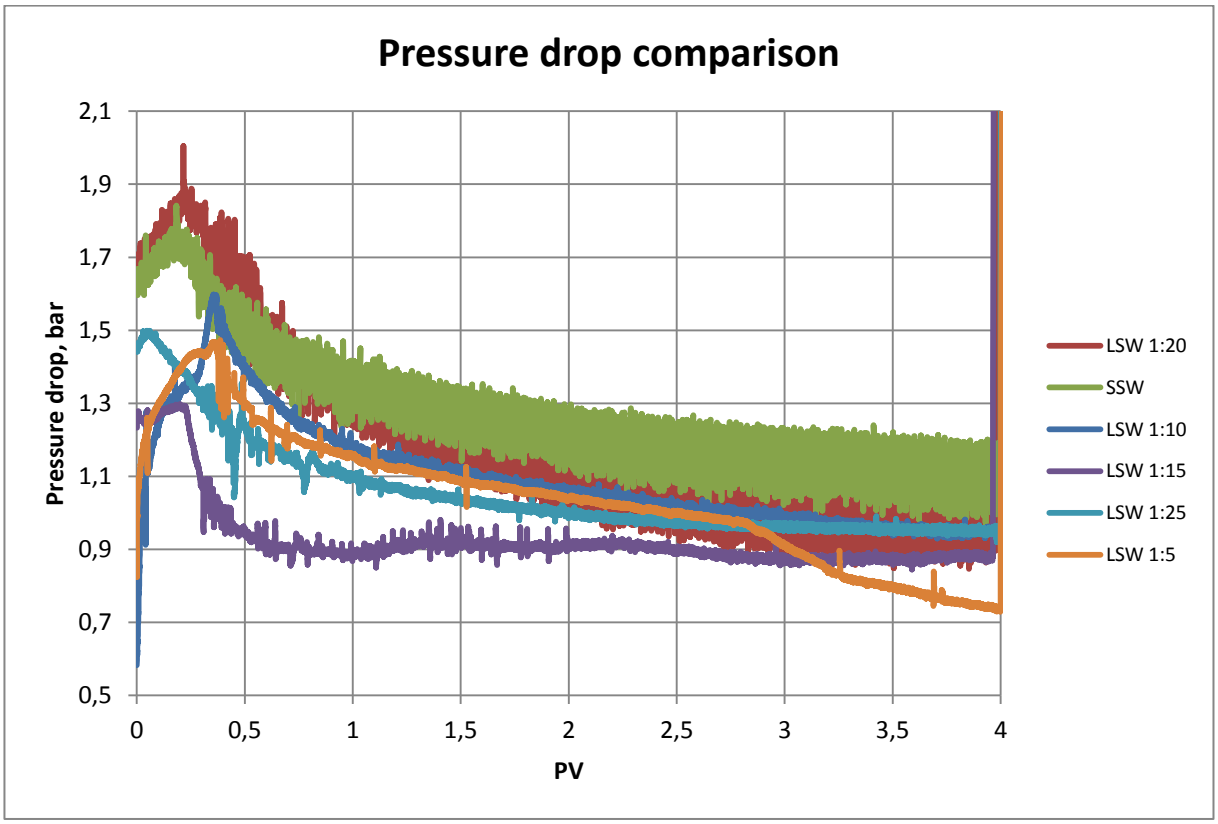

Figure 4.27 – Pressure drop trends on 4 PV/day for flooding with brines of different salinities.

We can see on the graph, that pressure drop for LSW 1:10, LSW 1:20 and LSW 1:25 stabilizes at approximately the same level of 1 bar. This is reasonable, because the LSW brines have

approximately the same viscosity. If we suppose that the cores have the same absolute permeability, the pressure drop trends should stabilize at the same level. The LSW 1:20 values deviate more from this level, but this is, as we discussed before, is most probably due to the sensitivity of manometer.

The LSW 1:5 values have the same trend with above mentioned three brines until about 2.75 PV of flooding, and then we observe a new trend, where a pressure drop decreases to about 0.75 bar at 4 PV. This can be an indication of flooding out of some flow restrictions.

The two cases which are completely different from the above mentioned with regard to the stabilization level are SSW and LSW 1:15. The SSW stabilization level is higher and equal to about 1.1 bar. This can be due to the fact, that the viscosity of the SSW brine is also higher than for LSW (0.44 cP versus 0.405 – 0.411 cP).

The LSW 1:15 case has the stabilization level lower than LSW 1:10 and other brines with the same viscosity. It can be due to different reasons. For example the core could have higher permeability. It was mentioned before, that all the cores were made out of the same piece of rock, but even such cores can have different permeabilities. The other possibility is the flooding out of fines. We can see also that the pressure drop peak in the beginning is lower than for the other cases. It can be the indication of lower amount of fine migration. After 1.25 PV the pressure drop for LSW 1:15 brine rises slightly after 2.25 PV. This phenomenon can be due to the redistribution of fines.

If we will take a look at pressure drop peak values, we can see that the LSW 1:10 has the highest one (we do not take into consideration SSW and LSW 1:20 brines now, because experiments with those brines were made on different equipment). Also the peak value here is observed after more amount of injection fluid pumped through the core than for other cases (you can see that the peak is located more to the right on the PV axis). These two observations correspond with the highest recovery for LSW 1:10 in comparison with other cases. LSW 1:5 peak is observed almost at the same time with LSW 1:10, but the peak value is lower. It can indicate lower amount of fines and worse sweep efficiency. As a result the recovery is slightly lower. LSW 1:25 pressure drop peak value is comparable with that of LSW 1:5, but it is located much more to the left. It can be the indication that the sweep efficiency does not increase very much. This corresponds with the earlier water breakthrough and the lowest recovery from all cases.

SSW and LSW 1:20 pressure drop peak values are higher than for other experiments. It can be due to the fact that those two experiments were made on the other equipment. You can see that pressure drop values for SSW and LSW 1:20 deviate much more from the average value, than for the other experiments. This can be due to the lower sensitivity of manometer. The peak values can also be different due to the error of manometer or due to other technical problems. But we can at least try to compare those peak values between each other. They are located at approximately the same point on PV axis, but the SSW peak value is lower than LSW 1:20. This corresponds with the lower recovery in case of SSW.

4.9 Simulation results

Another parameter which we can use in discussion of the experimental results is the relative permeability of water and oil. It can tell us about the relative movement of the water phase with respect to the oil phase inside the core, and as a result the sweep efficiency. As was discussed before in the theory review part, the mobility ratio for displacing fluid (water) and displaced fluid (oil) can tell us about the conditions of displacement of oil from the pore space to the production well. If the mobility ratio exceeds one it is considered unfavorable, because the injection fluid moves more readily inside the reservoir (or inside the core during laboratory experiments) than the oil. High mobility ratio can cause fingering, which will result in early water breakthrough and reduced sweep efficiency. In the end all of this will mean lower recovery factor.

The mobility ratio itself depends on the effective permeabilities of the displacing and displaced fluid, and also the viscosities of these fluids. The viscosities of the fluids are known and kept constant during experiments. For all LSW brines the viscosity is comparably the same (for flooding experiments temperature of 70 °C it changes depending on salinity in the range 0.405 cP – 0.411 cP), and for SSW brine it is slightly higher (0.44 cP). The effective permeability of the fluid depends on the absolute permeability of the core and the relative permeability of the fluid in the multiphase system (here during the experiments we have two-phase system of the water brine with special salinity and synthetic oil).

Calculation of the relative permeabilities is made by Sendra simulator (version 2013.1). It uses the 1D black-oil simulation model for the calculation of relative permeabilities for both phases. The results are presented as the plot of relative permeability curves and are very convenient for comparison of different experiments. The variety of other flow properties, such as capillary pressure, can be calculated and compared.

The variety of scenarios is available for running in Sendra. For our experiments steady-state horizontal imbibition is used, because we have constant flowrate of injection fluid which displace synthetic oil. Following core parameters are used us a basis for the simulation: length, diameter, porosity and absolute permeability. Following fluid parameters are used: viscosity and density of the injection fluid at the experiment temperature, viscosity and density of the displaced fluid at the experiment temperature, initial water saturation, water injection rate.

The important shortcoming of the program is that the simulation does not include such processes as the dissolution of calcite, fine migration and flow restrictions. These parameters, however, play important role in our experiments. The dissolution on the 16 PV/day is high and damages the core very much by channeling. As a result the absolute permeability is changing, and we can't use the same correlation for both flowrates. That's why the simulation is made only for 4 PV/day flowrate.

The experimental data, which are used during simulation, are the pressure drop graph and the oil production. For the calculation of relative permeability Corey correlation is used.

The Corey correlation is often used simplified model of relative permeability as a function of water saturation. If the normalized water saturation is defined as (Wikipedia, Relative permeability):

$$S_{wn} = \frac{S_w - S_{wi}}{1 - S_{wi} - S_{or}} \qquad (4.4)$$

where

S_{wi} irreducible water saturation

S_{or} residual oil saturation

Then the Corey correlations of the relative permeability of oil and water are (Wikipedia, Relative permeability):

$$k_{ro} = (1 - S_{wn})^{N_o} \qquad (4.5)$$

$$k_{rw} = k_{rw}^{o} {S_{wn}}^{N_w} \qquad (4.6)$$

where

k_{ro} relative permeability for oil

k_{rw} relative permeability for water

k_{rw}^{o} the end point of the water relative permeability

The empirical parameters N_o and N_w can be obtained from measured data either by optimizing to analytical interpretation of measured data, or by optimizing using a core flow numerical simulator to match the experiment (often called history matching) (Wikipedia, Relative permeability). It's exactly what we use Sendra for. We have our history data for oil recovery and pressure drop and we try to find an appropriate correlation which will match with our data. As a result we get simulated relative permeability curves during flooding process.

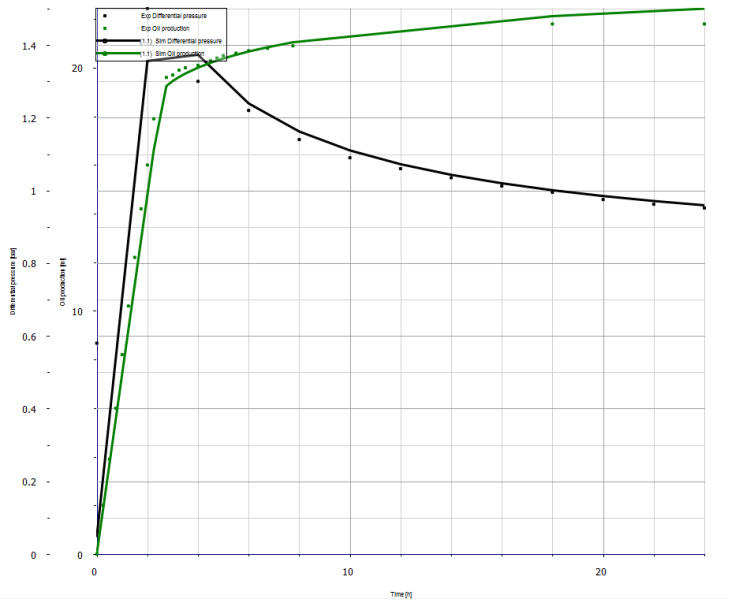

Figure 4.28 – Example of history matching in Sendra.

You can see an example of matching the experimental data (flooding with LSW 1:10) in Sendra on Figure 4.28. The first vertical axis is for pressure drop in bars and the second is for oil recovery in milliliters. The horizontal axis shows the time from the beginning of flooding in hours. On the graph the black dots represent the pressure drop during flooding, the green dots represent the recovery observed during flooding process. The black line shows the simulated curve of pressure drop, the green line shows the simulated recovery. As you can see, the simulated data correspond well enough with the experimental data, so we can suppose that the relative permeability curves will also be quite representative.

On Figure 4.29 you can see the simulated relative permeability curve for oil (green line) and for water (blue line) during flooding with LSW 1:5. On the vertical axis you can see the values for relative permeability of oil and water phase. Horizontal axis shows the water saturation (fractional). The curves cross at 0.508 water saturation. This value is important for comparison with other cases, because it can relatively show the time of water breakthrough. Before it was mentioned, that if the mobility ratio exceeds 1, it is considered as unfavorable. The mobility ratio depends on viscosity and effective permeability of oil and water phases. The viscosity for the synthetic oil is comparable with LSW brines (0.41 cP for n-decane against 0.405 – 0.411 cP for different LSW brines). So we can say that the cross point of relative permeability curves can tell us when the mobility ratio reaches the value equal 1 and the injection fluid stops to flood out oil phase effectively.

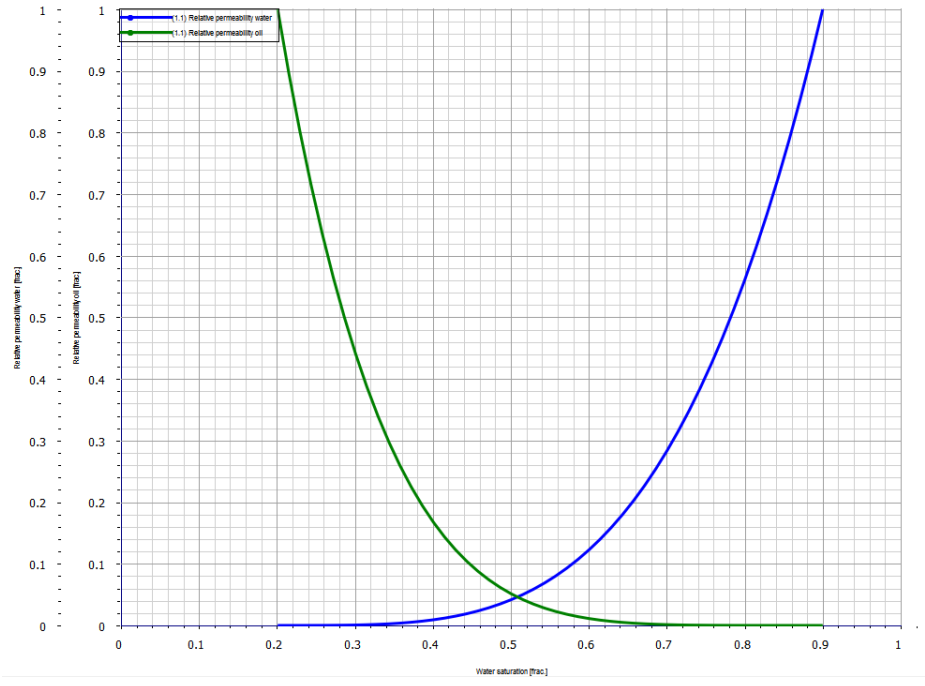

Figure 4.29 – Simulated relative permeability curves for flooding with LSW 1:5.

Figure 4.30 shows the relative permeability curves for LSW 1:10 flooding. The curves for oil and water cross at water saturation value 0.522. This is higher than in case of LSW 1:5, and it means that the water breakthrough happens later in present case than in previous case. It corresponds with the observed amount of recovery during flooding with these two brines, where LSW 1:10 had higher

amount of recovery on 4 PV/day flowrate (62.6% versus 61.5% in case of LSW 1:5). The shape of curves is almost the same, but the recovery is also not so different.

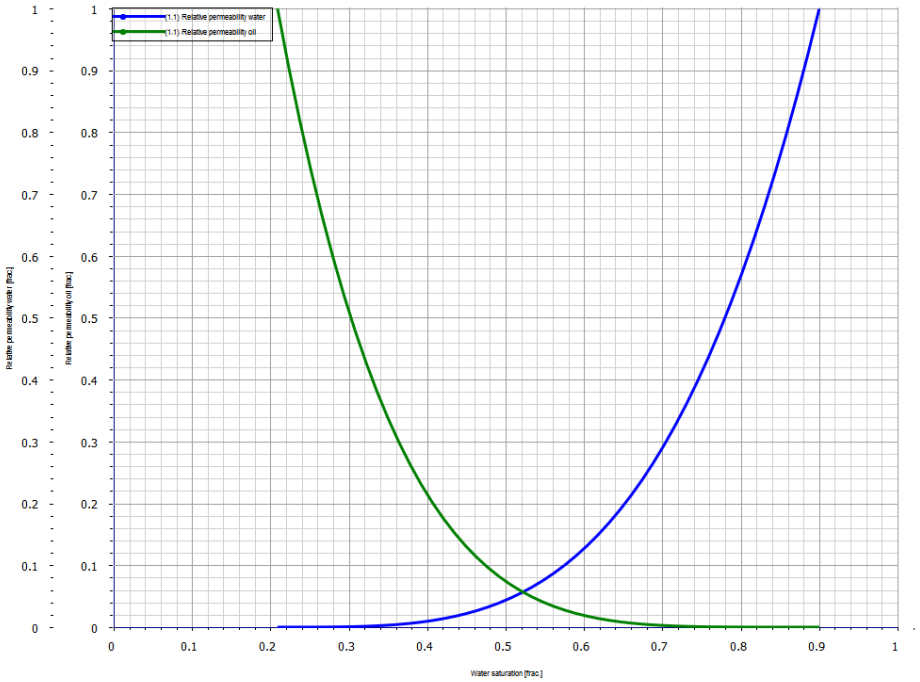

Figure 4.30 – Simulated relative permeability curves for flooding with LSW 1:10.

Figure 4.31 shows the simulated relative permeability curves for LSW 1:15 case. The cross point water saturation is equal to 0.472. This is lower than for two previous cases, which can mean that the water breakthrough happens earlier in case of flooding with LSW 1:15 brine. This corresponds with lower recovery in this case (54.2%). The other thing which you could notice is that the water relative permeability curve looks quite different from previously described cases. You can see that the water relative permeability is increasing faster than in case of LSW 1:5 and LSW 1:10. This corresponds with what we discussed before about dissolution-fine migration phenomenon and its effect on sweep efficiency. It was supposed that the dissolution in case of LSW 1:15 is low in comparison with LSW 1:5 and LSW 1:10 brines. Therefore the amount of fine migration and flow restrictions is also low. The sweep efficiency does not increase as much, as in case of LSW 1:5 and LSW 1:10. As a result the water floods through lower amount of pore space and we get the situation analogous to fingering. The simulation confirms this supposition by showing us that the water relative permeability increases faster in case of LSW 1:15, as it should be for low sweep efficiency.

On the Figure 4.32 you can see water and oil relative permeability curves for flooding with LSW 1:20. The shape of water relative permeability curve looks similar to LSW 1:5 and LSW 1:10, which corresponds with oil recovery, where for LSW 1:20 it is also high as in those two cases (59.2%). The cross point water saturation is equal to 0.479. It is lower than for LSW 1:5 and LSW 1:10 and higher than for LSW 1:15, which again corresponds with the recovery observations. The exact value is, however, more close to LSW 1:15, than to cases of high recovery. This phenomenon

can be explained by the fact, that the LSW 1:20 was done on different equipment and, as it was discussed before, the peak values seems to be overestimated in case of LSW 1:20 and SSW in comparison with other cases.

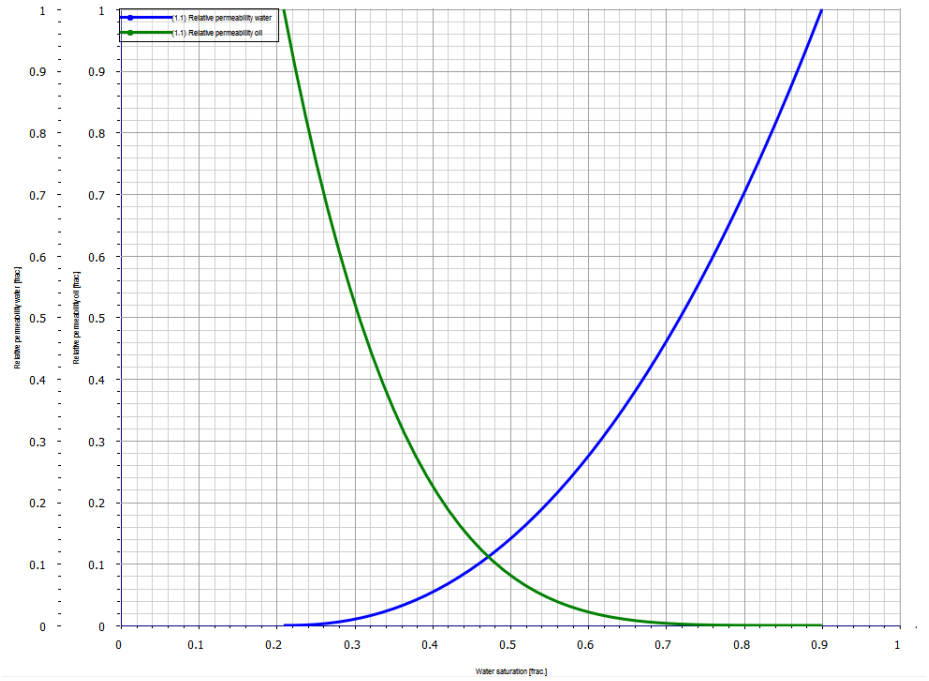

Figure 4.31 – Simulated relative permeability curves for flooding with LSW 1:15.

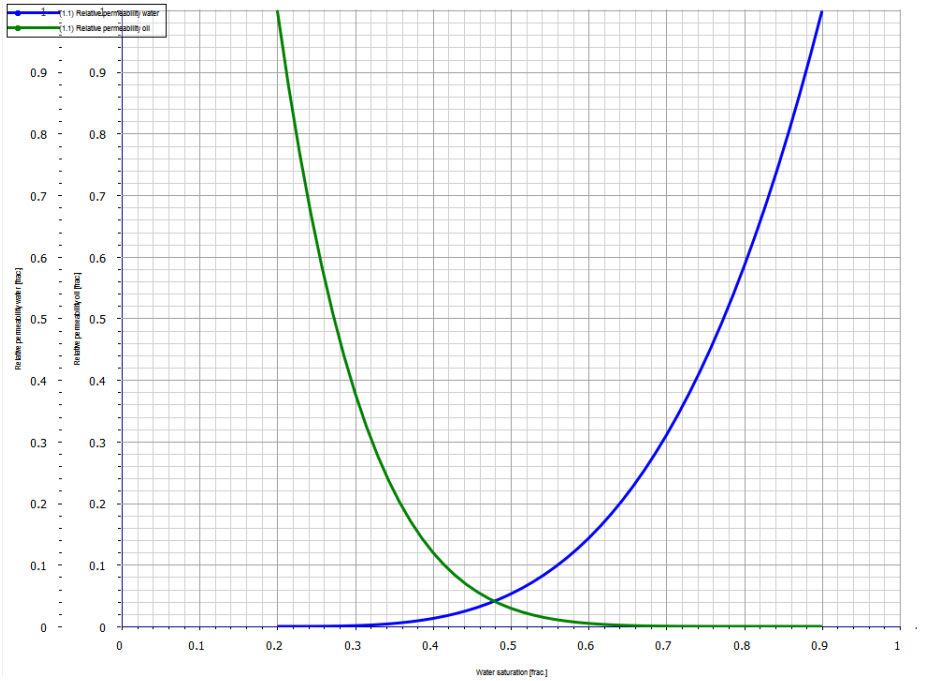

Figure 4.32 – Simulated relative permeability curves for flooding with LSW 1:20.

Figure 4.33 shows simulated relative permeability curves for LSW 1:25 flooding. The recovery with this brine was the lowest from all cases (51%). The water relative permeability curve shape is close to that with LSW 1:15, which was also the case of low recovery. The cross point water

saturation is equal to 0.437, which is the lowest from all described cases. This implies the early water breakthrough, and it is exactly what was noticed during experiment.

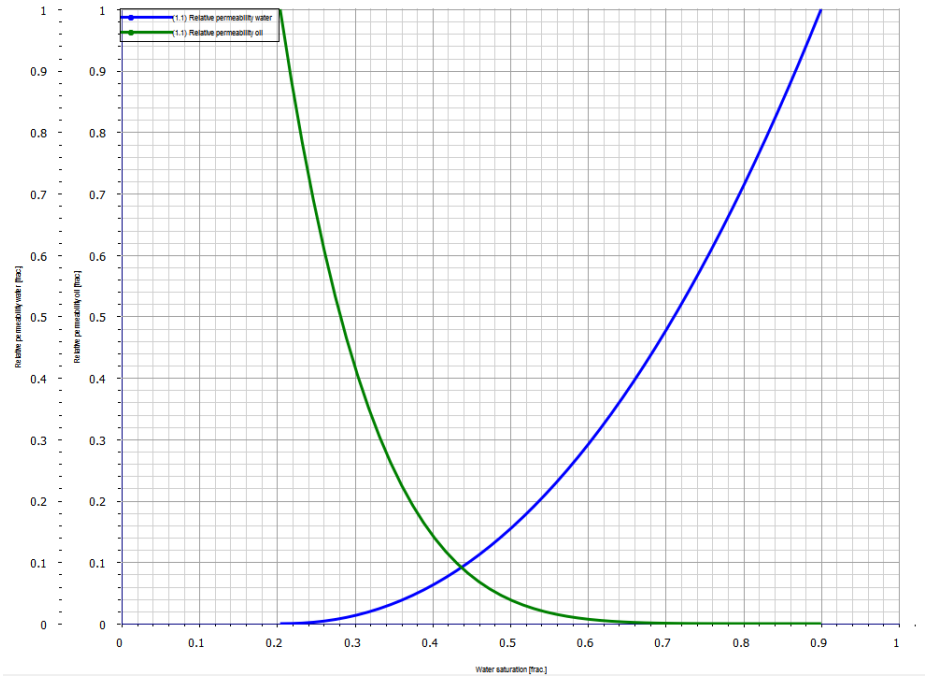

Figure 4.33 – Simulated relative permeability curves for flooding with LSW 1:25.

The last case that was simulated in Sendra is the flooding with SSW brine. On Figure 4.34 you can see water and oil relative permeability curves for this case. It is less convenient for comparison than other cases, because the dynamic viscosity of SSW at flooding temperature is equal to 0.44 cP, which is noticeably higher than for other cases. Besides this experiment was also made on different equipment (the same as LSW 1:20), and it was discussed before that the history data for pressure drop (the difference between the peak values due to possible technical problems with equipment) can influence the simulation results. However, the simulation results correspond more or less with other cases. The shape of the water relative permeability curve represents an average between high recovery cases (such as LSW 1:10) and low recovery cases (such as LSW 1:25). The observed recovery in case of SSW is also between those cases (56.6%). The cross point water saturation is equal to 0.465. This value is also the average between the highest and the lowest cases. However, the exact value is lower than for LSW 1:15 (where the recovery was lower), which can be explained partly by viscosity difference and partly by the pressure drop peak difference.

As a conclusion we can say, that the Sendra simulation results correspond with the ideas, which was proposed on the basis of data from flooding, pH measurements and ion chromatography. The relative permeability curves correspond with the supposed amount of fine migration and sweep efficiency. The cross point water saturation corresponds with the relative time of water breakthrough and its connection with recovery.

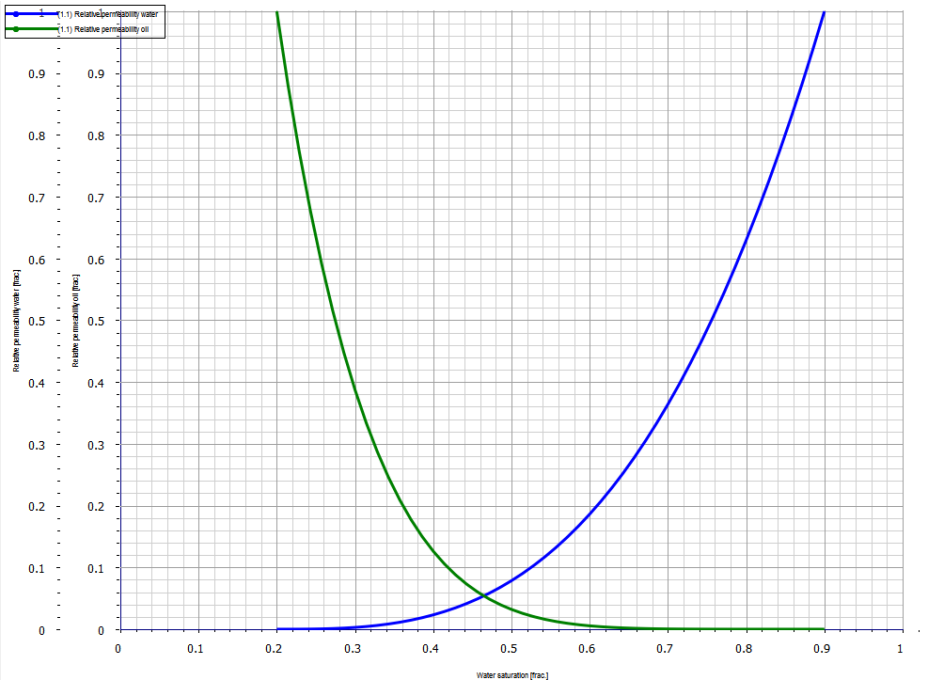

Figure 4.34 – Simulated relative permeability curves for flooding with SSW.

4.10 Flooding with SSW / LSW 1:10

The core #7 was flooded first with SSW brine, and then with LSW 1:10 to check for any possible EOR effects. The reason for choosing LSW 1:10 brine as an EOR fluid is that it brought the highest recovery on low flowrate, so it was considered to have more potential for changing the core properties, than the other fluids. The core was flooded with SSW on 4 PV/day (0,111 ml/min), then flowrate was switched to 16 PV/day (0.444 ml/min). Then the injection fluid was changed to LSW 1:10, and the core was flooded with it on 4 PV/day and 16 PV/day. The changing of flowrate in all cases was made only when it was clear that there will be no more incremental oil.

Figure 4.35 shows the recovery during flooding process for this case. The recovery on low flowrate with SSW is equal to 58%. When the flowrate was switched, the recovery increment of 4.7% was acquired. The total recovery with SSW brine is equal to 62.7%. When the injection fluid was switched to LSW 1:10 and the core was flooded with it on 4 PV/day flowrate, no additional oil was acquired. However, when the flowrate was switched to 16 PV/day the additional 0.3% recovery was observed. If we will compare recovery on low flowrate with SSW for core #7 and core #2, we will see that for the present case it is slightly higher (the difference is about 1.4%). This can be due to two possible reasons: the repeatability of the experiments and the absolute permeability of the core. First reason means, that the repeatability of the experiments is not perfect. Even if we flood the core with the same properties and use for it the same brine, the results still can be slightly different. The chalk itself is not an absolutely homogeneous system, and such processes as a dissolution of calcite and fine migration can bring slightly different results (even if the amount of dissolution is the same). There can be also technical reasons for the repeatability, such us precipitation of salts in the outlet and inlet line.

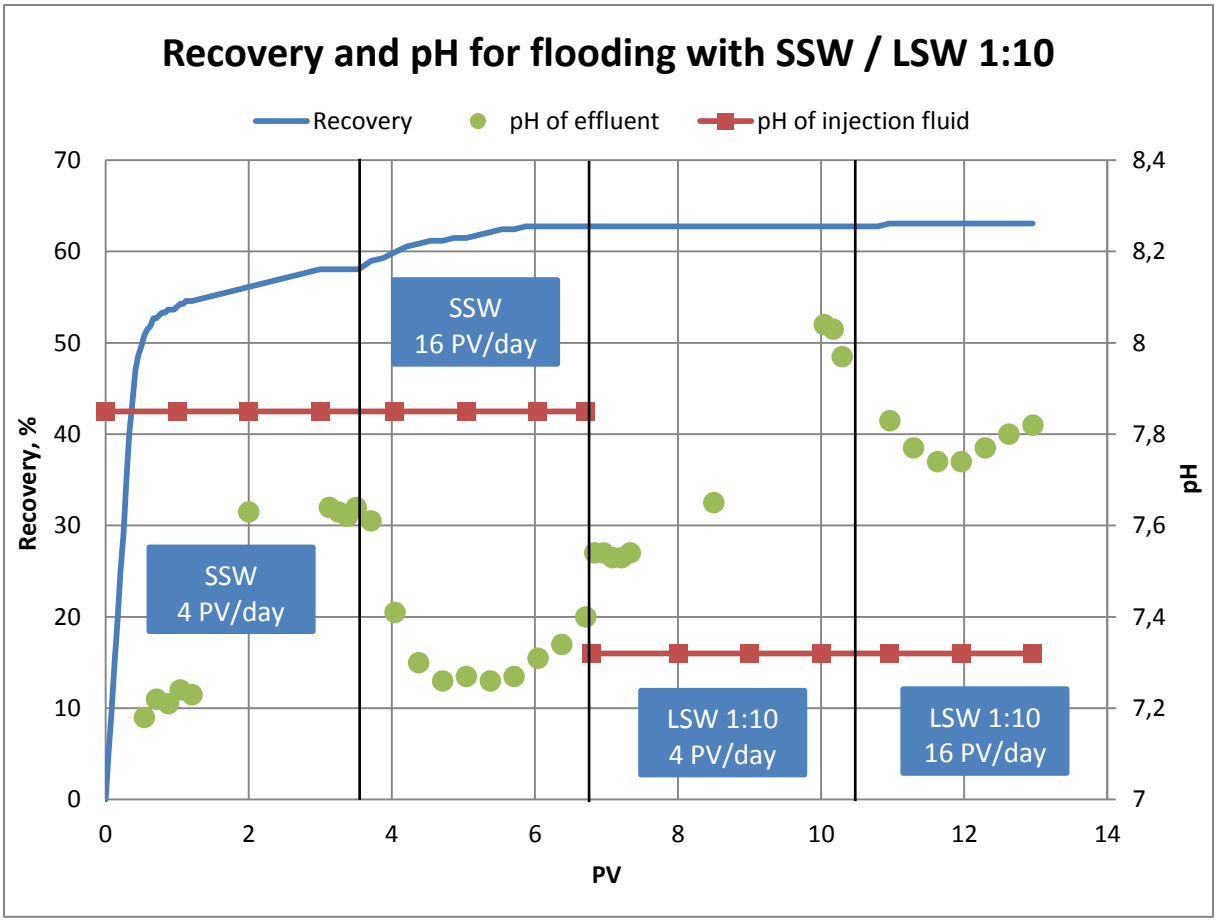

Figure 4.35 – Recovery and pH values during flooding with SSW / LSW 1:10.

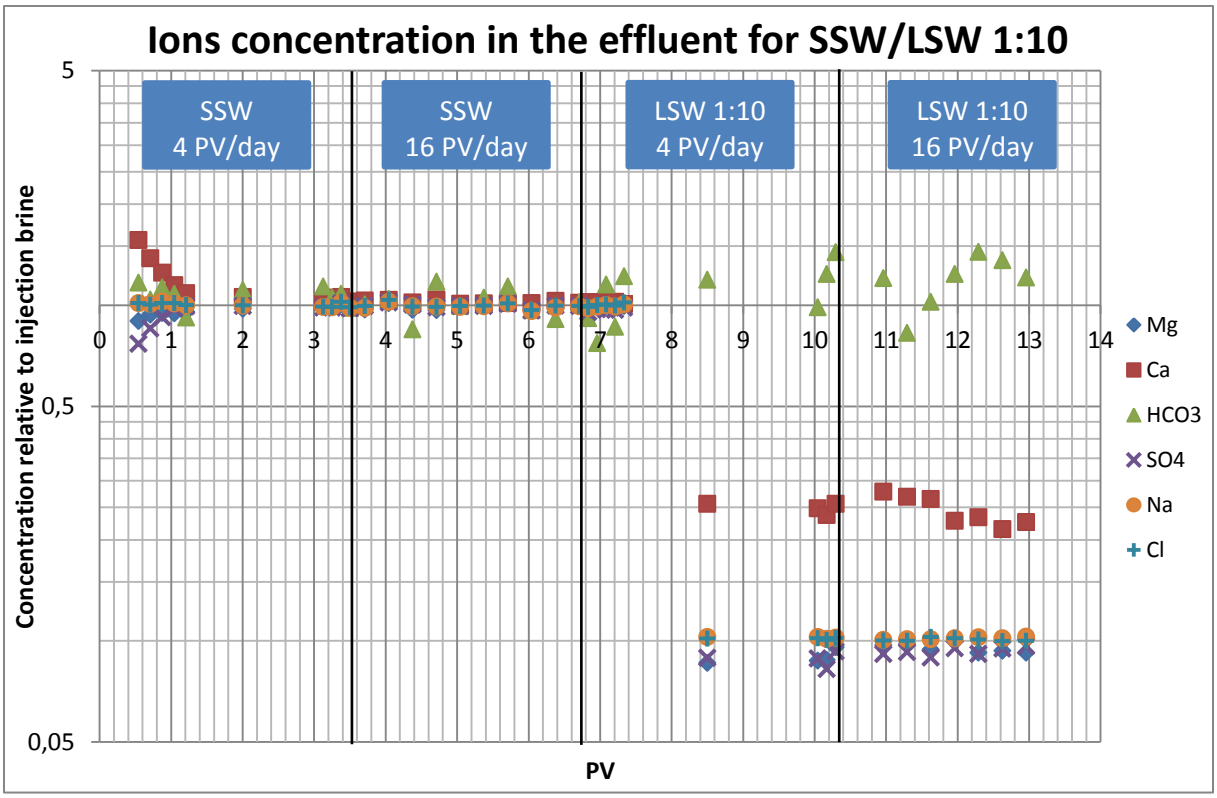

Figure 4.36 – Concentration of ions in the effluent samples, taken during flooding with SSW / LSW 1:10.

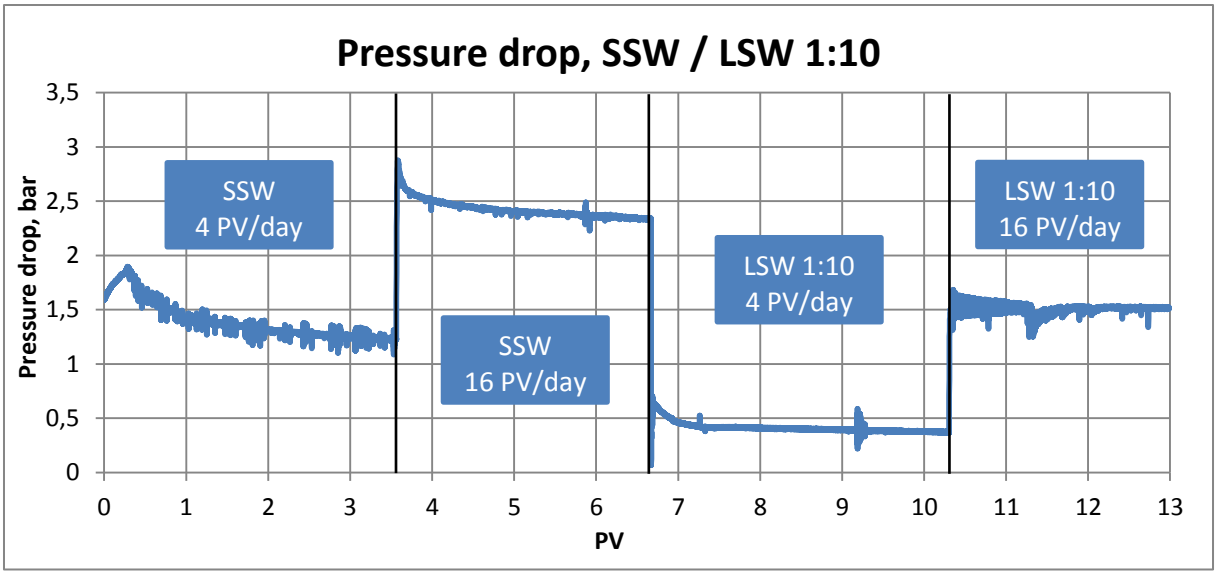

Figure 4.37 – Pressure drop across the core during flooding with SSW / LSW 1:10.

The second reason for the difference in results can be the absolute permeability of the core. It was mentioned before, that the cores of the same rock type (even if they are made out of the same piece of rock) can have slightly different permeabilities. Such thing was already noticed in case of flooding with LSW 1:15, where the stabilization level for pressure drop on 4 PV/day was lower than for other experiments, even so the viscosity of the brines is relatively similar. If we look at the pressure drop stabilization level for the present case (Figure 4.37, SSW, 4 PV/day), we will see that its value is equal to about 1.2 bar. In case of flooding the core #2 with SSW it was equal to 1.1 bar. This comparison indicates that there is a possibility that the cores have slightly different absolute permeabilities, and it can be the reason for difference in recovery.

The recovery increment with SSW brine after switching of flowrate for core #7 and core #2 is considerably different. In present case it is equal 4.7% versus 10.8% in previous case. During descriptions of all previous flooding experiments there was noticed a dependence between recovery on low flowrate and recovery increment after changing of flowrate, where the higher amount of oil on 4 PV/day means lower amount of oil on 16 PV/day. This was connected partly to the dissolution and fine migration and partly to the available amount of oil left in core after flooding on 4 PV/day flowrate. In present case the recovery on low flowrate is higher than in previous case, so in accordance with other experiments it leads to lower recovery increment after switching of flowrate.

Let's now look more closely on the data, acquired from flooding of the core #7. On pressure drop graph we can see a high peak in the beginning. It's not reasonable to compare it with the experiment done with core #2, because they were done on different equipment, and it was previously noticed that the peak values are not similar for two different flooding set-ups. The graph after the peak looks more chaotic, than other experiments, which were done on the same equipment. It is also the indication of a not perfect repeatability, because these high deviations of pressure values from the average can mean some technical problems with manometer.

If we will look at the ions chromatography results (Figure 4.36), we will see that the behavior for sodium and chloride ions is the same as in all previous cases, where their concentration is the same with the injection brine. So we can again use them as the base line for comparison with other ions.

The calcium ions show the same behavior, as in experiment with core #2, where their relative concentration in the beginning is higher, than for the base line. However, the difference is slightly higher than in previous case. This can be the indication of higher amount of dissolution and fine migration, which can explain higher recovery with SSW on 4 PV/day. The magnesium and sulfate behavior also corresponds with previous case, however, the difference between the base line and the relative concentration for these ions is again higher, the same as in case with calcium. This is reasonable, because it was supposed before that the Mg^{2+} ions substitute Ca^{2+} ions in calcite crystal lattice, and SO_4^{2-} ions can precipitate with Ca^{2+} in the form of $CaSO_4$ salts. So the amount of magnesium and sulfate in the effluent seems to be connected to the amount of calcite dissolution, and as a result to the amount of calcium.

The stabilization level for calcium is again slightly higher than the base line. For magnesium and sulfate the stabilization level has almost the same values with the base line. The bicarbonate deviates much, as in all previous cases, but the average value is higher than the base line. The behavior of all ions after switching to 16 PV/day is similar to flooding of the core #2.

The trend of pH values on both flowrates has the same shape, as in previous experiment, but the values are higher. This can be due to the fact that there are two processes, influencing the pH values: the amount of dissolution and the binding of OH^- ions by magnesium. It was already noticed that the amount of dissolution is different in this case, according to the ion chromatography results.

The pressure drop trend after changing of flowrate (as for both the peak and the stabilization level) looks similar with LSW 1:10 case, where we also had a low recovery increment.

The changing of the injection fluid salinity didn't bring additional oil recovery on 4 PV/day. We can see on the pressure drop graph that for flooding with LSW 1:10 on 4 PV/day flowrate the stabilization level is equal to about 0.4 bar. This is much lower than for SSW, where it was equal 1.2 bar. The pressure drop reduction is connected partly to the viscosity difference, but this can account only to about 0.1 bar, as it was noticed from the previous experiments (Figure 4.27). The viscosity difference between LSW 1:10 and SSW is not so great (0.407 cP versus 0.44 cP respectively) as to bring such big pressure difference. The main reason for severe pressure drop reduction is most probably the dissolution process. When we flood the core on 16 PV/day with SSW, we can see that the pressure drop has peak in the beginning and then stabilizes at a lower value. This reduction of pressure can mean the increasing of absolute permeability due to formation of channels. By this procedure we actually damage the core, and when we switch again to lower flowrate, the injection fluid just flows freely through the existing channels. That can be the reason, why we do not observe any recovery increment on low flowrate after changing of salinity. We have much more permeable structure, than in

the beginning of the flooding, so the possible brine/rock interactions cannot bring any sweep efficiency increase.

The ion chromatography results just after changing of the injection fluid (6.7 – 7.3 PV) shows the relative concentration values equal to SSW. This can be because the first effluent samples represent the SSW injection brine, and it can take some time to flood it out with the LSW 1:10. We do not observe any noticeable mixing between two injection brines during first pore volume of flooding with LSW 1:10. This stable displacement of previous injection fluid by the new one can also be the confirmation that the sweep efficiency does not increase.

However, if we will take a look at the pH values of the effluent samples taken just after changing of injection brine salinity, we will notice that they are slightly higher. This can be due to stopping of flooding process for the procedure of changing the injection fluid. It takes some time to perform and during this time the pH of fluid inside the core can slightly rise.

The ion chromatography for other effluent samples, taken during the 4 PV/day flooding with LSW 1:10, show the relative ions concentration trends similar to previous LSW flooding experiments. We can see sodium and chloride concentration equal to that of injection LSW brine. Calcium amount is higher than in the injection fluid, and the difference is equal to about 0.15 relative to SSW. This is lower, than in case of flooding with LSW 1:10 as a primary recovery fluid, but it still means that the dissolution process is going on. However, with 4 PV/day flowrate the amount of fine migration is not enough to create flow restrictions in dissolute channels. So the sweep efficiency does not increase.

We can see also the increased amount of bicarbonate in comparison with the injection fluid, which supports the dissolution theory. The magnesium amount in the effluent is reduced, probably because of substitution of calcium with magnesium in the calcite lattice. The sulfate concentration is also reduced, probably because of the precipitation of $CaSO_4$ salts.

We can also see the confirmation of the dissolution process in pH values. They are higher than for the injection fluid and in the end of flooding with LSW 1:10 on 4 PV/day reach the value equal 8.04. It can be the indication that the channels are very dissolute.

When the flowrate is switched to 16 PV/day, we get the recovery increment of 0.3%. The pressure drop graph shows us severe fluctuating in the beginning, which decreases slowly as the flooding proceeds. This can be an indication of fine migration. The reason that we do not see the clear peak can be due to the fact, that the channels are very dissolute and the pore throats are wide. That's why fines do not plug the pore throats completely, and this fluctuating of the pressure drop can mean continuous redistribution of fines. This process can increase the sweep efficiency slightly and can explain the small recovery increment.

The amount of calcium in the effluent is also slightly higher on 16 PV/day flowrate, than on 4 PV/day. It can support the idea, that the sweep efficiency is increased and we flood some new undissoluted channels. While the flooding proceeds, the amount of calcium in the effluent decreases.

The behavior for magnesium and sulfate ions trends is similar to flooding on 4 PV/day, only the difference between the injection fluid concentrations and the effluent is not so pronounced. It can mean that the most part of the substitution and precipitation happens just after the changing of injection fluid salinity. Partly this phenomenon can also be influenced by the fact, that the sweep efficiency is slightly increased and we flood some new undissoluted channels.

Bicarbonate concentration values keep on high level. The pH trend is similar to those observed before in previous experiments with different LSW brines.

4.11 Summary of results

The low salinity brines showed the potential for increasing the oil recovery both as a primary recovery injection fluid and as a secondary. The cores with the similar properties (including dimensions, porosity, absolute permeability and IWS) were chosen for performing flooding experiments. During the flooding experiments with different salinity brines as a primary recovery fluid, we observed the difference in recovery both on 4 PV/day and 16 PV/day. Besides of recovery, there is a difference in other parameters, such as pressure drop, pH of effluent and ions concentration.

The potential of the injection fluid with definite salinity to produce more oil from the core in comparison with other fluids can be connected to the amount of dissolution. If the dissolution of calcite in chalk core is high, it can make calcite lose its integrity. Calcite particles will peel off from the surface and it will lead to fine migration. Fines can block the pore throats and create flow restrictions, which can lead to increased sweep efficiency and as a result higher recovery.

However, after switching of flowrate the high dissolution in the beginning of the flooding can bring opposite results. It was observed during experiments that high recovery on low flowrate corresponds with low recovery increment on high flowrate. This can be due to the fact, that high dissolution on low flowrate will allow injection fluid just flow through existing channels after switching to high flowrate. Oppositely, low dissolution will make injection fluid to find new channels after switching of flowrate, and the sweep efficiency will increase more.

So the potential of the injection fluid to change rock properties shows itself on low flowrate, but the total recovery from the core depends on both flowrates. If the recovery on 4 PV/day was higher due to the high amount of dissolution, the total recovery can still become equal on 16 PV/day and even lower.

Several general observations were made during flooding with LSW and SSW brines as a primary recovery fluid. Mostly they support the proposed mechanism for increased oil recovery, where it is connected to the amount of dissolution. The observations are as follows:

- The pressure drop graphs have peak in the beginning of the flooding. The height of this peak and its location on PV axis can tell us about the amount of fine migration and as a result sweep efficiency. If the peak is high and it's located more to the right, this can mean that the amount of flow restrictions is high and the sweep efficiency increases.

- The stabilization level for pressure drop peak depends on the absolute permeability of the core and the viscosity of the injection fluid.
- The pressure drop peak after switching of flowrate (its height and the difference with the stabilization level) can tell us about efficiency of oil mobilization by the increasing of flowrate. If the peak value is high and also there is a high difference between it and the stabilization level, then it can mean that the sweep efficiency is increasing and the recovery increment will be high.
- The amount of chloride and sodium in the effluent is equal to the injection fluid with only slight deviations. During mixing of LSW injection fluid and SSW formation fluid the amount of these ions is higher due to mixing. Overall we can take them as the base line for compare of the other ions.
- The amount of calcium in the effluent, or most importantly its difference with the injection fluid, can tell about the amount of dissolution. If the calcium concentration is high, it can mean that the dissolution is also high.
- The amount of bicarbonate is always higher than in injection fluid. The deviations from the average are also high, because the bicarbonate amount in the solution represents a complex system, which depends on the interaction with air and the pH.
- Magnesium and sulfate amounts are close to base line, but there still exist a considerable difference. The magnesium amount in some samples is lower, than for the injection fluid. This can be due to substitution of dissolute calcium with magnesium ions. Sulfate amount can be either higher or lower, and it can be connected to dissolution/precipitation of $CaSO_4$ salts.
- The pH of the effluent samples for all LSW brines is higher than for the injection fluid. This can be the consequence of the dissolution process. The values of pH can increase partly because of creation of bicarbonate and partly due to hydrogen penetration in calcite crystal lattice. The bicarbonate amount is always high and has deviations from average value, so the pH trends are connected mostly to hydrogen penetration in calcite. The sharp increase in pH can mean that the channels are very dissolute. Also it was noticed on 16 PV/day flowrate that the time, when pH starts to increase, corresponds with sweep efficiency.

The relative permeability simulation done in Sendra corresponds with the observed recovery results and the sweep efficiency. In cases of high recovery the cross point between the oil and water relative permeability curves is located more to the right on water saturation axis. This corresponds with later water breakthrough in those cases. Besides the shape of the water relative permeability curve indicates in those cases, that injection fluid relative permeability increases slower with time than for low recovery cases. This can be the indication of higher sweep efficiency.

The LSW 1:10 was chosen to check the possible EOR effects. This salinity showed the most potential for brine/rock interaction during flooding as a primary recovery fluid. However, as an EOR injection fluid it gave only 0.3% oil increment. This was probably caused by the high amount of dissolution, done by SSW injection fluid on 4 PV/day and especially on 16 PV/day.

5 Conclusions

The flooding experiments with Stevns Klint chalk cores were performed with the intention to study the effect of the injection brine salinity on recovery. Many studies were performed before by different researchers both on chalk and sandstone cores. There are different opinions on the low salinity water flooding potential to increase oil recovery, and the results of different published works do not always correspond with each other. This is probably due to the fact that the conditions for experiments are also different. However, some results clearly indicate, that the low salinity water flooding can increase the recovery (Yousef et al., 2011; Al-Harrasi et al., 2012; Al-Attar et al., 2013). The effect is attributed to different parameters, such as wettability changing of the rock, formation of emulsions, fine migration. These parameters in its turn depend on rock, oil and water properties.

In this work the flooding of similar chalk cores was made with injection brines of different salinities. This was made in order to study the dependence between the recovery and injection brine salinity in a primary recovery waterflooding mode. Then the fluid that showed the most potential for brine/rock interaction was flooded as a secondary recovery injection fluid.

Results for primary recovery waterflooding show that the recovery from the core can depend on the amount of dissolution of calcite. Dissolution can lead to fine migration and creating of flow restrictions, which increase sweep efficiency. The pressure drop data, pH of the effluent and ion chromatography analysis support this theory. The pressure drop peak height and location can correspond with the amount of dissolution and fine migration. Increasing of pH of the effluent in comparison with the injection fluid can indicate the formation of bicarbonate and hydrogen substitution of calcium during calcite dissolution. Ion chromatography shows the increased amount of calcium in the effluent, and its difference with the injection brine corresponds with the amount of dissolution. The simulation of water and oil relative permeability curves in Sendra corresponds with the observed results and proposed mechanism of dissolution/fine migration.

The dependence of the amount of dissolution on brine salinity can be due to the difference in physical properties of those brines: viscosity, pH, IFT between brine and synthetic oil, and ions concentration. Viscosity of the brine decreases with decreasing salinity, however, the difference in it between LSW brines is not so high. We can actually see this by the stabilization level on the pressure drop graphs, where it is similar for different salinities (with the exception of SSW, where the viscosity is noticeably higher). The pH of the injection brine decreases with decreasing salinity. The lowering of the injection fluid pH can support the dissolution process. However, then the recovery would just increase with decreasing salinity, and as we observed, the recovery first increases and then decreases. Another parameter, which can influence this process, is IFT. It increases with decreasing of injection fluid salinity. Higher IFT ordinary means that there will be more capillary trapped oil inside the pore space of the core, and as a result recovery should lower with lowering of salinity. So pH and IFT can bring opposite results on recovery. It can explain the observed results and the dependence of calcite

dissolution on the injection brine salinity. The ions concentration itself can also influence the recovery, but the type of analysis performed in this work do not allow to judge about the amount of this influence.

The flooding with LSW 1:10 brine gave the best results as a primary recovery injection fluid on 4 PV/day flowrate with regards to recovery, so it was considered that this salinity has more potential for brine/rock interaction than the other brines which were studied. Therefore the secondary recovery waterflooding was performed with this brine. After flooding with SSW as a primary recovery fluid, LSW 1:10 brought only about 0.3% of additional oil recovery. The effect is low most probably because the dissolution done by SSW brine is high. The core is damaged during the flooding with SSW on 16 PV/day flowrate. This damage demonstrates itself in channeling and increased absolute permeability of the core.

The following propositions for future work can be made:

- The repeatability of the experiments should be checked. The chalk cores represent not an absolutely homogeneous system, so the results can deviate from core to core.
- Brines of other salinities should be checked in order to confirm the correlation between recovery and salinity on both flowrates.
- It was noticed by other researchers that the outcrop and reservoir cores sometimes can give different results. Since this work is done with Stevns Klint outcrop chalk, the reservoir rock should be checked for the possibility of giving the same results.
- The reservoir fluids should also be tried in experiments. This work is done with synthetic oil, so the crude oil can be used in order to study the effect. The IWS brine that was used in this work is the SSW brine. Formation brines ordinary have higher salinities than SSW. It can also influence the results, so the actual formation brine should be also studied.
- Analysis of another type can also be performed, such as contact angle measurements and mineral composition of the core before and after flooding.

References

1. Ahmadi, M.A. and Shadizadeh, S.R., 2013. *"Implementation of a high-performance surfactant for enhanced oil recovery from carbonate reservoirs."* Journal of Petroleum Science and Engineering 110, pp. 66–73.
2. Ahmed, T. and Meehan, N., 2011. *"Advanced Reservoir Management and Engineering (2nd Edition)."* Saint Louis, MO, USA, Elsevier Science & Technology Books.
3. Ahr, W.M., 2008. *"Geology of Carbonate Reservoirs: The Identification, Description and Characterization of Hydrocarbon Reservoirs in Carbonate Rocks."* Hoboken, NJ, USA, John Wiley & Sons.
4. Al-Attar, H.H., Mahmoud, M.Y., Zekri, A.Y., Almehaideb, R.A. and Ghannam, M.T., 2013. *"Low Salinity Flooding in a Selected Carbonate Reservoir: Experimental Approach."* Paper SPE 164788 presented at the EAGE Annual Conference & Exhibition incorporating SPE Europec, London, United Kingdom, 10-13 June.
5. Al-Harrasi, A.S., Al-Maamari, R.S., and Masalmeh, S., 2012. *"Laboratory Investigation of Low Salinity Waterflooding for Carbonate Reservoirs."* Paper SPE 161468 presented at the Abu Dhabi International Petroleum Exhibition & Conference, Abu Dhabi, UAE, 11-14 November.
6. Alotaibi, M.B., Nasralla, R.A. and Nasr-EI-Din, H.A., 2010. *"Wettability Challenges in Carbonate Reservoirs."* Paper SPE 129972 presented at the 2010 SPE Improved Oil Recovery Symposium, Tulsa, Oklahoma, USA, 24-28 April.
7. Austad, T., Strand, S., Hognesen, E.J. and Zhang, P., 2005. *"Seawater as IOR Fluid in Fractured Chalk."* Paper SPE 93000 presented at the 2005 SPE International Symposium on Oilfield Chemistry, Houston, Texas, U.S.A., 2-4 February.
8. Bell, F.G., Culshaw, M.G. and Cripps, J.C., 1999. *"A review of selected engineering geological characteristics of English Chalk."* Engineering Geology 54, pp. 237–269.
9. Chilingar, G.V., et al., 2012. Fundamentals of the Petrophysics of Oil and Gas Reservoirs. Somerset, NJ, USA, John Wiley & Sons.
10. Chukwudeme, E.A. and Hamouda A.A., 2009. *"Oil recovery from polar components (asphaltene and SA) treated chalk rocks by low salinity water and water containing SO_4^{2-} and Mg^{2+} at different temperatures."* Colloids and Surfaces A: Physicochemical and Engineering Aspects 336, pp. 174-182.
11. Cosgrove, T., 2010. *"Colloid Science: Principles, Methods and Applications (2nd Edition)."* Hoboken, NJ, USA, Wiley-Blackwell.
12. Cossé, R., 1993. "*Basics of Reservoir Engineering. Oil and Gas Field Development Techniques."* Editions Technip, Paris. ISBN 2-7108-0630-4. Printed in France by Imprimerie Nouvelle, 45800 Saint-Jean-de-Braye.
13. Dukhin, A.S. and Goetz, P.J., 2002. *"Ultrasound for Characterizing Colloids Particle Sizing, Zeta Potential Rheology."* Amsterdam, NLD, Elsevier Science & Technology Books.

14. Fanchi, J., 2005. *"Principles of Applied Reservoir Simulation."* Burlington, MA, USA, Gulf Professional Publishing.
15. Fathi, S.J., Austad, T. and Strand, S., 2010. *"Smart Water" as a Wettability Modifier in Chalk: The Effect of Salinity and Ionic Composition."* Energy and Fuels, Vol. 24, pp. 2514-2519.
16. Fathi, S.J., Austad, T., Strand, S. and Puntervold, T., 2010. *"Wettability Alteration in Carbonates: The Effect of Water-Soluble Carboxylic Acids in Crude Oil."* Energy and Fuels, Vol. 24, pp. 2974-2979.
17. Fink, J.K., 2012. *"Petroleum Engineer's Guide to Oil Field Chemicals and Fluids."* Waltham, MA, USA, Gulf Professional Publishing. ISBN 978-0-12-383844-5.
18. Frykman, P., 2001. *"Spatial variability in petrophysical properties in Upper Maastrichtian chalk outcrops at Stevns Klint, Denmark."* Marine and Petroleum Geology 18, pp. 1041-1062.
19. Gomari, K.A.R., 2009. *"Different Approaches to Understand Mechanism of Wettability Alteration of Carbonate Reservoirs."* Paper SPE 121952 presented at the 2009 SPE EUROPEC/EAGE Annual Conference and Exhibition, Amsterdam, The Netherlands, 8-11 June.
20. Gomari, K.A.R., Denoyel, R. and Hamouda A.A., 2006. *"Wettability of calcite and mica modified by different long-chain fatty acids (C_{18} acids)."* Journal of Colloid and Interface Science 297, pp. 470-479.
21. Gomari, K.A.R. and Hamouda A.A., 2006. *"Effect of fatty acids, water composition and pH on the wettability alteration of calcite surface."* Journal of Petroleum Science and Engineering 50, pp. 140-150.
22. Gomari, K.A.R., Karoussi, O. and Hamouda, A.A., 2006. *"Mechanistic Study of Interaction Between Water and Carbonate Rocks for Enhancing Oil Recovery."* Paper SPE 99628 presented at the SPE Europec/EAGE Annual Conference and Exhibition, Vienna, Austria, 12-15 June.
23. Goodwin, J., 2009. *"Colloids and Interfaces with Surfactants and Polymers : An Introduction (2nd Edition)."* Hoboken, NJ, USA, John Wiley & Sons.
24. Green, D. W. and Willhite, G. P., 1998. *"Enhanced Oil Recovery."* Society of Petroleum Engineer, Vol. 6, Richardson, Texas.
25. Gudmestad, O., et al., 2010. "Petroleum Resources with Emphasis on Offshore Fields." Ashurst, GBR, WIT Press.
26. Hamouda, A.A. and Gomari, K.A.R., 2006. *"Influence of Temperature on Wettability Alteration of Carbonate Reservoirs."* Paper 99848 presented at the 2006 SPE/DOE Symposium on Improved Oil Recovery, Tulsa, Oklahoma, U.S.A., 22-26 April.
27. Hamouda, A.A and Valderhaug O.M., 2014. *"Investigating Enhanced Oil Recovery from Sandstone by Low-Salinity Water and Fluid/Rock Interaction."* Energy and Fuels 28 (2), pp. 898-908.
28. Hamouda, A.A., Valderhaug, O.M., Munaev, R. and Stangeland, H., 2014. *"Possible Mechanisms for Oil Recovery from Chalk and Sandstone Rocks by Low Salinity Water (LSW)."*

Paper SPE 169885 presented at the SPE Improved Oil Recovery Symposium, Tulsa, Oklahoma, USA, 12-16 April.

29. Hansen, G., Hamouda, A.A. and Denoyel, R., 2000. *"The effect of pressure on contact angles and wettability in the mica/water/n-decane system and the calcite + stearic acid/water/n-decane system."* Colloids and Surfaces A: Physicochemical and Engineering Aspects 172, pp. 7-16.
30. Hermansen, H., Landa, G.H., Sylte, J.E. and Thomas L.K., 2000. *"Experiences after 10 years of waterflooding the Ekofisk Field, Norway."* Journal of Petroleum Science and Engineering 26, pp. 11-18.
31. Hjuler, M.L. and Fabricius I.L., 2009. *"Engineering properties of chalk related to diagenetic variations of Upper Cretaceous onshore and offshore chalk in the North Sea area."* Journal of Petroleum Science and Engineering 68, pp. 151-170.
32. Jabbar, M.Y., Al-Hashim, H.S. and Abdallah, W., 2013. *"Effect of Brine Composition on Wettability Alteration of Carbonate Rocks in the Presence of Polar Compounds."* Paper SPE 168067 presented at the SPE Saudi Arabia section Annual Technical Symposium and Exhibition, Khobar, Saudi Arabia, 19-22 May.
33. Jahn, F., et al., 2008. *"Developments in Petroleum Science, Volume 55: Hydrocarbon Exploration and Production (2nd Edition)."* Amsterdam, NLD, Elsevier.
34. Karoussi, O. and Hamouda A.A., 2008. *"Imbibition of Sulfate and Magnesium Ions into Carbonate Rocks at Elevated Temperatures and Their Influence on Wettability Alteration and Oil Recovery."* Energy and Fuels 22 (3), pp. 2129–2130.
35. Lehmann, O., Birnhack, L. and Lahav O., 2013. *"Design aspects of calcite-dissolution reactors applied for post treatment of desalinated water."* Desalination 314, pp. 1-9.
36. Liteanu, E., Spiers, C.J. and de Bresser, J.H.P., 2013. *"The influence of water and supercritical CO_2 on the failure behavior of chalk."* Tectonophysics 599, pp. 157-169.
37. Martavaltzi, C., Dakik, A., Agrawal S. and Gupta, A., 2012. *"Wettability Alteration of Carbonates by Optimizing the Brine and Surfactant Composition."* Paper SPE 163348 presented at the SPE Kuwait International Petroleum Conference and Exhibition, Kuwait City, Kuwait, 10-12 December.
38. Meybodi, H.M., Kharrat, R. and Araghi M.N., 2011. *"Experimental studying of pore morphology and wettability effects on microscopic and macroscopic displacement efficiency of polymer flooding."* Journal of Petroleum Science and Engineering 78, pp. 347-363.
39. Mihajlović, S.R., Vučinić, D.R, Sekulić, Z.T., Milićević, S.Z. and Kolonja, B.M., 2013. *"Mechanism of stearic acid adsorption to calcite."* Powder Technology 245, pp. 208-216.
40. Morrow, N. and Buckley, J., 2011. *"Improved Oil Recovery by Low-Salinity Waterflooding."* Journal of Petroleum Technology, Vol. 63, pp. 106-112.
41. Plank, P. and Bassioni, G., 2007 *"Adsorption of Carboxylate Anions on a $CaCO_3$ Surface."* Z. Naturforsch. 62b, pp. 1277-1284.

42. Risnes, R., Haghighi, H., Korsnes, R.I., Natvik, O., 2003. *"Chalk–fluid interactions with glycol and brines."* Tectonophysics 370, pp. 213-226.
43. Romero-Zerón, L., 2012. *"Introduction to Enhanced Oil Recovery (EOR) Processes and Bioremediation of Oil-Contaminated Sites."* Rijeka, Croatia, InTech. ISBN 978-953-51-0629-6.
44. Rosen, M. J., 2004. *"Surfactants and Interfacial Phenomena."* Hoboken, NJ, USA, John Wiley & Sons.
45. Selley, R. C., 2000. *"Applied Sedimentology."* San Diego, CA, USA, Academic Press.
46. Sen R., 2008. *"Biotechnology in petroleum recovery: The microbial EOR."* Progress in Energy and Combustion Science 34, pp. 714-724.
47. Shalabi, E.W.A., Sepehrnoori, K. and Delshad, M., 2014. *"Mechanisms behind low salinity water injection in carbonate reservoirs."* Fuel 121, pp. 11-19.
48. Speight, J. G., 2009. *"Enhanced Oil Recovery Handbook: A Guide to Heavy Oil."* Houston, TX, USA, Gulf Publishing Company.
49. Sposito, G., 2004. *"Surface Chemistry of Natural Particles."* Cary, NC, USA, Oxford University Press, Incorporated.
50. Standnes, D.C. and Austad, T., 2000. *"Wettability Alteration in Chalk 1: Preparation of Core Material and Oil Properties."* Journal of Petroleum Science and Engineering 28, pp. 111-121.
51. Surguchev, L.M., Manrique, E. and Alvarado, V., 2005. *"Improved Oil Recovery: Status and opportunities."* WPC Paper 18-0886 presented at the 18th World Petroleum Congress, Johannesburg, South Africa, 25-29 September.
52. Sydansk, R. D. and Romero-Zerón, L., 2011. "SPE Textbook, Volume 8: Reservoir Conformance Improvement." Richardson, TX, USA, Society of Petroleum Engineers.
53. Tabrizy, V.A., Denoyel, R. and Hamouda, A.A., 2011. *"Characterization of wettability alteration of calcite, quartz and kaolinite: Surface energy analysis."* Colloids and Surfaces A: Physiochemical and Engineering Aspects 384, pp. 98-108.
54. Tharwat, F.T., 2012. *"Dispersion of Powders in Liquids and Stabilization of Suspensions."* Hoboken, NJ, USA, Wiley-VCH.
55. Tiab, D. and Donaldson, E. C., 2011. *"Petrophysics : Theory and Practice of Measuring Reservoir Rock and Fluid Transport Properties (3rd Edition)."* Saint Louis, MO, USA, Elsevier Science & Technology Books.
56. Tucker, M.E., 2003. *"Sedimentary Rocks in the Field."* Chichester, England, John Wiley & Sons. ISBN 0-470-85123-6.
57. Water Density Calculator, 2011 from http://www.csgnetwork.com/h2odenscalc.html.
58. Water Properties Calculator, 2010 from: http://www.hamzasreef.com/Contents/Calculators/WaterProperties.php
59. Willhite, G.P., 1986. *"SPE Textbook Series, Volume 3: Waterflooding."* Richardson, TX, USA, Society of Petroleum Engineers.

60. Wikipedia, Ionic strength from http://en.wikipedia.org/wiki/Ionic_strength
61. Wikipedia, pH from http://en.wikipedia.org/wiki/PH
62. Wikipedia, Relative permeability from http://en.wikipedia.org/wiki/Relative_permeability
63. Yousef, A.A., Al-Saleh, S.H., Al-Kaabi, A. and Al-Jawfi, M.S., 2011. *"Laboratory Investigation of the Impact of Injection-Water Salinity and Ionic Content on Oil Recovery From Carbonate Reservoirs."* SPE Reservoir Evaluation & Engineering, Vol. 14, pp. 578-593.
64. Zahid, A., 2012. "Smart Waterflooding in Carbonate Reservoirs." PhD Thesis, Technical University of Denmark, Denmark.
65. Zhang, P., Tweheyo, M.T., and Austad, T., 2007. *"Wettability Alteration and Improved Oil Recovery by Spontaneous Imbibition of Seawater into Chalk: Impact of the Potential Determining Ions: Ca^{2+}, Mg^{2+} and SO_4^{2-}."* Colloids and Surfaces A: Physiochemical and Engineering Aspects 301, pp. 199-208.

Appendix

Table A.1 – Concentration of ions in mole/l for flooding of core #1 with LSW 1:5.

PV	Mg^{2+}	Ca^{2+}	HCO_3^-	SO_4^{2-}	Na^+	Cl^-
0,541667	0,03226	0,016303	0,002618	0,017546	0,380429	0,462095
0,666667	0,025963	0,013087	0,003436	0,017269	0,313979	0,370773
0,791667	0,016351	0,008631	0,002845	0,013779	0,203903	0,232185
0,916667	0,011782	0,006784	0,003736	0,010845	0,148386	0,165228
2	0,007854	0,005569	0,003082	0,00601	0,092062	0,105901
3,125	0,008262	0,004064	0,002982	0,004989	0,090986	0,104213
3,25	0,008219	0,003886	0,0029	0,004809	0,090298	0,103541
3,375	0,008239	0,003706	0,002873	0,004813	0,090568	0,103394
3,541667	0,008181	0,003579	0,002318	0,004824	0,088945	0,102588
3,708333	0,008157	0,00358	0,002591	0,004688	0,088616	0,102089
3,833333	0,008158	0,003446	0,001845	0,004732	0,088426	0,101689
4,166667	0,008156	0,003596	0,002727	0,004647	0,08853	0,101905
4,5	0,008239	0,003375	0,001418	0,004647	0,086687	0,101093
4,833333	0,008331	0,003364	0,002345	0,004648	0,088132	0,102318
5,166667	0,008333	0,003299	0,002109	0,004711	0,088258	0,103205
5,5	0,008294	0,003203	0,002191	0,004641	0,088126	0,102064
5,833333	0,008321	0,003053	0,002118	0,004704	0,08848	0,102082
6,166667	0,008354	0,003092	0,001218	0,004672	0,088281	0,101978
6,5	0,008457	0,00316	0,002473	0,004611	0,090164	0,102354
6,833333	0,008385	0,00306	0,002364	0,004632	0,088607	0,101834
7,166667	0,008362	0,003036	0,002209	0,004615	0,088472	0,102224
7,5	0,00842	0,003074	0,002564	0,004587	0,089682	0,102196
7,833333	0,008432	0,002973	0,0025	0,004677	0,08991	0,10262

Table A.2 – Concentration of ions in mole/l for flooding of core #3 with LSW 1:10.

PV	Mg^{2+}	Ca^{2+}	HCO_3^-	SO_4^{2-}	Na^+	Cl^-
0,666667	0,030723	0,015328	0,003149	0,017451	0,379661	0,440479
0,791667	0,016423	0,00921	0,002886	0,013592	0,201702	0,233606
0,916667	0,009322	0,006996	0,002583	0,009057	0,109039	0,129494
1,083333	0,006144	0,006122	0,002851	0,005821	0,067333	0,074644
1,208333	0,004671	0,005728	0,002731	0,004289	0,050799	0,058611
1,333333	0,004017	0,005623	0,003874	0,004063	0,04744	0,056976
2	0,003477	0,005025	0,002229	0,002615	0,045251	0,052447
3,125	0,003846	0,004725	0,001069	0,002283	0,045673	0,055835
3,25	0,003472	0,004725	0,002537	0,002308	0,045199	0,054713
4,333333	0,003633	0,004392	0,002183	0,00231	0,045816	0,052647
4,666667	0,003733	0,004465	0,002177	0,003153	0,045459	0,054706
5	0,004306	0,004083	0,003131	0,002254	0,045278	0,053954
5,333333	0,003699	0,003933	0,002394	0,002597	0,045088	0,052968
5,666667	0,004244	0,003969	0,002531	0,002442	0,045278	0,053017
6	0,004173	0,003912	0,003949	0,00236	0,045761	0,053482
6,333333	0,004315	0,003839	0,003143	0,002803	0,045756	0,052194
6,5	0,003879	0,003766	0,002509	0,002387	0,045789	0,051767
6,666667	0,003865	0,003855	0,002823	0,002354	0,04506	0,054502
6,833333	0,003842	0,003693	0,002703	0,002452	0,045798	0,055053

Table A.3 – Concentration of ions in mole/l for flooding of core #4 with LSW 1:15.

PV	Mg^{2+}	Ca^{2+}	HCO_3^-	SO_4^{2-}	Na^+	Cl^-
0,5	0,037719	0,01709	0,002118	0,019391	0,425975	0,509394
0,625	0,020061	0,010012	0,002509	0,017887	0,237885	0,281846
0,75	0,008263	0,005034	0,001782	0,011427	0,095138	0,111489
0,875	0,005319	0,00397	0,002827	0,006388	0,053645	0,061438
1	0,00431	0,003683	0,002555	0,004166	0,040019	0,046064
1,125	0,003813	0,003528	0,003173	0,003199	0,035	0,040512
2	0,002816	0,003262	0,003009	0,001856	0,030666	0,035283
3,125	0,002501	0,002834	0,0022	0,001565	0,029035	0,034787
3,25	0,002557	0,002786	0,001991	0,001627	0,030317	0,035277
3,375	0,002649	0,002793	0,002427	0,001571	0,030405	0,036213
4,166667	0,00249	0,002619	0,001364	0,001559	0,029286	0,034968
4,5	0,002484	0,00254	0,0028	0,001499	0,03016	0,034872
4,833333	0,002688	0,002444	0,002282	0,001493	0,029133	0,034692
5,166667	0,002584	0,002441	0,002845	0,001481	0,030762	0,035295
5,5	0,002696	0,002419	0,002682	0,001511	0,030813	0,036041
5,833333	0,003673	0,002704	0,002255	0,002464	0,041661	0,04907
6,166667	0,002608	0,002219	0,002491	0,001456	0,030137	0,034856
6,5	0,002652	0,002196	0,002627	0,001447	0,030588	0,035207
6,833333	0,002712	0,002123	0,001691	0,001451	0,02988	0,034901
7,166667	0,002688	0,002071	0,002664	0,001415	0,030466	0,034742
7,5	0,002863	0,002081	0,0016	0,001451	0,029794	0,034813
7,833333	0,002797	0,00205	0,002736	0,001403	0,030788	0,034663

Table A.4 – Concentration of ions in mole/l for flooding of core #5 with LSW 1:20.

PV	Mg^{2+}	Ca^{2+}	HCO_3^-	SO_4^{2-}	Na^+	Cl^-
0,583333	0,036687	0,017664	0,003166	0,019154	0,441677	0,517279
0,708333	0,022448	0,011984	0,003669	0,018409	0,277404	0,332479
0,833333	0,009535	0,00778	0,003034	0,012177	0,124859	0,146274
0,958333	0,008289	0,005992	0,002971	0,008897	0,09399	0,110196
2	0,002288	0,004119	0,002269	0,002118	0,025546	0,029512
3,5	0,001284	0,00405	0,003143	0,001868	0,022713	0,025767
3,666667	0,001213	0,004054	0,002457	0,001302	0,022871	0,026223
3,833333	0,001246	0,004079	0,002566	0,001357	0,022597	0,025906
4,166667	0,001388	0,00401	0,002794	0,001574	0,022792	0,026377
4,333333	0,001322	0,003636	0,003	0,001357	0,022277	0,027122
4,666667	0,001364	0,003721	0,002971	0,001419	0,022674	0,026655
5	0,002364	0,003664	0,002269	0,001411	0,022753	0,026227
5,333333	0,001843	0,003295	0,003126	0,002001	0,022528	0,026632
5,666667	0,00162	0,003209	0,003411	0,001709	0,022189	0,026999
6	0,001374	0,003218	0,002309	0,001315	0,022326	0,025679
6,333333	0,001653	0,00262	0,002634	0,001632	0,022331	0,025694
6,666667	0,001682	0,002738	0,002406	0,001298	0,022929	0,026026
7	0,001719	0,002624	0,002566	0,001331	0,022885	0,02598
7,333333	0,001852	0,002572	0,002211	0,001248	0,022078	0,026103

Table A.5 – Concentration of ions in mole/l for flooding of core #6 with LSW 1:25.

PV	Mg^{2+}	Ca^{2+}	HCO_3^-	SO_4^{2-}	Na^+	Cl^-
0,541667	0,035218	0,016661	0,0026	0,018228	0,431074	0,518043
0,666667	0,019763	0,009881	0,002745	0,015793	0,251383	0,299705
0,791667	0,01075	0,005883	0,002473	0,011545	0,136355	0,16133
0,958333	0,005834	0,003817	0,003036	0,007892	0,069044	0,083404
1,083333	0,00385	0,002853	0,0021	0,005612	0,042636	0,049787
2	0,001837	0,002316	0,003091	0,001635	0,020104	0,022692
3,166667	0,001077	0,001994	0,002918	0,000878	0,017931	0,020821
3,375	0,001099	0,001915	0,003055	0,000938	0,018414	0,020947
3,583333	0,001075	0,001981	0,003127	0,000869	0,018454	0,020807
3,791667	0,001054	0,001947	0,002882	0,000866	0,017807	0,020645
4,166667	0,001068	0,001858	0,002455	0,000923	0,018553	0,020947
4,5	0,001046	0,001799	0,002555	0,000858	0,017656	0,020649
4,833333	0,001077	0,00181	0,003027	0,000842	0,018379	0,020854
5,166667	0,001324	0,002108	0,003218	0,000838	0,018584	0,020579
5,5	0,001418	0,001985	0,002827	0,00089	0,018501	0,020456
5,833333	0,001416	0,001955	0,003018	0,000879	0,018377	0,020737
6,166667	0,001283	0,001835	0,002673	0,000853	0,018665	0,020482
6,5	0,001397	0,001887	0,003136	0,000871	0,018635	0,020647
6,833333	0,001324	0,001758	0,002564	0,000832	0,0184	0,020262
7,166667	0,001348	0,00173	0,002973	0,000836	0,01855	0,020796
7,5	0,001487	0,001843	0,002009	0,000801	0,018334	0,020448
7,833333	0,001464	0,001688	0,002555	0,000788	0,018267	0,020709

Table A.6 – Concentration of ions in mole/l for flooding of core #2 with SSW.

PV	Mg^{2+}	Ca^{2+}	HCO_3^-	SO_4^{2-}	Na^+	Cl^-
0,5	0,043408	0,019772	0,002434	0,020294	0,458833	0,536013
0,625	0,044339	0,017416	0,003343	0,022934	0,461784	0,536994
0,75	0,045436	0,016421	0,002806	0,023741	0,456096	0,533724
0,875	0,045256	0,014962	0,00256	0,024397	0,461923	0,537828
2	0,043934	0,014324	0,003503	0,024557	0,466952	0,533944
3,166667	0,045298	0,013955	0,00228	0,023983	0,46273	0,528551
3,333333	0,044556	0,013657	0,002629	0,023648	0,469652	0,536963
3,5	0,044493	0,013565	0,001577	0,023447	0,441993	0,516422
3,666667	0,045099	0,01354	0,001526	0,023818	0,459111	0,524085
4,333333	0,045981	0,01363	0,001491	0,024361	0,455929	0,529115
4,666667	0,044361	0,013187	0,002223	0,023831	0,443988	0,521634
5	0,043759	0,012996	0,001949	0,023345	0,442002	0,505131
5,333333	0,04482	0,013443	0,002126	0,024432	0,453544	0,528528
5,666667	0,044389	0,013033	0,003783	0,024077	0,445008	0,503255
6	0,044953	0,013045	0,001669	0,024042	0,451707	0,526374
6,333333	0,046454	0,012988	0,002549	0,024607	0,46106	0,53616
6,833333	0,045256	0,012703	0,002543	0,024522	0,460382	0,530528
7,5	0,045559	0,012602	0,002703	0,024148	0,454287	0,519823
8,166667	0,044417	0,012647	0,002091	0,024202	0,449239	0,52473

Table A.7 – Concentration of ions in mole/l for flooding of core #7 with SSW / LSW 1:10.

PV	Mg^{2+}	Ca^{2+}	HCO_3^-	SO_4^{2-}	Na^+	Cl^-
0,54166667	0,040334	0,020319	0,002333	0,018419	0,456704	0,532534
0,70833333	0,042193	0,017950	0,002076	0,020463	0,453248	0,526591
0,875	0,042620	0,016250	0,002257	0,022106	0,461775	0,532491
1,04166667	0,042501	0,014906	0,002162	0,023442	0,455123	0,532573
1,20833333	0,043022	0,014118	0,001838	0,023790	0,449238	0,525983
2	0,043922	0,013749	0,002219	0,023877	0,448535	0,524451
3,125	0,044594	0,013320	0,002276	0,023617	0,445033	0,520232
3,25	0,044890	0,013697	0,002105	0,023622	0,443435	0,519068
3,375	0,045228	0,013759	0,002162	0,024275	0,457944	0,537377
3,5	0,044571	0,013341	0,001962	0,023501	0,441387	0,517736
3,70833333	0,043677	0,013429	0,002010	0,023859	0,441312	0,522105
4,04166667	0,045607	0,013486	0,002086	0,024430	0,460887	0,543767
4,375	0,043552	0,013250	0,001695	0,024058	0,446088	0,520193
4,70833333	0,043511	0,013510	0,002352	0,023654	0,445090	0,519213
5,04166667	0,045015	0,013122	0,001990	0,023859	0,445021	0,521913
5,375	0,045059	0,013164	0,002105	0,023872	0,446567	0,523433
5,70833333	0,045835	0,013174	0,002276	0,024214	0,455238	0,531006
6,04166667	0,043810	0,013198	0,001933	0,023129	0,431752	0,507667
6,375	0,044793	0,013377	0,001819	0,023922	0,442529	0,523550
6,70833333	0,045335	0,013211	0,002038	0,023849	0,446088	0,522093
6,83333333	0,043881	0,013270	0,001829	0,022902	0,441121	0,518210
6,95833333	0,044408	0,013286	0,001543	0,023332	0,445240	0,525161
7,08333333	0,044686	0,013260	0,002305	0,023255	0,450162	0,527402
7,20833333	0,044331	0,013299	0,001724	0,023249	0,445737	0,523695
7,33333333	0,044754	0,013096	0,002438	0,023593	0,452135	0,534669
8,5	0,003869	0,003328	0,002381	0,002137	0,046155	0,053257
10,0416667	0,003929	0,003229	0,001971	0,002125	0,046191	0,053447
10,1666667	0,003940	0,003078	0,002476	0,001978	0,045576	0,052892
10,2916667	0,004304	0,003328	0,002876	0,002233	0,046011	0,053485
10,9583333	0,004358	0,003619	0,002410	0,002191	0,045240	0,052622
11,2916667	0,004399	0,003489	0,001653	0,002222	0,045483	0,052542
11,625	0,004242	0,003440	0,002048	0,002139	0,045448	0,053866
11,9583333	0,004478	0,002964	0,002476	0,002283	0,045757	0,053436
12,2916667	0,004148	0,003034	0,002886	0,002194	0,046086	0,052979
12,625	0,004201	0,002795	0,002724	0,002276	0,045779	0,052348
12,9583333	0,004151	0,002935	0,002419	0,002311	0,046314	0,052504